Aus der Klinik für Allgemeine, Unfall- und Wiederherstellungschirurgie
der Universität München
Direktor: Prof. Dr. med. Wolfgang Böcker

Molecular mechanisms of phrenic nerve outgrowth and innervation of the diaphragm

Dissertation
Zum Erwerb des Doktorgrades der Naturwissenschaften
an der Medizinischen Fakultät
der Ludwig-Maximilians-Universität zu München

vorgelegt von
Maximilian Michael Saller
aus München
2016

Mit Genehmigung der Medizinischen Fakultät

der Universität München

Erstgutachter:	PD Attila Aszodi, PhD
Zweitgutachter:	PD Dr. Christian Ries

Mitbetreuung durch die	
promovierte Wissenschaftlerin:	Dr. Andrea Huber Brösamle

Dekan:	Prof. Dr. med. dent. Reinhard Hickel

Tag der mündlichen Prüfung:	27.10.2016

"Here's to the crazy ones. The misfits. The rebels. The troublemakers. The round pegs in the square holes. The ones who see things differently. They're not fond of rules. And they have no respect for the status quo. You can quote them, disagree with them, glorify or vilify them. About the only thing you can't do is ignore them. Because they change things. They push the human race forward. And while some may see them as the crazy ones, we see genius. Because the people who are crazy enough to think they can change the world, are the ones who do."

Rob Siltanen

Abstract

The highly structured process of breathing is controlled by automatic respiratory centers in the brainstem, which signal to a specialized group of motor neurons in the cervical spinal cord that constitute the phrenic nerves. In mammals, the thoracic diaphragm that separates the thorax from the abdomen adopts the function of the primary respiratory musculature. Faithful innervation by the phrenic nerves is therefore a prerequisite for the functionality of this highly specialized musculature and thus, ultimately, the viability of the entire organism. Here, we employed a genetic approach to investigate the involvement of the Sema3-Npn-1 signaling pathway during phrenic nerve targeting and fasciculation, as well as during establishment of the diaphragm.

We utilized mouse lines in which either the binding site of Npn-1 for class 3 Semaphorins was mutated systemically (*Npn-1*$^{Sema-}$), or in which Npn-1 was removed selectively from somatic motor neurons (*Npn-1*^{cond}*;Olig2-Cre*) by tissue-specific activity of Cre-recombinase. Whole-mount immunohistochemistry revealed initial defasciculation of phrenic motor axons within the brachial plexus at developmental stage E10.5. Interestingly, the axons refasciculated and formed one distinct nerve bundle before reaching the primordial diaphragm, the pleuroperitoneal fold, at E11.5 in both mutant mouse lines. During the development of the costal muscles of the diaphragm, Sholl analysis revealed increased defasciculation of the phrenic nerve branches which persisted until the end of primary myogenesis at E16.5 and beyond. Additionally, significantly more axons extended into the central tendon region (CTR) of the diaphragm at all investigated embryonic stages when compared to littermate controls. Intriguingly, we observed formation of ectopic muscles patches within the CTR that were innervated by misprojecting axons in both mutant mouse lines. We therefore asked whether ectopic muscle development was a direct result of manipulating Sema3A-Npn-1 signaling, or a secondary

effect regarding interaction of ectopically migrating phrenic axons and muscle progenitor cells (MPCs). To elucidate the underlying mechanisms of ectopic recruitment of MPCs to the CTR, we focused on the Slit-Robo signaling pathway, which is employed by motor neurons during axon targeting and bundling, and was shown to be involved in targeted MPC migration at later developmental stages in Drosophila. We showed that Slit2 and it's corresponding Robo receptors are expressed in phrenic motor neurons and migrating MPCs during diaphragm development and innervation, respectively. *In vitro* chemotaxis experiments revealed an attractive effect of Slit1 and Slit2 onto primary MPCs, while Sema3A acts strongly repulsive.

Taken together, our data indicate that Sema3A-Npn-1 signaling cell-autonomously influences phrenic nerve growth and targeting, while aberrant muscle formation in the CTR of the diaphragm may be triggered by ectopically invading axons, independently of the Sema3A-Npn-1 signaling pathway. Thus, we postulate an influence of factors released by motor neuron growth cones on the migration properties of myoblasts during establishment of the diaphragm. Conditional genetic approaches may prove the interdependency of motor axon growth cones and myoblast progenitor cells for faithful establishment of neuromuscular connectivity during embryonic development.

Zusammenfassung

Der hochstrukturierte Atmungsprozess wird durch respiratorische Zentren im Stammhirn gesteuert, die Signale zu spezialisierten Motorneuronen im zervikalen Rückenmark weiterleiten und die phrenischen Nerven bilden, automatisch gesteuert. Das Zwerchfell trennt in Säugetieren den Thorax vom Abdomen ab und übernimmt die Funktion des primären Atemmuskels. Die korrekte Innervierung durch die phrenischen Nerven ist somit eine Voraussetzung für die Funktionalität dieses hochspezialisierten Muskels und sichert die Überlebensfähigkeit des gesamten Organismus. In dieser Arbeit verwendeten wir genetische Modellsysteme, um die Beteiligung des Sema3-Npn-1 Signalweges während der Projektion und der Faszikulierung der phrenischen Nerven sowie der Bildung des Zwerchfelles zu analysieren.

Hierfür untersuchten wir zwei verschiedene Mauslinien, in denen zum einen die Bindungsstelle von Npn-1 für Semaphorine der Klasse 3 mutiert wurde (*Npn-1*$^{Sema-}$), und zum anderen Npn-1 selektiv in Motorneuronen durch gewebespezifische Aktivität von Cre-Rekombinase entfernt wurde (*Npn-1*^{cond}*;Olig2-Cre*). Im Entwicklungsstadium E10.5 zeigten immunohistochemische Färbungen von ganzen Embryonen eine Defaszikulierung von phrenischen Motoraxonen im brachialen Plexus. Interessanterweise refaszikulierten die Axone und bildeten ausgeprägte Nervenbündel, bevor sie das primitive Zwerchfell (pleuroperitoneale Falten) bei E11.5 erreichten. Während der Entwicklung der kostalen Muskeln des Zwerchfells zeigte eine Shollanalyse eine erhöhte Defaszikulierung der phrenischen Nervenverzweigungen, die bis zum Ende der primären Myogenese bei E16.5 andauerte. Zusätzlich wuchsen im Vergleich zu Kontrollembryos signifikant mehr Axone bei allen untersuchten Embryonalstadien in die zentrale Sehnenregion (CTR) des Zwerchfelles ein. Faszinierenderweise konnten wir die Bildung von innervierten ektopischen Muskeln in der CTR in beiden mutanten Mauslinien

beobachten. Wir stellten uns die Frage, ob die Entwicklung von ektopischen Muskeln direkt durch die Manipulation des Sema3A-Npn-1 Signalweges bedingt wurde oder durch einen sekundären Effekt, der auf der Interaktion von ektopisch projizierenden phrenischen Axonen und Muskelvorläuferzellen (MPCs) beruht. Um den zugrunde liegenden Mechanismus der ektopischen Rekrutierung von MPCs in die CTR aufklären zu können, haben wir uns auf den Slit-Robo Signalweg konzentriert, der während der Zielfindung und Faszikulierung von Motorneuron zum Einsatz kommt und des Weiteren in die zielgerichtete Bewegung von MPCs in späteren Entwicklungsstadion der Drosophila involviert ist. Wir konnten zeigen, dass Slit2 und sein korrespondierender Robo Rezeptor in Motorneuronen des phrenischen Nervs bzw. in migrierenden MPCs, während der Entwicklung und Innervation des Zwerchfells exprimiert ist. *In vitro* Chemotaxisexperimente zeigten eine anziehenden Effekt von Slit1 und Slit2 auf MPCs während Sema3A stark abstoßend wirkte.

Zusammengefasst zeigen unsere Daten, dass der Sema3A-Npn-1 Signalweg zellautonom Wachstum und Zielfindung der phrenischen Nerven beeinflusst, während die abnormale Bildung von Muskel in der CTR des Zwerchfells möglicherweise durch ektopisch einwachsende Axone, unabhängig des Sema3A-Npn-1 Signalweges, ausgelöst wird. Somit postulieren wir, dass durch den Wachstumskegel der Motorneuronen freigesetzte Faktoren das Migrationsverhalten von Myoblasten während der Ausbildung des Zwerchfells beeinflussen können. Konditionalgenetische Herangehensweisen könnten die gegenseitige Abhängigkeit zwischen den Wachstumskegeln der Motorneuronen und Muskelvorläuferzellen, die in die genaue Etablierung der neuromuskulären Konnektivität während der embryonalen Entwicklung involviert sind, aufklären.

Contents

Abstract I

Zusammenfassung III

Contents V

List of Figures IX

List of Tables XI

1 Introduction 1

1.1 The establishment of breathing 1

1.1.1 Ryhthm patterning in the brainstem 1

1.1.2 The phrenic motor nucleus in the brachial spinal cord 5

1.1.3 Phrenic nerve outgrowth and innervation of the primordial diaphragm 7

1.2 Somitic origin of the thoracic diaphragm 8

1.2.1 Muscle precursor specification, proliferation and differentiation . 9

1.2.2 Migration of muscle progenitor cells towards their target sites . . 11

1.2.3 Fusion of myoblasts and formation of neuromuscular junctions . 13

1.2.4 Tendon development and formation of myotendinous junctions . 15

1.2.5 Development, innervation and defects of the thoracic diaphragm 16

1.3 Establishment of peripheral motor and sensory circuitry 19

1.3.1 Axon guidance mechanisms during target innervation 19

1.3.2 Secreted guidance cues that govern axon pathfinding, fasciculation and neuronal development 21

1.3.2.1 Class 3 Semaphorins – Neuropilins 21

1.3.2.2 Slit – Robo 24
1.3.2.3 Ephrins – Eph receptors 26
1.3.2.4 SF/HGF – cMET 27

2 Aim of the study **28**
2.1 Determination of the effects of class 3 semaphorin-Npn-1 signaling ablation on phrenic nerve targeting, fasciculation and innervation of the diaphragm 29
2.2 Unveil new mechanisms that influence the interaction between motor neuron growth cones and muscle progenitor cells 29

3 Material & Methods **31**
3.1 Animal husbandry 31
3.1.1 Ethics statement 31
3.1.2 Animal housing 31
3.1.3 Mouse lines 31
3.1.4 Genotyping 32
3.2 Immunohistochemistry 34
3.2.1 Embryo and diaphragm dissection 34
3.2.2 Whole-mount embryo staining 34
3.2.3 Whole-diaphragm staining 35
3.2.4 Motor neuron pool and myogenic progenitor cell staining 36
3.3 Histological analysis of ectopic muscles 37
3.4 Molecular biology 37
3.4.1 Midi prep with heat shock transformation of Escherichia Coli . . 37
3.4.2 Plasmid linearization and generation of RNA probes 38
3.4.3 *In situ* hybdridization 39
3.4.4 Quantitive PCR 41
3.5 Quantification of phrenic nerve defasciculation, misprojecting axons, ectopic muscle and *Npn-1* & *Slit2* positive motor neurons 42
3.6 Myoblast chemotaxis assay 43
3.7 Statistical analysis 44

4 Results **45**

4.1 *Npn-1* is expressed in motor neurons of the phrenic nucleus during PPF targeting and diaphragm innervation 45

4.2 Pre-diaphragm fasciculation of the PN is only mildly disturbed upon systemic or motor neuron specific ablation of Sema3-Npn-1 signaling . . . 47

4.3 Npn-1 cell-autonomously governs PN fasciculation within the diaphragm muscles 49

4.4 Misprojecting PN axons innervate ectopic muscles in the CTR of the diaphragm 55

4.5 Somatic motor neurons are not involved in normal muscle development but essential for EM formation 62

4.6 Ectopic muscles are likely to develop from muscle rather than transdifferentiation of tendon progenitor cells 64

4.7 Slits and Robo are expressed in pMN and myoblasts that will form costal muscles, respectively, during diaphragm development 66

4.8 A subpopulation of primary MPCs is attracted by Slit1 and Slit2 68

4.9 *Npn-1*$^{Sema-}$ and *Npn-1*$^{cond-/-}$*;Olig2-Cre*$^{+}$ mutant neonates show increased lethality 71

4.10 Systemic ablation of Robo1 and Robo2 showed no ectopic muscle formation, but a severe misalignment of muscle fibers in the diaphragm . . 76

5 Discussion **79**

5.1 Sema3-Npn-1 signaling is not involved in early targeting of the PPF . . . 79

5.2 Systemic and MN-specific ablation of Sema3-Npn-1 signaling shows a severe effect during innervation of the diaphragm musculature 81

5.3 Ectopic muscles in the CTR of the diaphragm are innervated by misrouted axons of the PN after ablation of Sema3-Npn-1 signaling 83

5.4 Diaphragm myoblasts from costal muscles are attracted by Slits 85

5.5 Ectopic muscles might be the cause of neonatal lethality after manipulation of Sema3-Npn-1 signaling 88

6 Conclusion & Outlook **90**

7 Supplementary data **92**

8 Bibliography **95**

10 Appendix **125**

Abbreviations 125

Acknowledgments 132

Declaration 134

List of Figures

1.1 Schematic illustration of CPGs within the hindbrain that are involved in mammalian breathing. 3
1.2 Simplified neuronal circuitry of CPGs within the hindbrain. 4
1.3 Specification of somatic MNs during development of the spinal cord. . . 6
1.4 Phrenic nerve outgrowth and targeting of the PPF. 8
1.5 Development of the dermomyotome and its anatomy. 10
1.6 Diaphragm development and innervation by the phrenic nerve. 17
1.7 Axon guidance mechanism during development. 20
1.8 Semaphorin classes and their corresponding Neuropilin and Plexin receptors. 22
1.9 Slit-Robo complex and stabilization by proteoglycans. 25

3.1 Quantification of EM orientation and illustration of Sholl analysis. 42

4.1 Expression of *Npn-1* in the phrenic nucleus in the cervical spinal cord during targeting and innervation of the thoracic diaphragm. 46
4.2 Whole-mount staining of the brachial plexus during diaphragm targeting. 48
4.3 Whole-mount staining of control and mutant diaphragm. 51
4.4 Sholl analysis of PN axon branching within the diaphragm. 52
4.5 Quantification of PN branching within the diaphragm during development. 54
4.6 PN axons misproject into the CTR after systemic ablation of Sema3-Npn-1 signaling. 56
4.7 Sema3A and its signaling receptors are express in myoblasts of the CoM during diaphragm development. 57
4.8 Quantification of misprojecting axons into the CTR during development after conditional ablation *Npn-1* in somatic MNs. 59

4.9 Quantification of EMs within the CTR during development and adulthood. 61
4.10 Complete removal of somatic MNs affects muscle development of the diaphragm. 63
4.11 Rostral-caudal localization of EMs within the CTR. 65
4.12 Expression of *Slit2* in the phrenic nucleus in the cervical spinal cord during targeting and innervation of the thoracic diaphragm. 67
4.13 Expression of *Robo1* and *Robo2* in MPCs of the diaphragm during development. 68
4.14 Characterization of primary MPCs and its response to chemokines. . . . 69
4.15 Chemotaxis assay of pMPCs in a 3D collagen matrix. 70
4.16 Quantification of FMI and COM of pMPCs during chemotaxis by soluble ligands. 71
4.17 Manipulation of Sema3-Npn-1 signaling is not affecting NMJ band width in the CoM of the diaphragm. 72
4.18 No difference of EM size and length between mutant and control embryos. 74
4.19 Mutant animals of both mouse lines have an increased cumulative EM area. 75
4.20 The majority of EMs show a nonlinear alignment towards CoM fibers. . 76
4.21 Robo1/Robo2 mutants have no misprojecting axons into the CTR, but also no ectopic muscle formation. 77
4.22 Robo1/Robo2 ablation leads to misalignment of CoM fibers. 78

5.1 Hypothesis of EM formation in the CTR of the diaphragm. 87

7.1 Whole mount staining of *Npn-1*$^{Sema-}$ heterozygote embryos. 92
7.2 Whole mount staining of *Npn-1*$^{Sema-}$ and quantification of defasciculation. 93
7.3 Quantification of EM formation and misprojecting axons of *Npn-1*$^{Sema+/-}$ embryos. 94

List of Tables

3.1 Instruments & chemicals for gDNA isolation. 32
3.2 Instruments & chemicals for genotyping of mouse lines. 33
3.3 Oligonucleotides for genotyping. 33
3.4 Primary antibodies and fluorescence-labeled secondary antibodies or toxins. 34
3.5 Chemicals, solutions & buffers for whole-mount embryo staining. 35
3.6 Chemicals, solutions & buffers for whole-diaphragm staining. 36
3.7 Buffers for immunohistochemistry & immunocytochemistry. 36
3.8 Chemicals for histology of embryo sections. 37
3.9 Chemicals for bacterical culture. 38
3.10 Restriction enzymes (RE) and polymerases (P) for ISH-Plasmids. 39
3.11 Chemicals & buffers for *in situ* hybridization. 40
3.12 Primer pairs for quantitative determination of gene expression. 41

Chapter 1

Introduction

1.1 The establishment of breathing

Most tetrapods, and all dipnoi and pulmonates, rely on direct oxygen exchange by lungs or lung variations (Brainerd, 1999; Jordaens et al., 2007; Perry et al., 2001). Breathing is indispensable for all higher organisms due to the requirement of molecular oxygen for synthesis of adenosine triphosphate (ATP) from adenosine diphosphate by phosphorylation as a chemical energy source. Diseases that directly or indirectly impair breathing in humans either cause longterm disability and pain or can ultimately result in lethality of the organism. Sources of respiratory diseases can be (developmental) genetic defects (Crone et al., 2012), bacterial or viral infections (De et al., 2001; Edelstein, 1982), or severe trauma of the hindbrain or the cervical spinal cord which cause a complete rupture of respiratory sensory and/or motor axon tracts. Breathing can be hierarchically divided in three distinct centers: rhythm patterning in the brainstem, phrenic/intercostal/abdominal motor neurons (MNs) and finally the innervated musculature, which create the physical force of inspiration and expiration.

1.1.1 Ryhthm patterning in the brainstem

Rhythmic movements, like swimming, running, breathing or flying, were long thought to purely rely on monosynaptic reflex arcs (Marder and Bucher, 2001). Graham Brown postulated over 100 years ago, that cats keep rhythmic respiration even when peripheral reflexes are completely abolished during deep anesthesia (Brown, 1914). These neuronal networks, which produce rhythmic action potentials, are nowadays referred to

as central pattern generators (CPGs). The respiratory system (RS) of the brain consists of several of these highly specialized CPGs, which contain expiratory, inspiratory and rhythm-generating neurons (Benarroch, 2007a,b). The nucleus of the solitary tract (NST) forwards sensory information (pH and O_2/CO_2 levels) of the periphery to regulatory centers like the parafacial respiratory group or retrotrapezoid nucleus (pFRG/RTN) or the pontine respiratory group (PRG), which is an arrangement of the Kölliker-Fuse nucleus (KF) and the lateral parabrachial subgroup (LPBr). While the Bötzinger complex (BötC) and the pre-Bötzinger complex (pre-BötC) refine signals prior transmission to terminal CPGs, the pre-BötC creates the rhythmic signal of breathing. Finally, the terminal rostral inspiratory ventral respiratory group (rVRG) and the caudal respiratory ventral respiratory group (cVRG) provide the ultimate signal for cervical, thoracic and abdominal MNs (Figure 1.1) (Alheid and McCrimmon, 2008; Janczewski and Feldman, 2006; Onimaru and Homma, 2003).

CPGs like the (sub)parabrachial Kölliker-fuse complex (PKFC) and lateral parabrachial subgroup (LPbr) in the dorsolateral pons are mainly involved in inspiratory-expiratory phase transitions of breathing by modulating inspiratory off-switch (IOS) mechanism (Bautista and Dutschmann, 2014; Berger, 1977; Dutschmann and Herbert, 2006). This IOS might also have physiological reasons, like swallowing or pathophysiological causes, i.e. lesions of the hindbrain, which can lead to complete apnea (Bonis et al., 2011).

Pacemaker neurons that provide the oscillatory signal for the RS are located in the pre-BötC (Smith et al., 1991). 50 to 500 of these highly interconnected neurons generate approximately every 5 sec an action potential (AP) burst, which results in around 18.000 respirations per day in humans (Butera et al., 1999a,b). The BötC is located rostral to the pre-BötC, which contains, in contrast to the pre-BötC, expiratory neurons that inhibit mono-synaptically phrenic motor neurons (pMNs), sensory neurons of the dorsal root ganglia (DRG) and neurons in the rostral VRG (Merrill and Fedorko, 1984; Merrill et al., 1983; Tian et al., 1999).

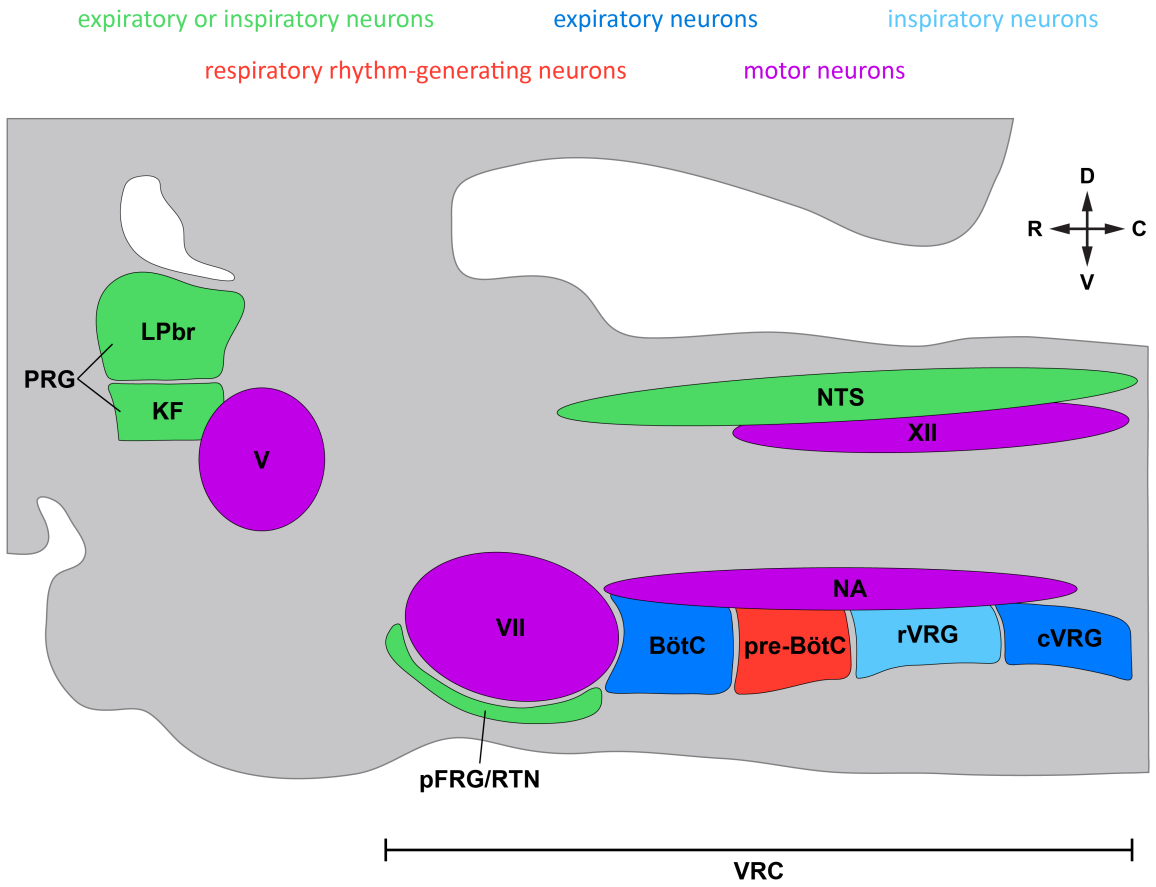

Figure 1.1: Schematic illustration of CPGs within the hindbrain that are involved in mammalian breathing.

Breathing is highly regulated by neuronal circuits in the brainstem, which is comprised of several specified CPGs. The CPGs of the RS are located in the pontine respiratory group (PRG), the nucleus of the solitary tract (NTS) and the rostral and caudal ventrolateral respiratory groups (VRG), the Bötzinger complex (BötC), (pre-)Bötzinger complex (pre-BötC) and the parafacial respiratory group or retrotrapezoid nucleus (pFRG/RTN), which together compose the ventrolateral respiratory column (VRC). NA: nucleus ambiguous, V: motor trigemal nucleus, VII: facial nucleus, XII: hypoglossal motor nucleus, VRC: bentral respiratory column. Modified and adapted from (Ballanyi et al., 2010; Benarroch, 2007b; Bianchi et al., 1995; Smith et al., 2013).

Caudal to BötC and pre-BötC, two groups of inhibitory and excitatory neurons are situated, namely the rostral and caudal VRG (Hayakawa et al., 2004). While the rostral VRG consists of inspiratory neurons, the caudal VRG is comprised mainly of expiratory neurons (Alheid and McCrimmon, 2008). Rostral VRG neuron activity is regulated by excitatory pre-BötC neurons and expiratory neurons of the BötC that interconnect to MNs of the phrenic nerves (PNs) which innervate the thoracic diaphragm (Smith et al., 2013). During expiration, caudal VRG neurons excite MNs at thoracic and lumbar spinal

levels, which innervate intercostal and abdominal muscles (Smith et al., 2013).

Sensory information from pulmonary mechanoreceptors, chemoreceptors of the vascular system and visceral sensory neurons are accumulated within the NTS and forwarded to the PRG (Alheid et al., 2011; Smith et al., 2013). Furthermore, anterograde tracings provide evidence of neuronal projections towards higher brain centers, i.e. hypothalamus, amygdala or various other forebrain areas (Ricardo and Koh, 1978).

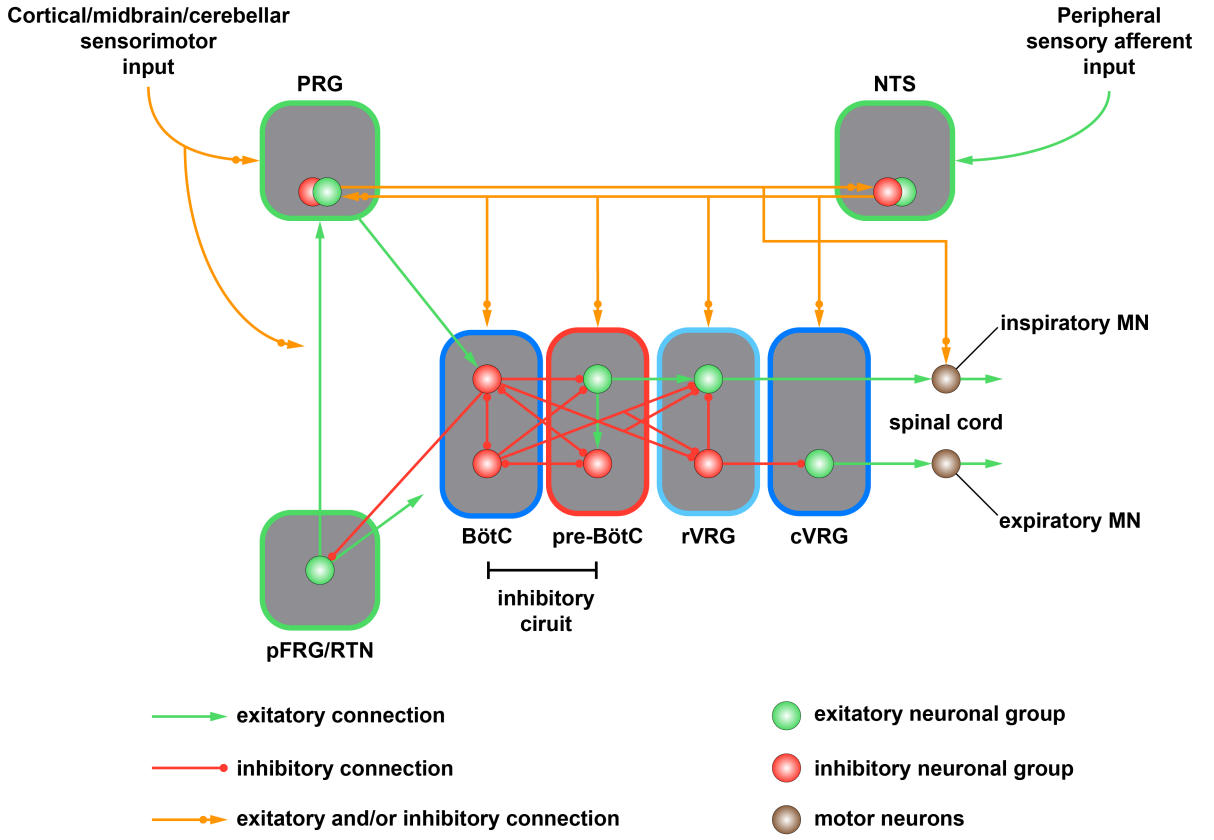

Figure 1.2: Simplified neuronal circuitry of CPGs within the hindbrain.

The respiratory center of the brainstem in mammalians receives sensory information of the periphery and higher brain centers. The rhythmic patterning of the pre-BötC is modified by an inhibitory circuitry with the BötC which finally deliver either an inspiratory (rVRG) or an expiratory (cVRG) signal to intercostal, diaphragm and abdominal innervating MNs. Modified and adapted from (Ballanyi et al., 2010; Smith et al., 2013).

All CPGs of the RS are highly cross-linked to provide a proper adaptation for changing physiological conditions (Figure 1.2). Sensory information, like O_2 and CO_2 concentrations or mechanoreceptors of the airway system, are received by afferent projecting

neurons of the vagal nerve in the upper airways (nasopharyxn, oropharynx, larynx and extrathoracic trachea) and the lower airways (trachea and lungs) (Kubin et al., 2006; Sant'Ambrogio et al., 1995).

Interestingly, besides the metabolic factor of breathing, its frequency is also influenced by emotions in mammalians. Such emotions might be rage or fear (Boiten, 1994), where subconscious enhancement of breathing compensates the higher oxygen requirement for subsequent probable escape. In contrast, several human cultures established conscious breathing techniques like Indo Tibetan Yoga, to actively reduce depression, post-traumatic disorders or anxiety (Brown and Gerbarg, 2009). Furthermore, anatomical and physiological adaptation, together with conscious control of breathing, facilitated the evolution of speech in humans approximately 1.6 million to 100,000 years ago (MacLarnon and Hewitt, 1999).

1.1.2 The phrenic motor nucleus in the brachial spinal cord

Efferent projection axons from the RS of the hindbrain innervate MNs that provide the signal for costal as well as abdominal muscles. Furthermore, mammalians have developed an additional breathing specific muscle, namely the thoracic diaphragm, which is mainly innervated by MNs in the phrenic nucleus (Philippidou et al., 2012). In the last two decades, genetic approaches have revealed several important transcription factors that are required for MN proliferation, sorting and specification (Davis-Dusenbery et al., 2014; Jessell, 2000).

The initial fate of developing neurons to specific interneurons or MNs is determined by opposing gradients of Sonic hedgehog (Shh) and/or members of the bone morphogenic proteins (Bmp) or wingless-type MMTV integration site family (Wnt) (Jessell, 2000). While Shh is released from the notochord and the floorplate, Bmps and Wnts are released from cells within the roofplate (Figure 1.3 A). Those ligands have distinct functions during the specification of various types of neurons. Ectoderm derived factors like BMP4 or BMP7 mediate the specification of dorsal progenitor cells towards interneurons (Liem et al., 1995). In contrast, low concentrations of Shh, which is released by the floorplate, drives the specification of late born progenitor cells into MNs

(Ericson et al., 1996; Pfaff et al., 1996). Beside ligands that act in a dorsal-ventral axis, retinoic acid (RA), which is released in the somites, positively influences the specification of somatic MNs by the activation of momentous transcription factors (Maden, 2007; Novitch et al., 2003). These well-defined extracellular signals initialize an orchestrated sequence of transcription factor upregulation (Pax6, Olig2, Nkx6.1 and Nkx6.2) that specify somatic MNs (Lu et al., 2002; Novitch et al., 2001). The expression onset of the terminal transcription factor motor neuron and pancreas homebox 1 (Mnx1 or Hb9) defines the determination of post-mitotic MNs during their migration from the midline towards the ventrolateral position (Arber et al., 1999; Tanabe et al., 1998).

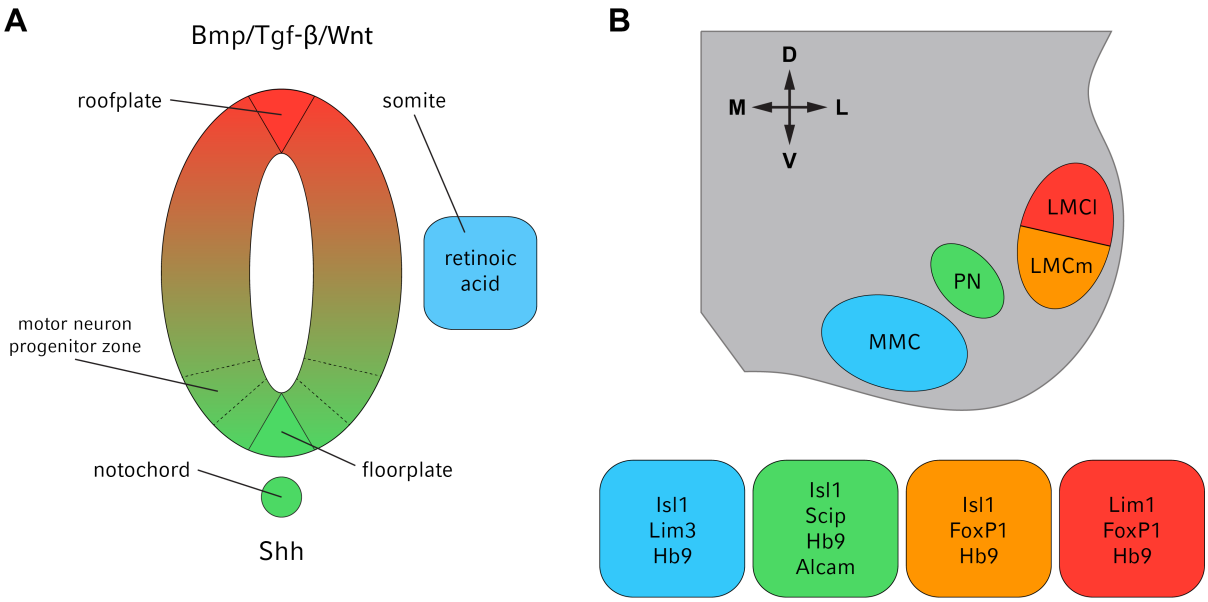

Figure 1.3: Specification of somatic MNs during development of the spinal cord.

Somatic MNs arise from a specific progenitor zone in the ventral part of the spinal cord. This specification of MNs is encouraged by the release of Sonic hedgehog (Shh) from the notochord and the floorplate (A). Shh induces a transcriptional sequence which finally results in a $Hb9^{+}$ progenitor MN pool. During developmental progression, MNs form columns which later project to their final muscular targets (B). D: dorsal, V: ventral, M: medial, L: lateral. Modified and adapted from (Davis-Dusenbery et al., 2014; Jessell, 2000; Philippidou et al., 2012).

Somatic MNs form columns within the spinal cord in respect to their subsequent innervation target (Figure 1.3 B). Brachial or lumbar MNs that project to the limbs express the forkhead transcription factor P1 (FoxP1) and are located in the lateral motor columns (LMC) (Dasen et al., 2008). MNs which later innervate axial musculature ex-

press the transcription factors Isl1 as well as Lim3 and are combined to medial motor column (MMC) (Thor et al., 1999), MNs within the phrenic motor column (PMC) express Isl1 and the POU domain, class 3, transcription factor Pou3f1 (also known as Scip or Oct6) (Philippidou et al., 2012).

Scip, which is a specific marker of MNs in the PMC, is expressed in the cervical levels C3 to C6 in and respiratory centers of the brain stem in mice (Bermingham et al., 1996). In rats, retrograde labeling from the PNs revealed that the main population of neurons in the phrenic nucleus is localized between spinal levels C3 and C5 (Mantilla et al., 2009). The specification of Scip$^+$ MNs relies on the two homebox transcriptions factors Hoxa5 and Hoxc5, which influence column formation, axonal branching of phrenic nerve axons in the diaphragm, and MN survival during embryonic development (Philippidou et al., 2012). Systemic deletion of Scip results in a reduction of the breathing frequency, which is caused by a lack of final wrapping of axonal myelin sheets (Bermingham et al., 1996; Jaegle et al., 1996).

Thus, the tight regulation of somatic MN specification and their subsequent organization in specific columns are the prerequisite for a faithful innervation of later forming muscles.

1.1.3 Phrenic nerve outgrowth and innervation of the primordial diaphragm

After the specification of somatic MNs in the ventral horn of the spinal cord, axons begin to extend towards their target sites. In mice, PNs separate bilaterally from limb innervating motor nerves and form two distinct branches at developmental stage E10.5 (Figure 1.4 A). One day later, PNs project between the primitive heart and lung towards the liver and have reached the pleuroperitoneal folds (PPFs), which mark the primordial diaphragm structures (Figure 1.4 B and Figure 6A). By developmental stage E12.5, PN axons start to form three distinct branches towards their final muscle targets (Figure 1.4 C and Figure 6B). Diaphragm musculature is innervated in a distinct topographical manner. While dorsal costal myofibers are innervated by more rostral pMNs, the ventral proportion is innervated by pMNs in the rostral PMC (Laskowski and

Sanes, 1987). During subsequent development, PNs form secondary and tertiary axon branches at the midline of both muscle proportions (Figure 1.4 D) (Allan and Greer, 1997; Greer et al., 1999). At the time of targeting and sophisticated innervation of the diaphragm by PN axons, a plentitude of axon guidance/bundling molecules like Gap43 (growth associated protein 43), Ngfr (nerve growth factor receptor) and Ncam (neuronal adhesion molecules) are strongly expressed by phrenic motor neurons (pMNs) (Allan and Greer, 1997; Cremer et al., 1997; Lee et al., 1992; Strittmatter et al., 1995).

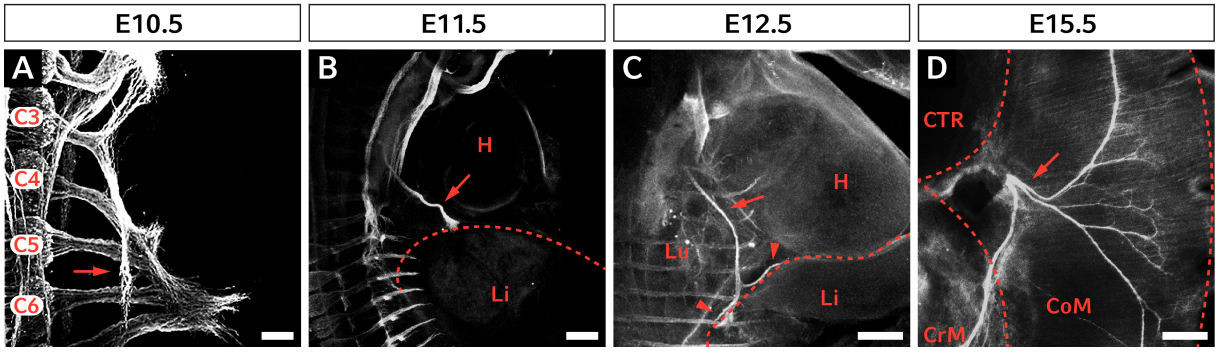

Figure 1.4: Phrenic nerve outgrowth and targeting of the PPF.

Whole mount antibody staining of wildtype mouse embryos against neurofilament. At E10.5, the PNs exit the spinal cord between cervical levels C3 to C5 and forms bilateral nerves within the brachial plexus (A, arrow). One day later, at E11.5, PN projections (B, arrow) have formed a distinct nerve bundle exiting the brachial plexus and targeting the developing diaphragm (B, dashed line). At E12.5, each PN (C, arrow) branches into three distinct nerve bundles (C, arrow heads), which later bilaterally innervate the costal and crural muscles of the diaphragm (D, arrow). H: heart, Li: Liver, CTR: central tendon region, CrM: crural muscle, CoM: costal muscle. Scale bar: 200 μm.

1.2 Somitic origin of the thoracic diaphragm

Breathing of mammalians is highly optimized when compared to other living tetrapods due to the large pulmonic surface of the lungs in combination with a specified thoracic diaphragm muscle, which provides a mechanical source for forced ventilation (Hirasawa and Kuratani, 2013). The current opinion of diaphragm evolution is based on two major steps: First, diaphragm muscle progenitor cells (MPCs) arise from cervical somites which lie caudally to limb somites and form a primitive diaphragm. During evolution, forelimbs translocated, together with a primitive diaphragm, caudally in mammalians.

Second, a spatial controlled genetic development of the pulmonary system occured in mammalian cynodonts (a Jurassic mammaliaform) (Hirasawa and Kuratani, 2013).

Somites are segments of paraxial mesoderm which are formed from cells of the presomitic mesoderm (PSM). It was shown that oscillating gene expression of the chicken hairy homologue 1 (c-hairy1) in an antero-posterior manner is involved in somitogenesis (Palmeirim et al., 1997). The expression of c-hairy1 and other genes, which are involved in oscillating gene expression like Hes1 or Her1, depend on the Notch-Delta signaling pathway (Rida et al., 2004; Saga and Takeda, 2001). After successful separation of the somites from the PSMs, somitic cells begin to differentiate over the dorsoventral axis into the main structures, namely the dermomyotome, myotome, syndetome and the sclerotome. All epaxial, hypaxial and some facial muscles arise from the dermomyotomes (Scaal and Christ, 2004).

1.2.1 Muscle precursor specification, proliferation and differentiation

The specification of the dermomyotomes (DM) partially depends on members of the Wnt family (Wnt1, Wnt3a, Wnt4 and Wnt6) (Figure 1.5), which was shown for co-cultures of PSM explants and Wnt expressing COS (CV-1 in Origin with SV40 genes) cells (Fan et al., 1997). While members of the Wnt family, which are released from the dorsal neural tube (Wnt1 and Wnt3a) or the dorsal ectoderm (Wnt4 and Wnt6), promote development of the DM, Shh, which is released by the notochord, influences the ventral development towards the sclerotome (Fan et al., 1997). Analysis of Wnt1/Wnt3a double mutant mouse embryos revealed the importance of this signaling for proper development of medial DM and further differentiation of MPCs by the suppression of noggin or engrailed 1 (En1) (Ikeya and Takada, 1998).

After full formation of the DM within the dorsal proportion of the somite, the majority of primitive progenitor cells express the two paired box transcriptions factors Pax3 and Pax7 (Kassar-Duchossoy et al., 2005). The medial DM is also the major source of highly proliferative and unspecified MPCs, which later migrate to all precise target sites (Gros et al., 2005). One of the earliest genes that positively influence initial proliferation

are sine oculis-related homeobox (Six) 1 and Six4, as simultaneous genetic depletion leads to a significant reduction of DM size in mice (Grifone et al., 2005). Furthermore, temporal silencing of Six1a and Six1b in zebrafish with morpholinos showed a similar reduction of proliferation of $Pax7^+$ MPCs (Nord et al., 2013). Beside such essential transcription factors, extracellular proteins, like Fgf4 (fibroblast growth factor 4) or Wnt3a, that increase proliferation of MPCs in the DM, also hold an important role for the creation of MPCs by the upregulation of Pax3 and Pax7 (Galli et al., 2004; Kahane et al., 2001). Proliferation of $Pax3^+$ cells in the medial DM is tightly regulated by dorsal ectoderm-derived Bmp4, as its depletion leads to a premature cell-cycle exit and initiation of the myogenic cascade by the upregulation of the transcription factor MyoD1 (myogenic differentiation 1) (Amthor et al., 1999). Thus, it is obvious that the consistent proliferation of MPCs is essential to provide sufficient cells for later fusion and elongation of MPCs to multinucleated myofibers during each myogenic wave.

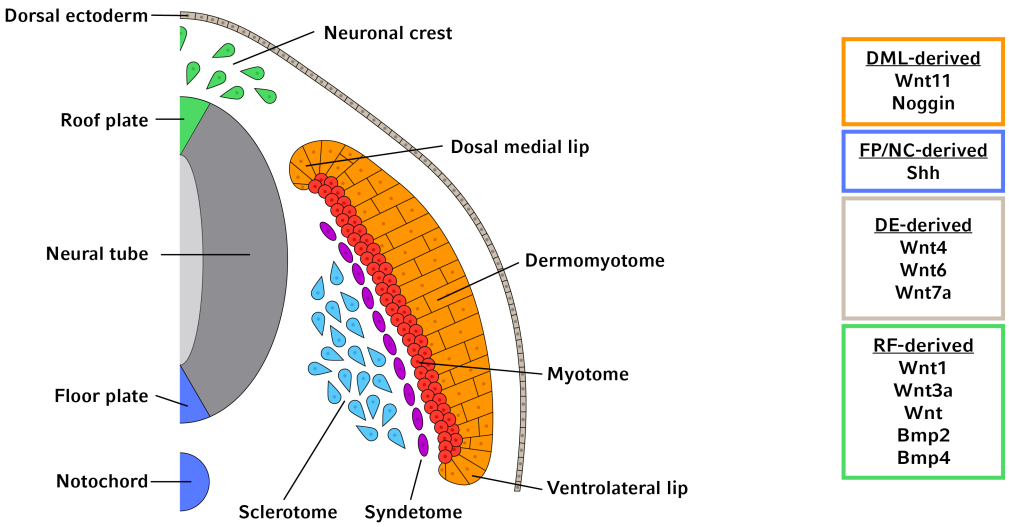

Figure 1.5: Development of the dermomyotome and its anatomy.

Specification of different somite compartments is tightly orchestrated by various molecules. While members of the Wnt or Bmp family are responsible for the dorsalization of the somites, Shh is involved in the formation of ventral structures by directly inducing differentiation and blocking of dorsal-derived Wnt signaling. Modified and adapted from (von Maltzahn et al., 2012).

Subsequent a highly proliferative phase, progenitor cells undergo an orchestrated genetic program of myogenic regulatory factors (MRFs) during the formation of the myotome out of the dorsolateral (DLL) and the ventrolateral lip (VLL) of the DM (Bentzinger et al., 2012). These MRFs consist of the basic helix loop helix (bHLH) transcription fac-

tors MyoD1, Myf5 (Myogenic factor 5), MyoG (Myogenin) and Mrf4 (Myogenic regulatory factor 4) that differentially influence various aspects of muscle differentiation (Pownall et al., 2002) and their transcriptional activity is tightly modulated by a complex formation with Tcf12 (transcription factor 12) during differentiation of MPCs (Hu et al., 1992; Londhe and Davie, 2011). One significant drawback of understanding muscle development in detail is the complex reciprocal regulation of MRFs. Remarkably, Shh, which initially represses Pax3 expression to favor upregulation of Pax1 in the PSM, mediates the expression of the Pax3 downstream targets MyoD1 and Myf5 during early differentiation of MPCs (Kahane et al., 2013). Following this initial activation of the MRF cascade, Myf5 activates, by binding directly to the bHLH promoter site, MyoG, which in turn initiates the expression of Mrf4 (Naidu et al., 1995; Yee and Rigby, 1993). Finally, MRFs upregulate (directly or indirectly) muscle specific sarcomeric proteins, like Acta1 (actin, alpha 1, skeletal muscle), Des (Desmin) or Myh1 (myosin, heavy polypeptide 1, skeletal muscle, adult) (Chen et al., 2010; Kassar-Duchossoy et al., 2004; Venuti et al., 1995). Even if MRFs can partially compensate each other, e.g. genetic deletion of MyoG in mice leads a severe loss, fusion deficit or misalignment of myofibers of the musculature, depending on the axial location of individual muscles (Nabeshima et al., 1993). Furthermore, posttranscriptional regulatory mechanisms that cause a cell-cycle exit are controlled by microRNAs (miRs) (Chen et al., 2010; Crist et al., 2009; Dey et al., 2011; Koutsoulidou et al., 2011). In example, miR-1, miR-206 and miR-486 can drive satellite cells or C2C12 cells towards a myogenic program *in vitro* by blocking Pax7 expression and therewith initiate differentiation (Chen et al., 2010; Dey et al., 2011).

Hence, the spatiotemporal up- or downregulation of genes that either influence cell proliferation or differentiation during development is crucial for the proper formation of muscles at their target locations.

1.2.2 Migration of muscle progenitor cells towards their target sites

In contrast to epaxial muscles of the back, MPCs of the lateral trunk, limbs and also the diaphragm have to migrate over long distances to reach their final position (Nabeshima et al., 1993). Silencing of MRFs during migration is crucial for the proper formation of individual muscles. It was shown that Msx1 (msh homeobox 1 or Hox7) is dominantly

suppressing Pax3 activity by direct competition during delamination and migration of MPCs into avian limb buds (Bendall et al., 1999). Pax3, together with Pax7, are the earliest genetic markers during muscle development and have distinct function during developmental progression of the musculature. While Pax3 is specifically expressed in cells of the DLL and VLL, Pax7 is present in the DM and myotome (Amthor et al., 1999; Kahane et al., 2013). Spontaneous mutations of Pax3 ($Pax3^{Sp}$) in mice leads to a disruption of MPC migration into the limb buds during development (Bober et al., 1994). Furthermore, genetic replacement of Pax3 by Pax7 mimics the loss-of-function of Pax3 and shows that Pax3 and Pax7 are functionally not redundant (Relaix et al., 2004).

This inhibition of cell migration is most likely provoked by the downregulation of the receptor c-Met (met proto-oncogene), as Pax3 can directly regulate c-Met expression (Epstein et al., 1996). C-Met deficient mice form normal $Pax3^{+}$ DMs at all spine levels, but MPCs fail to migrate into the developing limb buds (Bladt et al., 1995). Moreover, delamination from the VLL by c-Met-dependent signaling is also essential for the development of the thoracic diaphragm and some facial muscles, like the orbicularis oculi of the eye, or the longitudinalis linguae of the tongue (Bladt et al., 1995; Dietrich et al., 1999; Prunotto et al., 2004). The only currently known ligand of c-Met is SF/HGF (scatter facor/hepatocyte growth factor) (Organ and Tsao, 2011) and ectopic application of SF/HGF at interlimb levels of chicken embryos can induce delamination of $Pax3^{+}$ cells (Brand-Saberi et al., 1996). During normal development of limb buds, SF/HGF is probably upregulated by Fgf2, which is released by cells in the apical ectodermal ridge (AER) (Fallon et al., 1994), as ectopic release of Fgf2 mimics the results of SF/HGF beats at interlimb levels (Heymann et al., 1996). Furthermore, SF/HGF blocks the upregulation of MyoD1 in migrating MPCs, which keeps them in a consistent migratory state (Scaal et al., 1999). Interestingly, systemic overexpression of SF/HGF leads to ectopic muscle formation and deformation of the spinal cord that finally results in paralysis within the first weeks after birth (Takayama et al., 1996).

Another essential factor for MPCs migration towards distant targets is the conserved transcription factor Lbx1 (ladybird homeobox homolog 1) which is strongly expressed in MPCs of the VLL and during their migration towards their final targets (Jagla et al., 1998; Martin and Harland, 2006; Mennerich et al., 1998). Lbx1 expression is mainly initialized,

with an intermediate step of Pax3, by Six1 and Six4 (Grifone et al., 2005). Interestingly, contrary to c-Met or SF/HGF knock out mice, systemic or conditional (Myf5-Cre) deletion of Lbx1 is only affecting migration of dorsal forelimb and all hindlimb MPCs at limb levels as well as some myogenic precursor cells of the hypoglossal cord (Brohmann et al., 2000; Schäfer and Braun, 1999; Watanabe et al., 2011), while ventrally migrating MPCs, including the diaphragm and the tongue, are not affected (Gross et al., 2000). However, no definite mechanism is currently known that specifically directs MPCs of the diaphragm.

1.2.3 Fusion of myoblasts and formation of neuromuscular junctions

Cell-cell fusion is essential for a variety of different tissues. For example, haematopoietic stem cells within the bone-marrow fuse to hepatocytes that can support to regenerate liver tissue in fumarylacetoactate hydrolase (Fah) deficient mice (Vassilopoulos et al., 2003; Wang et al., 2003). Moreover, mononucleated bone-marrow-derived cells are able to fuse with embryonic stem cells (ESCs) *in vitro* and transplantation of these fused cells into the spleen of mice induced chondrocytes and striated muscle cell differentiation *in vitro* (Terada et al., 2002). Despite these regenerative events of cell-cell fusion, one of the most important mechanisms for all organisms with muscular locomotion is the fusion of myocytes to myofibers. This fusion cascade consists of cell-cell recognition, cell-cell adhesion, cellular alignment, and, finally, fusion of the lipid bilayers via pore formation and recycling of membrane vesicles in other cellular compartments (Rochlin et al., 2010). Each step during myocyte fusion is tightly regulated by different receptors and intracellular signaling mechanisms.

Currently, no specific mechanisms are known that direct the primary recognition of two myocytes prior myofiber fusion. The spatiotemporal arrangement of Drosophila founder cells (FCs) and fusion competent myoblasts (FCMs) may have an important role for the initiation of cell fusion in a two-phase model (Beckett and Baylies, 2007). Within the first stage, FCs and FCMs tightly condense without high fusion rates. During the second stage, FCMs separate from each other and start to fuse. Nevertheless, a possible candidate which regulates myocyte fusion might be the recognition/adhesion protein

Dumbfounded (Duf) due to its constricted regulation during fusion (Beckett and Baylies, 2007; Menon et al., 2005). An essential intermediate step before cell-cell adhesion relies on the expression of RhoE, as it provokes the elongation and alignment of C2C12 myogenic cells prior fusion by modulating M-cadherin, RhoA (ras homolog family member A) and RockI (Rho-associated coiled-coil containing protein kinase 1) expression (Fortier et al., 2008). Furthermore, the morphology of cardiomyocytes influences the prepatterning of the sarcomere before fusion (Bray et al., 2008). In addition, conditional deletion of the small GTPases Rac1 (RAS-related C3 botulinum substrate 1) and Cdc42 (cell division cycle 42) in migrating myoblast during development by Lbx1-Cre results in a profound reduction of myocyte fusion, which could be correlated to a downregulation of Vinculin, F-actin and Vasp (vasodilator-stimulated phosphoprotein) (Vasyutina et al., 2009). During the last step of myofiber development, cellular membranes are fused and it was shown that integrin β_1 has a major influence on myofiber maturation and therewith formation of the sarcomere (Schwander et al., 2003).

Shortly after terminated fusion of myofibers, they are innervated by MN axons and form highly specialized synaptic sites, namely neuromuscular junctions (NMJs), at the midline of myofibers, which condensate acetylcholine receptors (AChRs) in small areas (Burden, 1998). The diffuse prepatterning of AChRs at the midline of myofibers is independent of innervating MN axons and heavily relies on Musk, a muscle/skeletal receptor tyrosine kinase (DeChiara et al., 1996; Yang et al., 2001). One of the main activators of Musk and therewith tightening of the NMJ band is Agrin, a heparin sulfate proteoglycan, which is secreted by MNs amongst others (Glass et al., 1996). Agrin binds to the low density lipoprotein receptor-related protein 4 (Lrp4), which subsequently forms a receptor complex with Musk (Zhang et al., 2008). Furthermore, continuous stabilization of Musk is maintained by the muscle intrinsic activator Dok7 (docking protein 7) during postnatal development, even in the absence of Agrin or Lrp4 (Tezuka et al., 2014). In addition to cell autonomous regulation of NMJ development and maintenance, Neuregulin, released by motor endplates, and its receptor ErbB2 (erb-b2 receptor tyrosine kinase 2), expressed at NMJs, contribute to the efficiency of signal transduction via positively regulating AChRs expression (Leu et al., 2003). Furthermore, systemic deletion of the transcription factor OC1 (one cut domain, family member 1) results in downregulation of Agrin in hindlimb musculature, which leads to a severe reduction of locomotion of the

lower extremities due to a loss of sufficient NMJ formation and maturation (Audouard et al., 2012).

1.2.4 Tendon development and formation of myotendinous junctions

The function of the musculoskeletal system relies on the proper connection of muscles and bones to transmit force during muscle contraction. This linkage is provided by tendons that arise from Scleraxis^{+} (Scx) cells between the dermomyotome and the sclerotome (Schweitzer et al., 2001). Scx, a bHLH transcription factor, is a specific marker for tendons and ligaments (Schweitzer et al., 2001) and its genetic deletion leads to the loss of condensation and differentiation of tendon progenitor cells (TPCs) (Murchison et al., 2007). Scx is expressed, in the central tendon region (CTR) of the thoracic diaphragm, together with another tendon-related glycoprotein, namely Tenomodulin (Tnmd) (Brandau et al., 2001; Cserjesi et al., 1995). Despite the common origin of skeletal TPCs, which arise from the syndetome (Brent et al., 2003; Dubrulle and Pourquie, 2003), it was thought for a long time that progenitor cells of the CTR are differentiated cells of the septum transversum (Babiuk et al., 2003; Greer et al., 2000). Nevertheless, a recent detailed study has clarified that the bilateral PPFs give rise to the CTR and connective tissue fibroblasts of the costal muscle proportion (Merrell et al., 2015), while the septum transversum might have an important role during hepatogenesis by release of BMPs and direct contribution of hepatic stellate and perivascular cells (Asahina et al., 2011; Rossi et al., 2001).

The recognition of muscle attachment sides (MAS) during migration of MPCs is provided by several attractive ligand-receptor systems. In Drosophila, Robo expressing MPCs are initially repelled by Slit at the midline and later attracted the final MAS by the same Slit ligand, which is released by TCPs (Kramer, 2001). In addition, cleavage of Slit after the fifth EGF (epidermal growth factor) domain was shown to be essential for repulsive signaling, which leads towards myofiber alignment (Ordan et al., 2015). Furthermore, the transmembrane protein Kon-tiki (Kon) is enriched at myotube tips of Drosophila during tendon cell targeting and influences motility and later stabilization of MAS cell-autonomously (Schnorrer et al., 2007). After initial formation of myotendinous

junctions (MTJ), TPCs and MPCs start to produce unoriented ECM (extracellular matrix) proteins, like collagens, laminins, or the RNA helicase P68 (Tidball, 1994), which are reorganized to aligned ECM fibers during neonatal maturation (Trotter, 2002). Moreover, it could be shown that integrin α_7 has an important role in formation and maturation of MTJs without influencing muscle or tendon development (Mayer et al., 1997). These data could be emphasized by the upregulation of integrin α_7 during exercise and a reduction of micro-injuries in MTJs (Boppart et al., 2008).

Thus, the close relation between MPCs and TPCs at the intermediate layer of muscles and tendons is crucial for proper development, maturation and maintenance of MTJs.

1.2.5 Development, innervation and defects of the thoracic diaphragm

The mature thoracic diaphragm is formed by three distinct major anatomical structures: 1) the crural muscle (CrM) that surrounds the esophagus and the aorta, 2) the costal musculature (CoM) that is provides the major contraction for mammalian breathing and 3) the CTR that acts as a mechanical connection of contralateral muscles (Merrell and Kardon, 2013). After population of the PPFs with myoblasts and targeting by phrenic nerve axons at E11.5 in mice (Figure 1.6 A), muscle related fibroblasts start to migrate dorsally and ventrally in advance of following MPCs that slowly begin to form first myofibers at E12.5 (Figure 1.6 B) (Merrell and Kardon, 2013). Interestingly, these muscle connective tissue fibroblasts do not reside at the site where the crural musculature develops, which might indicate a different origin of MPCs that form costal and crural muscle proportions (Merrell et al., 2015). During the fast progression of CrM and CoM formation, PN axons start to shape initial secondary branches and innervate the first NMJs at E13.5 (Figure 1.6 C). The first myogenic wave and therewith anatomical completion of the diaphragm is finished by E16.5, when myofibers and PN axons reached the ventrally located sternum (Figure 1.6 D). Until birth and during postnatal maturation, both muscle compartments are undergoing massive hypertrophy of myofibers by fusion with following MPCs of the secondary myogenic wave (Figure 1.6 E) (Allan and Greer, 1997, 1998). While the capillary network of the diaphragm muscles is provided by ventrally

projecting phrenic arteries from the dorsal aorta and lateral invading intercostal arteries from the ribs, the venous system is located at the border between the CTR and both muscles (Stuelsatz et al., 2012).

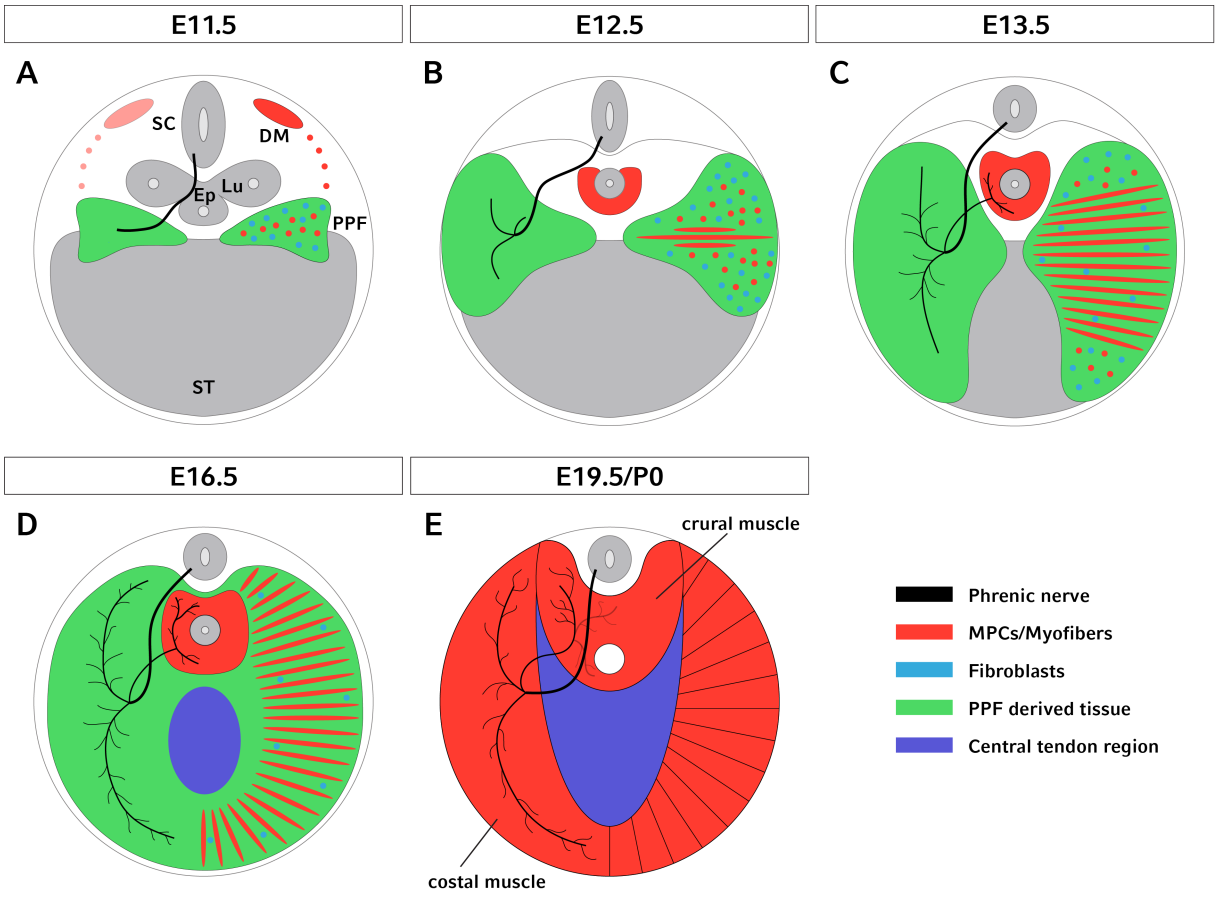

Figure 1.6: Diaphragm development and innervation by the phrenic nerve.

The bilateral PPFs, consisting of fibroblasts and MPCs, mark the initial primordial diaphragm and the PPFs are reached by the PN around E11.5 in mice (A). During dorsal and ventral migration of fibroblasts and MPCs, PNs start to innervate first myofibers and the middle of the PPFs at E12.5 (B) and continues with the formation of first NMJs around E13.5 (C). This dorsal/ventral extension and fusion continues, together with the full innervation by the PNs, until E16.5 (D). Until birth and in the following postnatal phase, myofibers undergo a strong hypertrophy by fusing with myocytes of the secondary myogenic wave (E). Note that the bilateral development of the diaphragm is simultaneous and innervation by the PN and the migration/fusion of MPCs is separated for a better illustration. SC: spinal cord, DM: dermomyotome, Lu: lung, Ep: esophagus, PPF: pleuroperitoneal fold, ST: septum transversum, MPCs: muscle progenitor cells. Modified and adapted from (Merrell et al., 2015).

Developmental defects of the diaphragm can have lethal consequences directly after birth due to the inability to breathe. Besides the main function of the diaphragm as a contractile muscle for breathing, it also separates the thoracic and the abdominal cavi-

ties (Merrell et al., 2015). Thus, genetic defects that circumvent the formation of muscles, such as mutations of Pax3, Lbx1, c-Met or SF/HGF causes severe impairments of this barrier (Bober et al., 1994; Brand-Saberi et al., 1996; Dietrich et al., 1999; Martin and Harland, 2006). Developmental abnormalities that are caused by such defects are named congenital diaphragmatic hernias (CDHs) which account for approximately 1-2 % of neonatal cause of death (Pober et al., 2005; Yang et al., 2006). The proportion of CDHs in neonatal deceases is increasing, even when the overall morality after birth is decreasing due to a better clinical monitoring (Brownlee et al., 2009).

Modern high-throughput sequencing techniques have uncovered a plentitude of human CDH associated genetic defects, like the Beckwith-Wiedemann and the Pallister-Killian syndrome or chromosomal aneuploidies like Trisomy 9 and 21 (Holder et al., 2007). Furthermore, several knockout mouse models could reveal single genes that lead to diaphragm malformations. In example, Zfpm2 (zinc finger protein, FOG family member 2) is responsible for primary lung development and diaphragm formation, possibly by modulating SF/HGF expression (Ackerman et al., 2005). Additionally, Gata4 (GATA binding protein 4) acts as a transcriptional co-regulator of Fog2 and heterozygous animals for Gata4 showed fusion of the CTR with the liver (Jay et al., 2007). Likewise, mice that lack the Robo ligand Slit3 show ruptures of CTR, which are caused by a thinning of the tendon, while muscle development and innervation seems normal (Liu et al., 2003; Yuan et al., 2003). Similar results have been reported for endothelial expressed Ndst1 (N-deacetylase/N-sulfotransferase (heparan glucosaminyl) 1) that can stabilize Slit-Robo signaling by modifying heparan sulfates (Zhang et al., 2014). Another important transcription factor for normal diaphragm muscle development is Pbx1 (pre-B-cell leukemia homeobox 1), as systemic deletion leads to fusion of the heart to anterior diaphragm structures and a severe disorganized muscle development (Russell et al., 2012).

Thus, even if some genes that are involved in CDHs formation during development have been uncovered in the last couple of years, further studies need to complete the entire genetic background of diaphragm development in respect to MPC migration, proliferation and fusion.

1.3 Establishment of peripheral motor and sensory circuitry

Newly formed neurons in the brain or spinal cord have to build highly interconnected neuronal circuitries to provide the background for everyday conscious motions or vegetative functions. Appropriate connection of interneurons and innervation of target muscles by MNs are crucial prerequisites. Distant axonal target innervation is tightly regulated in a stepwise progression by various mechanisms in a spatiotemporal manner.

1.3.1 Axon guidance mechanisms during target innervation

In contrast to interneurons, somatic MNs and sensory neurons have to project over long distances to reach their final targets. Guidance of outgrowing axons from the spinal cord is orchestrated by receptors in the leading edge of axons, the so called growth cone (GC) which react to membrane-bound or secreted molecules in an attractive or repulsive manner (Figure 7A) (Huber et al., 2003). Many guidance cues, e.g. the ligand receptor complex Slit-Robo, act bifunctional and depend on receptor complex formation, intracellular signaling or the current sensitivity of the GC. Such modifiers are varying ratios of cyclic adenosine monophosphate (cAMP) and cyclic guanosine monophosphate (cGMP) which act as second messenger molecules during intracellular downstream signal transduction and is in part depending on appropriate calcium homeostasis (Ming et al., 1997; Movshon et al., 2003; Song et al., 1997). Besides the gradual uncovering of complex intracellular downstream signaling pathways, research for new candidate molecules in the last 30 years discovered a plentitude of new membrane-bound or secreted axon guidance cues.

Such contact-mediated signaling enables proper axon bundling (fasciculation) to specify premature nerves branches before guidance decision points. These cell-cell interactions rely on membrane-bound molecules like the cellular adhesion molecules (CAMs), cadherins, receptor tyrosine kinases (RTKs) or receptor tyrosine phosphatases (RPTPs) (Van Vactor, 1998). Members of the CAM family, amongst others, are NCAM, L1-CAM (or L1), F11, members of integrin family or neurofascin (Nfasc) (Rutishauser, 1992). Interestingly, it was shown that a dynamic equilibrium of NCAM and L1 is es-

sential for intramuscular branching and innervation. While L1 mediates axon-axon fasciculation, NCAM favors defasciculation of axons within the muscle (Landmesser et al., 1988). Furthermore, axonal differentially expressed polysialic acid (PSA), which is an effective modulator of axon-axon and axon-matrix interaction, promotes axon sorting in the plexus region (Tang et al., 1992, 1994).

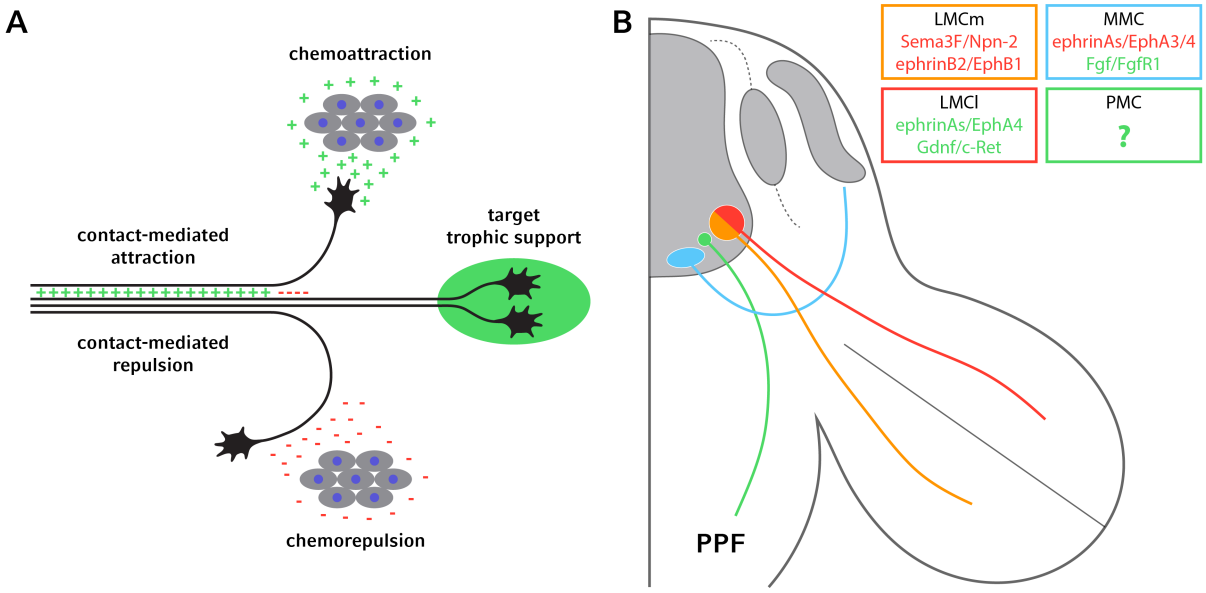

Figure 1.7: Axon guidance mechanism during development.

Axons of sensory and motor neurons have to navigate over long distances towards their final targets. Furthermore, axons have to tie up at specific guidance decision points. The mechanisms that drive these events might be either contact-mediated repulsion or attraction between neighboring axons, cells or ECM molecules or long-/short-range attractive/repulsive cues. Furthermore, axonal GCs sense trophic factors at their final target site (A). While several attractive (green) and repulsive (red) ligand-receptor-depended axon guidance mechanism of LMC and MMC are uncovered, no PN specific guidance mechanism towards the PPF is currently known (B, text boxes). Modified and adapted from (Bonanomi and Pfaff, 2010; Huber et al., 2003).

Other important proteins of contact-mediated signaling during axon targeting are members of the integrin family. Integrins are heterodimeric transmembrane proteins which consist of α and β subunits in an opulence of different variations (Docheva et al., 2014). They transmit extracellular signals to the actin cytoskeleton to activate different downstream mechanisms including protein tyrosine kinase 2 (Ptk2), mitogen-activated protein kinase 1 (Mapk1), or small guanosine triphosphateases (GTPases) like CDC42, Rac1 or RhoA (Legate et al., 2009). It is conspicuous that integrin-mediated downstream signaling is a major aspect of growth cone response to ECM components (Huber

et al., 2003). For example, integrin β_1 is strongly expressed in axons and soma of MNs and sensory neurons in the dorsal root ganglia (DRG) during target innervations. Conditional deletion of integrin β_1 in a Nestin-Cre background reduced neurite outgrowth *in vitro* and occasionally revealed misprojecting axons in the thoracic diaphragm (Schwander et al., 2004). Additionally, Caenorhabditis elegance Ina-1 (Integrin alpha ina-1), a close relative to the mammalian integrin α_1, promotes axon fasciculation and growth cone migration (Baum and Garriga, 1997). In contrast, semaphorin 7A (Sema7a) promotes axon outgrowth of murine cortical, olfactory and DRG neurons *in vitro*, which relies on the RGD-binding of Sema7a to integrin β_1 (Pasterkamp et al., 2003).

1.3.2 Secreted guidance cues that govern axon pathfinding, fasciculation and neuronal development

Additionally to short range guidance cues, which mainly act for axon bundling and growth cone condensation at specific decision points, secreted proteins play a fundamental role during axon guidance over long distances during development. Furthermore, interference of different ligands or receptors can silence or modify normal canonical pathways by complex formation. For example, Netrin-mediated attraction of growth cones towards the midline of the spinal cord is recognized by the receptor deleted in colorectal carcinoma (DCC). After crossing the midline of the spinal cord, cytoplasmic binding of the Slit receptor Robo to DCC is silencing the attractive effect of Netrin-DCC while canonical repulsion by Slit-Robo is maintained (Stein and Tessier-Lavigne, 2001). Up to now, numerous ligand-receptor complexes were uncovered within the last decades, which differently influence various neurons of the central and peripheral nervous system.

1.3.2.1 Class 3 Semaphorins – Neuropilins

Semaphorins form a large family of highly conserved signaling molecules and currently include eight classes with 27 members in total that share a common 500 amino acid long extracellular semaphorin (Sema) and domain and a plexin, semaphorin, and integrin (PSI) domain (Figure 1.8 A) (Goodman et al., 1999; Kozlov et al., 2004). While class 1 and 2 semaphorins and the family member Sema5c are only expressed in invertebrates, semaphorins 3 to 7 are expressed in vertebrates (Neufeld and Kessler, 2008).

Additionally, viral class V semaphorins are closely related to Sema7a and are encoded by pox- or herpesviruses (Myster et al., 2015).

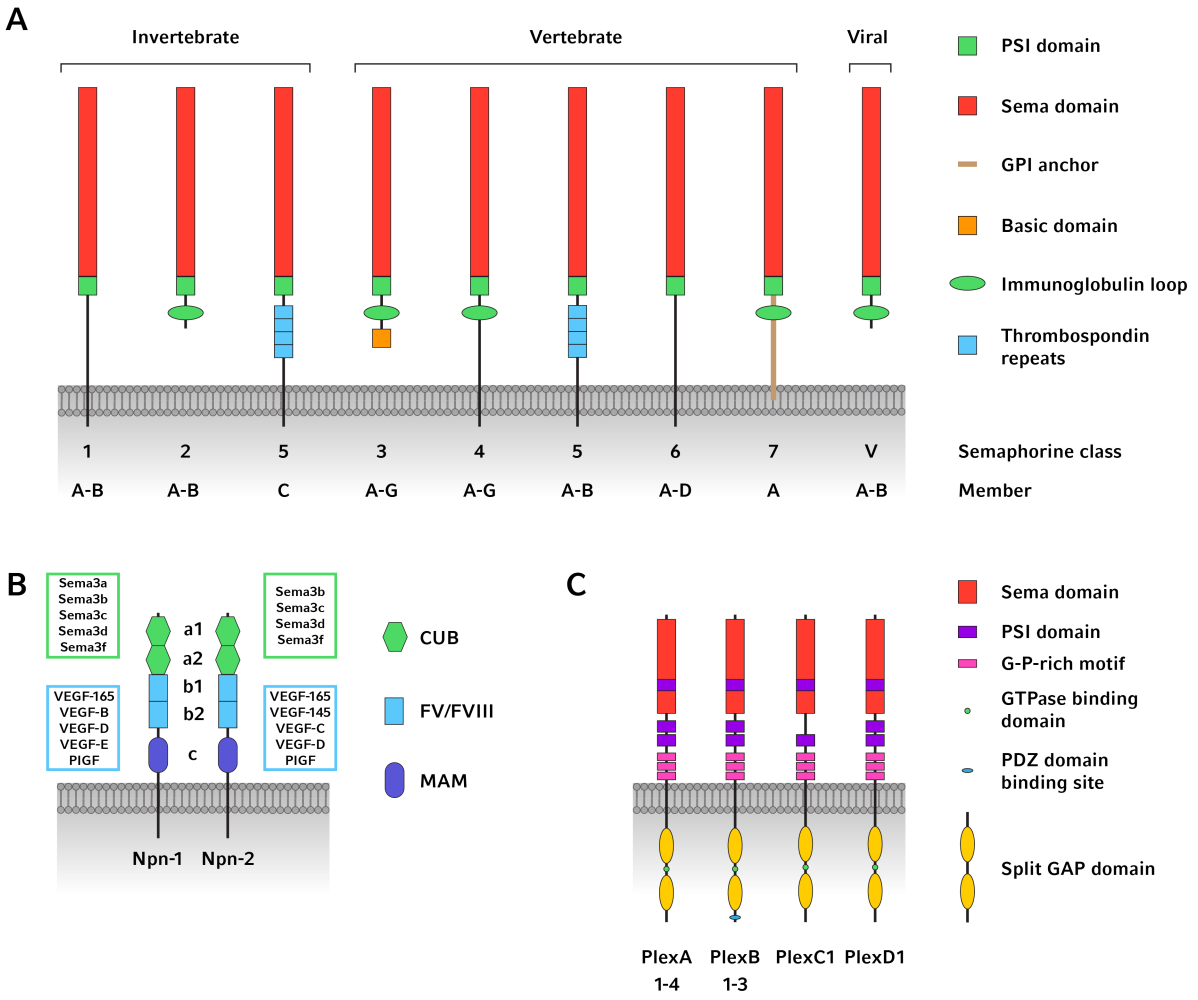

Figure 1.8: Semaphorin classes and their corresponding Neuropilin and Plexin receptors.

Semaphorins build a large family of secreted or membrane-bound proteins (A). All Semaphorins have a large phylogenetically conserved extracellular Sema and PSI domain. Additionally, different classes have thrombospondin repeats, basic domains or immunoglobulin loops. Furthermore, viral Semaphorins can mimic the GPI-anchored (Glycosylphosphatidylinositol) Sema7a. Neuropilin 1 and 2 are the main binding receptors for class 3 Semaphorins (B). They consist of two (a1 & a2) CUB domains (complement C1r/C1s, Uegf, Bmp1), two (b1 & b2) FV/FVII (coagulation factor V/VIII homology) domains and a single (c) MAM (meprin A5) domain. While the CUB domains are responsible for binding of Semaphorins, the FV/FVIII domains mediate VEGF binding. Due to the lack of an intracellular domain of Neuropilins, signaling is transmitted via complex formation between Plexin As and Neuropilins, even though some Semaphorins can directly bind to Plexins (C). Downstream signaling of activated Neuropilin-Plexin A mainly consists of small GTPases. Modified and adapted from (Grandclement and Borg, 2011; Neufeld and Kessler, 2008).

A central component of development is constituted by class 3 semaphorins A-G (Sema3s) as genetic deletion of individual Sema3s members have distinct biological functions in angiogenesis, immune system, neurogenesis or skeletogenesis (Fukuda et al., 2013; Hayashi et al., 2012; Kumanogoh and Kikutani, 2003; Neufeld et al., 2012; O'Malley et al., 2014). Intracellular downstream signaling via Sema3s is transmitted by a receptor complex composed of one of the two Neuropilins, Npn-1 and Npn-2, (Figure 1.8 B) as well as members of the Plexin A (1-4) family (Figure 1.8 C). While Neuropilins are the main binding receptors for class 3 Semaphorins, signal transduction to activate downstream mechanisms is mediated by Plexin As, as neuropilins lack a cytoplasmic C-terminal domain (He and Tessier-Lavigne, 1997; Kolodkin et al., 1997; Yu and Kolodkin, 1999). Furthermore, plexins trigger the same small GTPases as integrins in Drosophila, which underlines their indispensability for growth cone actin dynamics (Whitford and Ghosh, 2001). In addition to binding of Sema3s, Npn-1 also contains binding sides for vascular endothelial growth factor isoform 165 ($VEGF_{165}$), or transforming growth factor-beta 1 (Tgfb1) in T-cells (Glinka and Prud'homme, 2008; Soker et al., 1998, 2002) which make Npn-1, amongst other signaling pathways, indispensable for development of the cardiovascular system in mice (Kawasaki et al., 1999).

Sema3-Npn-1 signaling has a profound impact on countless biological aspects, like development, maturation or regeneration of the nervous system. An important class 3 semaphorin is Sema3a which initially showed to cause collapse of neuronal DRG growth cones and was therefore referred as Collapsin more than 20 years ago (Luo et al., 1993). Furthermore, functional *in vitro* assays revealed that expression of class 3 Semaphorins within the ventral part of the spinal cord prohibits nociceptive sensory axons from dorsal ingrowth, while proprioceptive can pass this repulsive border to form synapses with MNs (Messersmith et al., 1995). This repulsive guidance is true for various other axons of the central and peripheral nervous system, such as olfactory, cranial sensory or hippocampal neurons (Chédotal et al., 1998; Kobayashi et al., 1997). While the majority of growth cones are repelled by Sema3a, cortical apical dendrites are attracted by the ligand towards the marginal zone in murine brain slices (Polleux et al., 2000). Alongside this relatively short range guidance of axons and dendrites in the central nervous system, it has been also shown that Sema3a-Npn-1 signaling is crucial for the pause of axonal growth of motor and sensory axons at the brachial plexus of the

limb and thus MN axons prematurely enter the developing limb bud (Huber et al., 2005). Furthermore, conditional ablation of Npn-1 from motor or sensory neurons revealed that after loss of Npn-1 on sensory neurons, both motor and sensory neurons loss their tight fasciculation. In contrast, motor neuron-specific deletion of Npn-1 only affected somatic MNs and thus acts cell autonomously (Huettl et al., 2011). Such developmental defects are still observable during adulthood and disclose loss of muscles and bone density, possibly due to the reduction of MNs (Helmbrecht et al., 2015).

1.3.2.2 Slit – Robo

The Robo receptors (Robo1 & Robo2) and their main ligands Slit (Slit1 and Slit2) have been intensively studied in regards to axon pathfinding during midline crossing within the spinal cord (Figure 1.9) (Ypsilanti et al., 2010). Since the first discovery of the repulsive effect of Slit on commissural Robo^{+} neurons of the Drosophila spinal cord that enable a bilateral coordination of locomotion (Kidd et al., 1999; Talpalar et al., 2013), an immense progress has been made in validating Slit-Robo-mediated cellular guidance mechanisms in other neuronal compartments and organisms (Brose et al., 1999). For example, sensory axons of nodose ganglia neurons are repelled by Slit2 (Goldberg et al., 2013). Furthermore, Slit2-Robo2 signaling in cerebellar Purkinje cells is responsible for cell-autonomous circumvention of dendrite crossing during postnatal formation of neuronal circuits (Gibson et al., 2014).

Downstream signaling of Slit-Robo also involves small GTPases like Cdc42, RhoA or Rac1 (Ypsilanti et al., 2010). An important regulator of such GTPases is the Rho GTPase activating protein 39 (Arhgap39 or Vilse) that promotes hydrolysis of Rac1 and Cdc42 after intracellular binding to Robo (Lundström et al., 2004). Furthermore, Canoe (Cno), a Drosophila scaffold protein, stabilizes Robo receptors on filopodia *in vitro* by directly transmitting Slit-Robo signaling to the actin cytoskeleton (Slovakova et al., 2012). Systemic deletion of Afadin (the mammalian homologue of Cno), leads to a severe misdevelopment of the central nervous system, which might implicate a similar mechanism in mammalians when compared to Drosophila (Zhadanov et al., 1999).

Despite the participation of Slit-Robo signaling in axon pathfinding, the association

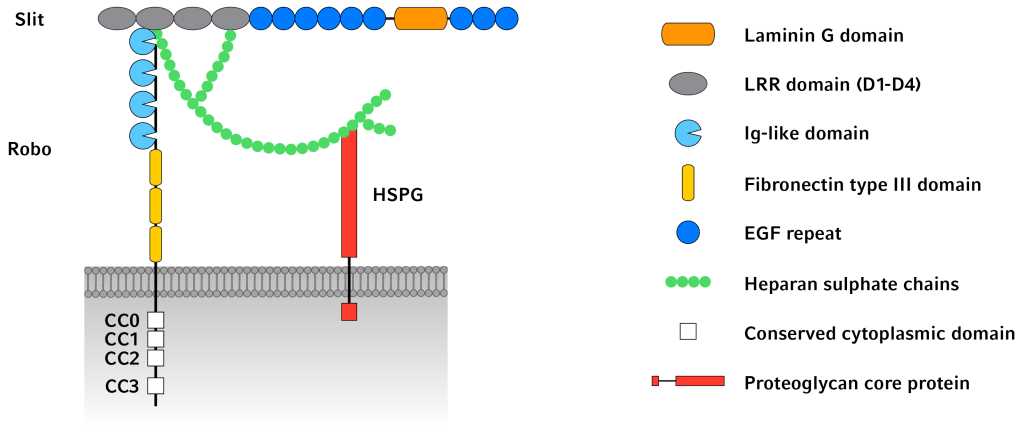

Figure 1.9: Slit-Robo complex and stabilization by proteoglycans.

The Slit-Robo family currently consists of three Slit proteins (Slit1-3) and four Robo receptors (Robo1-4) in mammalians. Slit binds, as monomer or homodimer, with the second LRR (leucine-rich repeats) to the Ig-like domain of the Robo receptor. Various intracellular mechanism (like small GTPases, Afadin or Dock) modify, often in combination with other receptors, cytoskeletal dynamics and therewith attraction or repulsion. Heparan sulphate proteoglycans (HSPGs) like Syndecan (Sdc) act as co-receptors, by forming a ternary stabilizing complex heparin sulphate chains. Modified and adapted from (Fujiwara et al., 2006; Ypsilanti et al., 2010).

of Robo1 and Robo4 during angiogenesis and heart development becomes more and more important (Fujiwara et al., 2006; Mommersteeg et al., 2015). In addition, diseases like ocular neovascularization which is caused by viruses, contact lenses or degenerative disorders, have a high socio economical impact on the health system (Lee et al., 1998). Recent findings revealed the participation of Slit2 and Robo1/Robo2 in vascularization of the retina by an increase of endothelial cell migration (Rama et al., 2015). Furthermore, Slit and/or Robo might be promising candidates to treat various types of cancer as both protein classes are downregulated in prostate, brain, kidney or lung cancer (Gara et al., 2015). Interestingly, due to the close correlation of Slit-Robo signaling and cytoskeletal dynamics, it might also be involved in metastatic progression of these types of cancers (Morlot et al., 2007). Moreover, combined knock-down of Npn-1 and Slit2 in chicken neuronal tube causes ectopic migration of MNs (Kim et al., 2015; Lee et al., 2015). These facts show that Slit-Robo signaling has profound effects on a plentitude of developmental and regenerative mechanisms.

1.3.2.3 Ephrins – Eph receptors

After the discovery of the ephrin-Eph signaling pathway more than 25 years ago (Hirai et al., 1987; Holzman et al., 1990), several more ephrin ligands and Eph receptor family members could be verified. Ephrin ligands are separated in two subclasses, namely ephrin As (ephrinA1-A5) and ephrin Bs (ephrinB1-3), which bind specifically to their corresponding classes of Eph receptors (Palmer and Klein, 2003). One current expectation is EphA4 that can bind both ephrin subtypes (Kullander and Klein, 2002). The Eph receptor family currently consists of a nine class A Eph (EphA1-8 and EphA10) and five class B Eph (EphB1-4 and EphB6) receptors in humans (Pitulescu and Adams, 2010). Ephrin-Eph signaling is a key mechanism for a variety of developmental processes in different tissues, like respiratory and cardiovascular system as well as bones (Gerety et al., 1999; Matsuo and Otaki, 2012; Peixoto et al., 2015). Interestingly, the majority of ephrins or Eph receptors are involved in several malignant degeneration of tissues (Pasquale, 2010).

Furthermore, ephrin-Eph signaling pathways have distinct roles during development of the central nervous system and plasticity during adulthood (Flanagan and Vanderhaeghen, 1998; Klein, 2004; Lai and Ip, 2009; O'Leary and Wilkinson, 1999). In this regard, the ephrin-Eph signaling pathway, e.g., was shown to be crucially involved in guidance decisions of motor axons originating in the medial (LMCm) or lateral (LMCl) aspects of the LMC to faithfully target ventral (ephrinB-EphB1) and dorsal (ephrinA-EphA4) limb musculature, respectively (Helmbacher et al., 2000; Wang and Anderson, 1997). These guidance mechanisms towards specific muscles are further fine-tuned by a tight spatiotemporal regulation of ephrin A expression (Feng et al., 2000). Additionally, ephrinA5 repels retinal axons of the lateral geniculate nucleus from inferior colliculus region (Frisén et al., 1998). Migration of neurons or neuronal crest cells (NCCs) and therewith the final position of are essential for later physiological function. For instance, *in vivo* blockage of ephrinB1 by soluble Fc-fusion proteins leads to inappropriate migration of NCCs in the dorsolateral pathway (Santiago and Erickson, 2002). Similar blocking experiments, with ephrinB2 or EphB2 as targets, disturb migration of neuroblasts within the subventricular zone (SVZ) that is accompanied by an increased cell proliferation (Conover et al., 2000). Furthermore, the secreted glycoprotein Reln (Reelin) binds

to the extracellular domain of ephrin Bs and modifies downstream signaling in neurons of the cerebral cortex that leads finally to a loss of cortical layer formation (Sentürk et al., 2011).

1.3.2.4 SF/HGF – cMET

Apart from the utilization of SF/HGF-cMet signaling in myoblast migration to the PPFs and limb buds (see section 1.2.2), it has also roles in axon guidance, neuronal survival and neurotrophic support (Birchmeier and Gherardi, 1998). Cranial MNs of the hindbrain i.e. are attracted by co-cultures with trigeminal ganglia or branchial arches *in vitro*, and blocking with antibodies against SF/HGF diminished the attractive effect (Caton et al., 2000). Furthermore, similar experiments with spinal cord explants expanded the attractive effect of SF/HGF releasing limb buds and sclerotome explants to somatic MNs (Ebens et al., 1996; Maina et al., 1997). Remarkably, SF/HGF-cMet signaling in combination with NGF (nerve growth factor (beta polypeptide)) also enhances the survival of somatic MNs as well as sensory neurons (Ebens et al., 1996; Maina et al., 1997). This neurotrophic support could also be shown for neurons of the neocortex or hippocampus that are correlated to diseases like Alzheimer's or Parkinson (Hamasaki et al., 2014; Koike et al., 2006).

Chapter 2

Aim of the study

Functional muscle innervation by somatic MNs is pivotal for the survival of all organisms that rely on muscle-dependent locomotion. One of the main muscular anatomical structures in mammalians is the thoracic diaphragm that provides the mechanical source for respiration. Proper bilaterally targeted innervation of the diaphragm by cervical arising phrenic MNs (pMNs), together with muscle development, is therefore crucial to facilitate myofiber contraction. Exploring the underlying mechanisms of PN axon pathfinding and diaphragm muscle development might be profitable to various postnatal acquired or developmental defects for future treatment of paraplegia or muscle-nerve related diseases like amyotrophic lateral sclerosis (ALS) or progressive muscular atrophy (PMA), which also result in impairment of breathing due to the loss of motor innervation and subsequent degeneration of the thoracic diaphragm.

Thus, we aimed to uncover novel mechanisms that are involved in axonal targeting of the diaphragm by pMNs and their subsequent innervation of myofibers. Furthermore, we revealed new insight how MN growth cones and migrating myoblasts are influencing each other. Therefore, we employed two different genetic mouse models to address this question.

2.1 Determination of the effects of class 3 semaphorin-Npn-1 signaling ablation on phrenic nerve targeting, fasciculation and innervation of the diaphragm

Class 3 Semaphorin-Neuropilin-1 signaling was shown be crucial for axon guidance and fasciculation. While systemic disruption of Sema3-Npn-1 signaling (*Npn-1^{Sema-}*) leads to a premature ingrowth of motor and sensory axons into the developing limb bud (Huber et al., 2005), motor neuron specific ablation of Npn-1 (*Npn-1^{cond};Olig2-Cre*) induces defasciculation of motor axons but not sensory axons (Huettl et al., 2011). Interestingly, approximately 40 % of *Npn-1^{Sema-}* and 30 % of *Npn-1^{cond};Olig2-Cre* newborn mutant animals die neonatally (Gu et al., 2003; Söllner, 2012), due to respiratory failure as deceased neonates appeared cyanotic. As intercostal motor axons are also defasciculated in both mouse models, it is possible that Npn-1 is likewise affecting the main respiratory nerve, namely the cervical arising PNs.

Therefore, we investigated the influence of Sema3-Npn-1 signaling on initial PN targeting and subsequent innervation of the thoracic diaphragm by whole-mount staining of embryos or dissected diaphragms, respectively. Furthermore, we quantified axonal innervation by a Sholl analysis and, remarkably, some axons innervated ectopic muscles in the CTR and we aimed therefore to uncover the underlying effect of EM formation.

2.2 Unveil new mechanisms that influence the interaction between motor neuron growth cones and muscle progenitor cells

Formation of ectopic muscles (EMs) has been reported for various genetic modified mouse lines. For example, MT-I driven overexpression of SF/HGF in mice leads to EM development around the spinal cord (Takayama et al., 1996). Furthermore, muscle-specific stabilization of β-catenin also leads to innervated EMs within the CTR of the diaphragm (Liu et al., 2012; Wu et al., 2012). The authors concluded that newly formed EMs attract axons and therewith ensure their innervation. Nevertheless, as systemic

or motor neuron specific deletion of the Sema3-Npn-1 signaling pathway also leads to striated muscle formation in the CTR of the diaphragm and misprojecting axons are visible before EMs are shaped, muscle intrinsic Npn-1 depended signaling is unlikely the underlying cause for EM creation.

Thus, we investigated new ligand-receptor signaling mechanism that affects the growth cone and myoblast interaction. Therefore, we employed functional *in vitro* experiments with primary MPCs from the CoM of the diaphragm and tried to validate newly obtained data *in vivo*.

Chapter 3

Material & Methods

3.1 Animal husbandry

3.1.1 Ethics statement

Animals were handled and housed according to the federal and institutional guidelines for the care and use of laboratory animals, approved by the Helmholtz Zentrum München Institutional Animal Care and Use Committee, and the government of Upper Bavaria.

3.1.2 Animal housing

Mice were housed under standard animal laboratory conditions with controlled temperature with a 12 h light/dark cycle and fed ad libitum in individually ventilated cages (IVC, Biozone Global, UK) with an effective area of 530 cm^2. A maximum of 5 female mice per cage for maintenance or 3 mice (2 female/1 male) for breeding were accommodated. Male mice were always housed alone if not used for breeding.

3.1.3 Mouse lines

Following mouse lines were used: *Npn-1*$^{Sema-}$ and *Npn-1*^{cond} (Gu et al., 2003), *Olig2-Cre* (Dessaud et al., 2007), *Robo1* (Long et al., 2004), *Robo2* (Lu et al., 2007), and *Hb9::eGFP* (Wichterle et al., 2002). *Npn-1*$^{cond-/-}$*;Olig2-Cre*$^{+}$ mutant embryos were compared to littermate controls (*Npn-1*$^{cond-/-}$*;Olig2-Cre*$^{-}$) in all experiments with motor neuron specific

ablation of *Npn-1*.

3.1.4 Genotyping

Genomic DNA (gDNA) was isolated from short tail tip tissue by digestion with 100 µl of 50 mM NaOH at 95 °C for 30 min. Alkaline reaction was neutralized with 30 µl of 1 M Tris-HCl (pH 7.0) to stabilize gDNA, which was used directly for PCR after short centrifugation to spin down non-digested tissue.

Table 3.1: Instruments & chemicals for gDNA isolation.

Instruments	
Centrifuge 5417R	Eppendorf, Germany
Thermomixer 5436	Eppendorf, Germany
Chemicals	
Hydrochloric acid (HCl)	Sigma-Aldrich, USA
Sodium hydroxid (NaOH)	Merck, Germany
Tris(hydroxymethyl)aminomethane (Tris)	Carl Roth, Germany

PCR reaction was carried out with mouse line specific primer pairs at amplification parameters: preheating at 95 °C for 5 min, 35 cycles of denaturation (95 °C for 30 sec), annealing (primer specific temperature for 60 sec), elongation (72 °C for 30 sec), and a final extension step at 72 °C for 10 min. Finally, amplicon size was visualized by gel electrophoresis on a 2 % agarose gel in 1x TAE buffer with 0.05 µl/ml ethidium bromide on a UV gel imager.

Table 3.2: Instruments & chemicals for genotyping of mouse lines.

Instruments	
Labcycler Gradient	SensoQuest, Germany
Mastercycler EP Gradient 5341	Eppendorf, Germany
peqSTAR 2x thermocycler	peqlab (VWR), Germany
PowerPac Basic Power Supply	Bio-Rad, USA
PerfectBlue Gel System Midi S	peqlab, (VWR) Germany
Serial N Gel Documentation System	Vilber Lourmat, Germany
Chemicals	
10x CoralLoad PCR Buffer	Qiagen, Netherlands
Agarose	Biozym, Germany
Desoxynucleotides (dNTPs)	Thermo Scientific, USA
Ethidium bromide	Sigma-Aldrich, USA
Ethylenediaminetetraacetic acid (EDTA)	Sigma-Aldrich, USA
GeneRuler 100bp Plus DNA Ladder	Thermo Scientific, USA
$MgCl_2$ (25 mM)	Qiagen, Netherlands
MilliQ-H_2O	Millipore, USA
Oligonucleotides	Metabion, Germany
Taq DNA Polymerase	Qiagen, Netherlands
Tris-Acetat	Carl Roth, Germany
Buffers	
1x TAE buffer	40 mM Tris-Acetat
	1 mM EDTA-HCl (pH 8.0)

Table 3.3: Oligonucleotides for genotyping.

Gene		Primer Sequence	Temperature
Npn-1	fwd	AAA CCC CCT CAA TTG ATG TTA ACA CAG CCC	63.0 °C
	rev	AGG CCA ATC AAA GTC CTG AAA GAC AGT CCC	
Cre	fwd	GTG TCC AAT TTA CTG ACC GTA CAC	59.5 °C
	rev	GAC GAT GAA GCA TGT TTA GCT GG	
GFP	fwd	TCC TTG AAG AAG ATG GTG CG	60.0 °C
	rev	AAG TTC ATC TGC ACC ACC G	

3.2 Immunohistochemistry

Table 3.4: Primary antibodies and fluorescence-labeled secondary antibodies or toxins.

Alexa647-conjugated phalloidin (1:75)	Life Technologies, USA
donkey anti-goat Alexa546 (1:200)	Life Technologies, USA
donkey anti-mouse Alexa488 (1:200)	Life Technologies, USA
donkey anti-rabbit Alexa546 (1:200)	Life Technologies, USA
goat anti-FoxP1 (1:250)	R&D Systems, USA
goat anti-Scip (1:250)	Santa Cruz, USA
mouse anti-Isl1/2 (1:50)	DSHB, USA
mouse anti-neurofilament 2H3 (1:50)	DSHB, USA
mouse anti-synaptophysin (1:200)	Sigma-Aldrich, USA
rabbit anti-GFP (1:2000)	Life Technologies, USA
Rhodamin-conjugated α-bungarotoxin (1:100)	Life Technologies, USA

3.2.1 Embryo and diaphragm dissection

The morning of vaginal plug formation was considered as embryonic day 0.5 (E0.5) and pregnant mice were sacrificed by cervical dislocation at desired developmental stages. Mouse embryos from E13.5 to E19.5/P0 were fixed in 4 % paraformaldehyde (PFA, Sigma-Aldrich, USA) in phosphate buffered saline (PBS, pH 7.4) overnight (ON) at 4 °C after decapitation while adult thoraces were fixed for 2 days at 4 °C. Embryos or thoraces were rinsed 3x in PBS and fixated on Sylgard (Dow Corning, USA) coated bacterial dishes in supine position with insect pins. Diaphragms with a tiny proportion of the distal end of the PN were carefully dissected under a stereo microscope (M50, Leica, Germany) with micro scissors and stored in PBS at 4 °C until later use.

3.2.2 Whole-mount embryo staining

The protocols for whole-mount embryo staining and immunohistochemistry have been described previously (Huber et al., 2005; Huettl et al., 2011). Embryos at developmental stage E11.5 and E12.5 were prepared as descripted for diaphragm dissection but without decapitation. Following initial fixation, embryos were bleached in Dent's bleach

for 24 h at 4 °C. Afterwards, embryos were rinsed five times in 100 % methanol and finally fixed in Dent's fix for at least 24 h and stored in the same solution until staining. Embryos were rinsed three times in PBS (pH 7.4) and washed three times for 1 h at room temperature (RT) prior staining with primary antibodies for neurofilament (sensory and somatic motor neurons) and green fluorescence protein (GFP, somatic motor neurons) in blocking solution for 3 to 5 days at RT. Next, unbound primary antibody was removed by rinsing embryos three times in PBS followed by five washing steps for 1 h at RT. Fluorochrome-conjugated secondary antibodies were incubated for two days at RT. Subsequently, embryos were rinsed three times in PBS and washed five times for 1 h at RT and final cleared with BABB. All washing and incubation steps were performed on a rotating tube holder (PTR-35, Grant, UK).

Table 3.5: Chemicals, solutions & buffers for whole-mount embryo staining.

Chemicals	
Methanol (MeOH)	Merck, Germany
Dimethylsulfoxid (DMSO)	Sigma-Aldrich, USA
Benzyl alcohol	Sigma-Aldrich, USA
Benzyl benzoate	Sigma-Aldrich, USA
Hydrogen peroxide (H_2O_2)	AppliChem, Germany
Heat-inactivated horse serum (HS)	Life Technologies, USA
Solutions & Buffers	
Dent's Fix	20 % DMSO, 80 % MeOH
Dent's Bleach	33% H_2O_2, 67 % Dent's Fix
BABB	33 % benzyl alcohol, 67 % benzyl benzoate
Blocking buffer	5 % horse serum, 20 % DMSO, 75 % PBS (pH 7.4)

3.2.3 Whole-diaphragm staining

Diaphragm were dissected from pre-fixed embryos, rinsed in PBS, incubated for 15 min in 0.1 M glycine in PBS to reduce autofluorescence and blocked ON in blocking solution. Afterwards, diaphragms were incubated with primary antibodies for neurofilament and synaptophysin in blocking solution ON at RT. Diaphragms were washed three times for 30 min in washing buffer, blocked for 1 h in blocking solution and subsequently in-

cubated with secondary antibodies in blocking solution ON at RT. Finally, diaphragms were incubated with fluorescence-conjugated phalloidin and α-bungarotoxin in blocking solution for 1 h at RT, rinsed three times for 30 min in PBS and flat-mounted with Mowiol.

Table 3.6: Chemicals, solutions & buffers for whole-diaphragm staining.

Chemicals	
Bovine serum albumin (BSA)	Sigma-Aldrich, USA
Triton X-100	Sigma-Aldrich, USA
Mowiol mounting medium	Merck, Germany
Buffers	
Blocking buffer	3 % BSA, 5 % HS, 0.5 % Triton X-100 in PBS (pH 7.4)
Washing buffer	0.5 % Triton X-100 in PBS (pH 7.4)

3.2.4 Motor neuron pool and myogenic progenitor cell staining

Dissected fixed embryos were cryoprotected with 30 % sucrose in PBS ON at 4 °C and frozen in TissueTek (Sakura, Japan). Transversal 12 µm sections were cut with a cryostat (CM1950, Leica, Germany) and stored at -80 °C until later use. Dried slides were washed for 10 min in PBS and subsequently blocked for at least 30 min at RT in blocking buffer. Antibodies against FoxP1, Isl1/2 and Scip for motor neuron pools and against Desmin for myogenic progenitor cells (MPCs) were incubated ON at 4 °C in blocking buffer. Slides were washed three times for 5 min in washing buffer and appropriate secondary antibodies in blocking were incubated for 1 h at RT. Finally, sections were counterstained with DAPI (4,6-Diamidin-2-phenylindol) and washed 3 three times in PBS before mounting with Mowiol.

Table 3.7: Buffers for immunohistochemistry & immunocytochemistry.

Buffers	
Blocking buffer	10 % HS, 0.1 % Triton X-100 in PBS (pH 7.4)
Washing buffer	0.1 % Triton X-100 in PBS (pH 7.4)

3.3 Histological analysis of ectopic muscles

Embryos at developmental stage E16.5 were fixed in 4 % PFA after deskinning, dehydrated with an increasing ethanol row and embedded in paraffin. 8 µm frontal sections were deparaffinized, rehydrated in a decreasing ethanol row and incubated for 2 h in a 0.1 % Direct Red 80 in saturated aqueous picric acid. Sections then were washed in 0.005 % acidic acid in water and dehydrated in an increasing ethanol row before mounting with Roti-Mount. Sections were imaged by bright field and polarization microscopy (Axiovert, Zeiss, Germany). Ectopic muscle location within the CTR was determined by collagen I distribution as organized collagen fibers birefringence red under polarized light, whereas muscle tissue appears yellow-green (Laws, 2004).

Table 3.8: Chemicals for histology of embryo sections.

Chemicals	
Acidic acid	Carl Roth, Germany
Direct Red 80	Sigma-Aldrich, USA
Roti-Mount	Carl Roth, Germany
Saturated aqueous picric acid (1.3 %)	Sigma-Aldrich, USA

3.4 Molecular biology

All plasmids used for *in situ* hybridization (ISH) have been descripted previously: *Npn-1* (Huettl et al., 2011), *Slit1*, *Slit2*, *Robo1*, and *Robo2* (kindly provided by Prof. Dr. Nilima Prakash, Hochschule Hamm-Lippstadt, (Prakash et al., 2009)).

3.4.1 Midi prep with heat shock transformation of Escherichia Coli

Sufficient amount of ISH plasmid templates to create ISH probes were produced in competent Escherichia Coli (E.Coli, strain: DH5α) by heat shock transformation. Therefore, bacteria were thawed on ice for 30 min and approximately 2 µg of plasmid-DNA was added with further 30 min incubation on ice. Transformation was performed by incubation of the bacteria/DNA solution for 60 sec at 42 °C. Following a 2 min relaxation time on ice, bacteria were incubated for 60 min in SOC medium (Invitrogen, USA) at 37 °C with

continuous shaking. To eliminate non-transformed clones, 100 µl of transformed bacteria were plated on a LB agar plate with 100 µg/ml ampicillin an incubated ON at 37 °C. The following day, single colonies were picked and transferred to 3 ml LB medium with 100 µg/ml ampicillin for preparatory culture. After 6 to 8 h of oscillating culture at 37 °C, 200 µl were transferred to 100 ml LB medium with 100 µg/ml ampicillin at cultured ON at 37 °C on a shaker. Amplified plasmid-DNA was extracted with a plasmid column midi kit (Qiagen, USA) and DNA concentration was measured optically (Nanodrop, Thermo Scientific, USA).

Table 3.9: Chemicals for bacterical culture.

Chemicals	
Agar	Becton Dickinson, USA
Ampicillin	Carl Roth, Germany
NaCl	Becton Dickinson, USA
Tryptone	Becton Dickinson, USA
Yeast extract	Becton Dickinson, USA

3.4.2 Plasmid linearization and generation of RNA probes

DNA templates were linearized with appropriate restriction enzymes for sense and antisense RNA *in vitro* transcription (Table 3.10). First, circular 5-10 µg plasmid-DNA was linearized with appropriate restriction enzymes and buffers according to the instructions of the company (all enzymes from Thermo Scientific, USA). Linearized DNA was purified with column binding tubes following the manual (Nucleospin, Macherey-Nagel, Germany). Afterwards, linearized plasmid DNA was *in vitro* transcripted with either Sp6, T7 or T3 RNA polymerases in 10x transcription buffer with digoxigenin (DIG) labelled ribonucleotides (all from Roche, Germany) for at least 2 h at 37 °C and transcription was validated by electrophoresis in a 2 % agarose gel. Sense and antisense RNA was purified after DNA digestion with spin columns (G 50, GE Healthcare Life Sciences, USA) and RNA was suspended in hybridization solution (see 3.4.3) and stored at -80 °C until later use.

Table 3.10: Restriction enzymes (RE) and polymerases (P) for ISH-Plasmids.

	antisense		sense	
Nucleotide	RE	P	RE	P
Npn-1	XhoI	Sp6	HindIII	T7
Robo1	EcoRI	T7	XhoI	T3
Robo2	NotI	T7	XhoI	T3
Slit1	SpeI	T7	NcoI	T3
Slit2	NcoI	T7	SpeI	T3

3.4.3 *In situ* hybdridization

In situ hybridization (ISH) was carried out as described previously with slight modifications (Huber et al., 2005). In brief, dissected embryos were fixed for 1 h in 4 % PFA in PBS (pH 7.4), cryoprotected in 30 % sucrose in PBS ON and sectioned at 12 µm thickness on a cryostat. All cuvettes were treated with RNAse inhibitor prior use. Slides were thawed and washed three times in diethyl dicarbonate (DEPC) treated PBS for 5 min at RT followed by an incubation in acetylation solution for 10 min at RT under continuous stirring. Afterwards, slides were rinsed three times in PBS and incubated in hybridization solution for at least 6 h at RT. RNA (approximately 200 ng) in hybridization solution was heated for 5 min at 90 °C and cooled for 5 min on ice to remove possible hairpins. Reaction was performed at 65 °C ON followed by washing slides two times for 30 min in preheated 0.2 % SSC buffer (pH 7.0) at 65 °C. Samples were temperature equilibrated in 0.2 % SSC, incubated in buffer 1 (both for 5 min at RT) and blocked for at least 6 h in blocking solution proceeded by incubation with alkaline phosphatase (ALP) conjugated anti-DIG-FAB-fragments (1:2000) in blocking buffer ON at 4 °C. The following day, sections were washed three times for 5 min in buffer 1, incubated two times in NTMT buffer for 10 min each and color reaction was carried out in NBT/BCIP (nitro-blue tetrazolium / 5-bromo-4-chloro-3-indolyphosphate) staining solution after a sufficient color reaction. Finally, slides were washed three times in distilled H_2O (dH_2O) for 5 min each, followed by IHC staining for motor neuron column specific markers described in 3.2.4.

Table 3.11: Chemicals & buffers for *in situ* hybridization.

Chemicals	
50x Denhardt's Solution	Sigma-Aldrich, USA
Anti-Digoxigenin-AP, Fab fragments	Sigma-Aldrich, USA
tRNA from bakers yeast	Sigma-Aldrich, USA
Blocking reagent	Sigma-Aldrich, USA
Diethyl dicarbonate (DEPC)	Carl Roth, Germany
Deionized formamide	Thermo Scientific, USA
Magnesium chloride	Sigma-Aldrich, USA
NBT/BCIP stock solution	Sigma-Aldrich, USA
Polyvinyl alcohol (PVA)	Sigma-Aldrich, USA
RNaseZap	Thermo Scientific, USA
Sodium chloride	Sigma-Aldrich, USA
Tween 20	Sigma-Aldrich, USA
UltraPure 20x SSC	Thermo Scientific, USA
Solutions & Buffers	
2x NTMT	5 % 4 M NaCl
	20 % 1 M Tris-Hcl (pH 9.5)
	10 % 1 M $MgCl_2$
	2 % Tween-20 (10 % in H_2O)
	63 % dH_2O
Buffer 1	100 mM & 150 mM NaCl in dH_2O
Hybridization solution	10 % 50x Denhardt's solution
	10 mg baker yeast tRNA
	2 % herring sperm DNA (10 mg/ml)
	25 % 20x SSC
	50 % deionized formamide
	13 % dH_2O
Staining solution	50 % PVA (10 % in dH_2O)
	20 µl NBT/BCIP stock solution per ml of desired volume
	50 % 2x NTMT

3.4.4 Quantitive PCR

Diaphragms of E13.5 embryos were dissected and costal muscles were cleaned from crural muscles as well as the septum transversum. Tissue was minced with a micro scalpel, homogenized with a QiaShredder and total RNA was isolated using the RNeasy Micro Kit according to the manufacturer's instructions (all from Qiagen). In brief, isolated cells were washed once with PBS, subsequently incubated in RLT buffer, supplemented with 1 % β-mercaptoethanol (Merck, Germany) and cell lysate was purified by spin columns. Obtained RNA was reverse-transcribed using the first strand cDNA synthesis kit (Roche). Quantitative PCRs were performed on a LightCycler 96 with a fast-start essential DNA green master mix (Roche). Samples were normalized to the house-keeping gene GAPDH. Obtained data was evaluated by the -$\Delta\Delta C_t$ method. The following primers from Integrated DNA Technologies were used:

Table 3.12: Primer pairs for quantitative determination of gene expression.

Gene	ID
Npn-1	Mm.PT.56a.30361019
Sema3A	Mm.Pt.56a.10918712
Slit1	Mm.PT.56a.43938322
Slit2	Mm.PT.56a.30206904
Robo1	Mm.PT.56a.32204547
Robo2	Mm.PT.56a.29354525
PlxnA1	Mm.PT.56a.28536398
PlxnA2	Mm.PT.56a.7849172
PlxnA3	Mm.PT.56a.8074864.gs
PlxnA4	Mm.PT.56a.43201967
MyoD1	Mm.PT.56a.5271235
GAPDH	Mm.PT.39a.1

3.5 Quantification of phrenic nerve defasciculation, misprojecting axons, ectopic muscle and *Npn-1* & *Slit2* positive motor neurons

To assess phrenic nerve defasciculation within the diaphragm, a Sholl analysis (Sholl, 1953), centered at the PN entry point (PNEP) to the diaphragm, was performed. Intersections of the phrenic nerve with concentrical circles at every 50 µm were counted until the end of the major PN branches and afterwards fitted to a Gaussian regression curve (Figure 3.1 A). Statistics were calculated for the Gaussian curve amplitude.

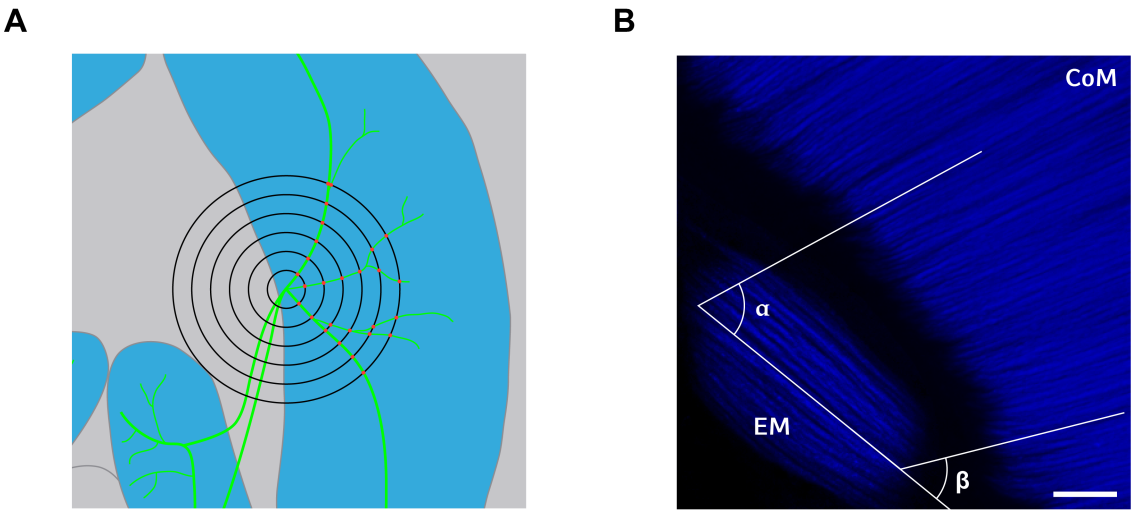

Figure 3.1: Quantification of EM orientation and illustration of Sholl analysis.

Branching of the PN within costal diaphragm muscles was quantified by counting the intersections of axons (red dots) with concentrical circles around the PN entry point at every 50 µm (A). EM myofiber orientation in comparison to fibers of the CoM was measured by calculating the mean of two angles at both ends of the EMs (B).

For quantification of misprojecting axons into the CTR, only the initial axon entry and not each individual axonal tip within the CTR was counted. Ectopic muscle quantity and size were evaluated in phase contrast images from developmental stage E15.5 onwards, when EMs were visible the first time. Only muscles with clearly visible myofibers from at least three diaphragms per develop-mental stage and mouse line were included in the analysis. The orientation of EMs in relation to CoM myofibers was quan-

tified by measurement of the shifted angle be-tween both ends of an EM and normal myofibers (Figure 3.1 B). Afterwards, the mean value of both angles was calculated.

The proportion of *Npn-1* and *Slit2* ISH$^+$ positive motor neurons in the phrenic was quantified by counting Isl1$^+$/Scip$^+$ neurons which were apparently positive for ISH color reaction. Furthermore, consecutive sections were stained for FoxP1 and aligned in Photoshop (Adobe, USA) to exclude counting of ISH$^+$ cells within the LMC. Quantification of expression level was carried out as described (Huettl et al., 2012). In brief, gray value intensity of ISH stained slides was measured for unspecific background staining within the white matter of the spinal cord. ISH signal was measured in the phrenic nucleus and in the LMC and background values were subtracted. Finally, expression level was calculated by dividing LMC values by phrenic nucleus values. At least four sections per animal were evaluated and left and right values were pooled.

3.6 Myoblast chemotaxis assay

Diaphragms of eight to ten E14.5 embryos per experiment were dissected and costal muscles were cleaned from crural muscles as well as the septum transversum. Muscle tissue was pooled, minced with a micro scalpel, and incubated under continues agitation in 250 U/ml collagenase type II in Dulbecco's Modified Eagle Medium (DMEM) for 10 min with final trituration. Non-digested tissue pieces were allowed to settle down for 30 sec and supernatant was transferred to a new collection tube. This procedure was repeated three times. Collected primary cells were strained with a 100 µm sieve, counted with a hemocytometer and directly used for chemotaxis experiments. A small proportion of primary cells was directly stained against muscle-specific Desmin following the protocol for immunohistochemistry and fluorescence activated cell sorted (FACSCalibur, BD, USA) to determine the proportion of MPCs. Acquired data was evaluated after appropriate gating in FlowJo 7.6.5 (FlowJo, USA).

Trans-well invasion assays were carried out as follows: invasion chambers (8 µm pore size) were pre-coated ON with 10 µg/ml rat tail collagen I in PBS. The following day, inserts were rinsed three times in PBS to remove excess collagen. Lower storage compartments were filled with either control medium alone (DMEM and 10 % FBS),

or with recombinant Slit1 (400 ng/ml), Slit2 (400 ng/ml), Slit1/Slit2 (400 ng/ml each), or Sema3A (500 ng/ml) in control medium. Invasion chambers were inserted into the lower storage slot and 2.5 * 10^3 freshly isolated myoblasts were seeded in the upper compartment in control medium. Seeded inserts were incubated for 24 h and subsequently fixed for 10 min in 4 % PFA. Afterwards, membranes were cut out, stained with DAPI and mounted with Mowiol on glass slides after two washing steps for 3 min in PBS. For data analysis, only fully visible cell nuclei were counted on both sides and subsequently the ratio of invaded to non-invaded cells was calculated for four independent experiments.

Time lapse 3D chemotaxis assays were performed in a linear gradient chemotaxis chamber slide. Primary MPCs in a concentration of 2,000 cells/µl were mixed together with collagen I and 10 mM NaOH in order to obtain a final suspension of 1,000 cells/µl in a 1 mg/ml collagen I gel matrix. The cell/collagen suspension was injected directly into the chemotaxis channel and allowed to polymerize for 3 h at 37 °C. Subsequently, µ-slides reservoirs were filled with either control medium (DMEM and 10 % FBS) or Slit1 (400 ng/ml), Slit2 (400 ng/ml), Slit1/Slit2 (400 ng/ml each), or Sema3A (500 ng/ml) in control medium. Cell migration was imaged every 15 min for 24 h in a controlled environment at 37 °C and 5 % CO_2 using a Zeiss Axiovert microscope. Cells were tracked manually with the MTrackJ plugin for ImageJ (Meijering et al., 2012), evaluated using the chemotaxis and migration tool (Ibidi), and shown as center of mass (COM) and forward migration index (FMI) of the total cell population. Cells which did not migrate more than 25 µm were determined as non-migrating.

3.7 Statistical analysis

Data were evaluated for statistical significance with GraphPad 5.0 (USA). All results are shown as mean values ± standard error of mean (SEM). For all experiments and time points at least three mutants and littermate controls were evaluated. Cell culture experiments were repeated at least three times in triplicates. A p-value of 0.05 or lower was considered as significant. After testing for normal data distribution with a D'Agostino and Pearson test, either a Mann-Whitney-U (no Gaussian distribution) or a two-tailed unpaired t-test (Gaussian distribution) was performed.

Chapter 4

Results

4.1 *Npn-1* is expressed in motor neurons of the phrenic nucleus during PPF targeting and diaphragm innervation

Npn-1 is strongly expressed in motor neurons of the LMC at brachial and lumbar levels as well as in MMC neurons (Huber et al., 2005; Huettl et al., 2011). Given the fact that *Npn-1*$^{Sema-}$ as well as *Npn-1*$^{cond-/-}$*;Olig2-Cre*$^{+}$ mutant embryos are born according to Mendelian inheritance, and dead pups appeared to be cyanotic (data not shown), not only intercostal, but also phrenic projections might be affected by manipulation of the Sema3-Npn-1 signaling pathway (Huber et al., 2005; Huettl et al., 2011). To analyze whether Npn-1 is also expressed by pMN during initial targeting of the primordial diaphragm and later innervation of the developing muscle, we performed *in situ* hybridization against *Npn-1* and fluorescent immunohistochemistry against the PMC markers Scip and Isl1/2 (Figure 4.1 C-D) as well as the LMC marker FoxP1 on consecutive sections (Figure 4.1 A'-D') to localize motor neurons of the phrenic nucleus at the spinal levels C3 to C6 (Philippidou et al., 2012).

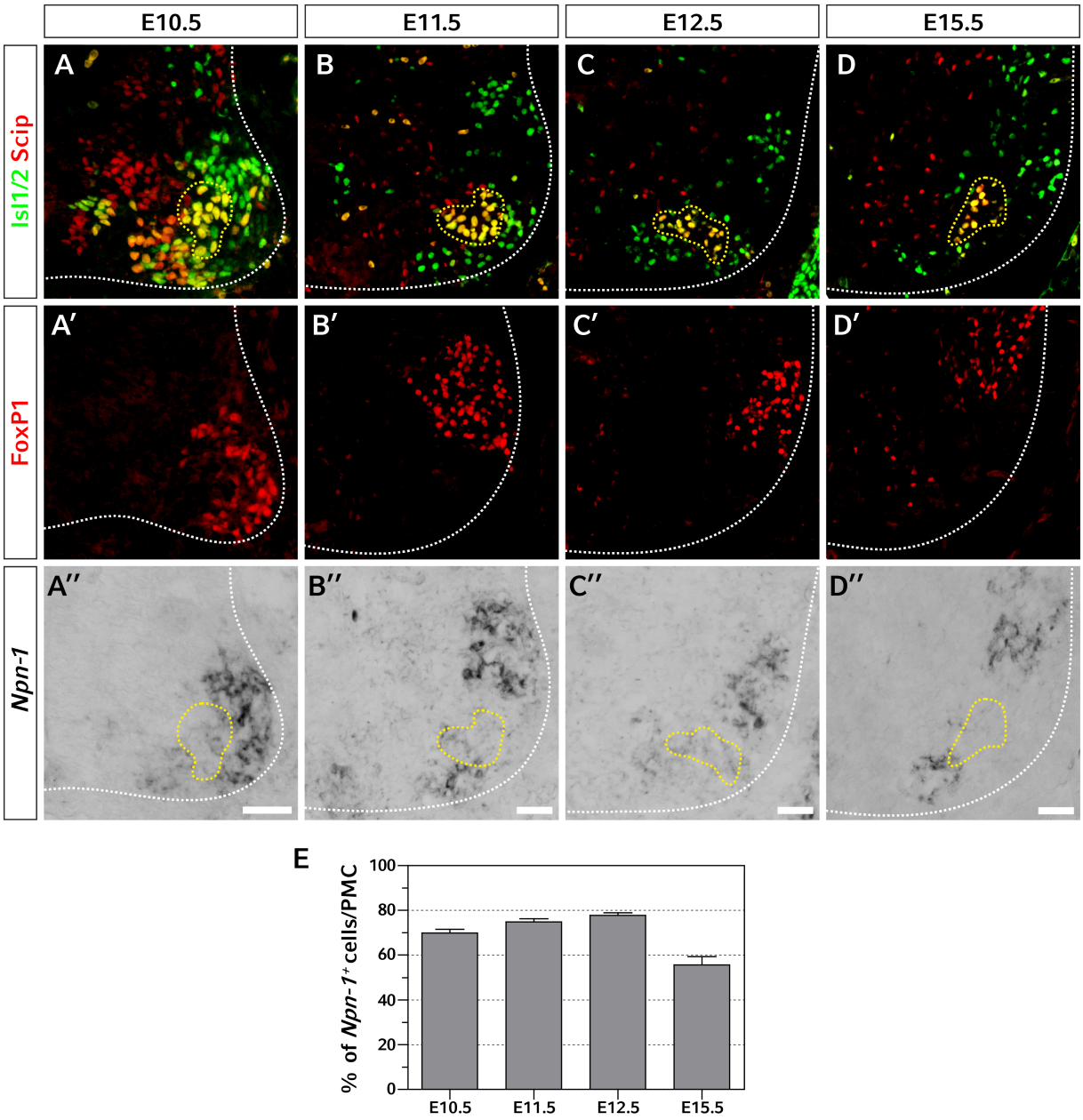

Figure 4.1: Expression of *Npn-1* in the phrenic nucleus in the cervical spinal cord during targeting and innervation of the thoracic diaphragm.

PN motor neurons express Scip (A-D, red) and Isl1/2 (A-D, green) and are negative for FoxP1 (A'-D', red), which marks limb innervating motor neurons. During PN outgrowth and innervation of the diaphragm, a subpopulation of Scip^{+}/Isl1^{+}/FoxP1^{-} motor neurons expresses *Npn-1* (A"-D", yellow dotted line). Quantification showed that approximately 70 % of somatic MNs in the PMC express *Npn-1* between developmental stage E10.5 to E12.5 and later decreased to approximately 56 % at E15.5 (E). Scale bar: 200 μm.

During the time course of initial diaphragm targeting, a subset of Scip^{+}/Isl1^{+} (Figure 4.1 A-D, yellow dotted line) motor neurons in the phrenic nucleus expresses *Npn-1*

(Figure 4.1 A"-D", yellow dotted line) during targeting of the PPF and subsequent innervation of the diaphragm muscles by the PNs. Quantification of ISH$^+$ cells showed that 69.87 $\pm$ 1.66 % SEM of pMNs express *Npn-1* at E10.5 and the numbers increased slightly to 74.83 $\pm$ 1.38 % SEM at E11.5, and 77.68 $\pm$ 1.17 % SEM at E12.5. By E15.5, crural and costal diaphragm muscle development and innervation are mostly finished, and the PNs have nearly reached the cartilaginous sternum at (Fig.1D, D'). Interestingly, the subpopulation of *Npn-1* expressing pMNs is noticeably, but not significantly, reduced during diaphragm innervation by E15.5 to 55.60 $\pm$ 3.71 % SEM, when compared to earlier developmental stages ($p = 0.1$).

Taken together, our findings demonstrate that a subpopulation of pMNs express *Npn-1* during initial targeting of the PNs towards the PFF, as well as at later stages, when sophisticated innervation of the thoracic diaphragm muscles is established. However, the expression level of *Npn-1* in the PMC seems to be lower when compared to the LMC.

4.2 Pre-diaphragm fasciculation of the PN is only mildly disturbed upon systemic or motor neuron specific ablation of Sema3-Npn-1 signaling

After verification of *Npn-1* expression in pMN during innervation of the diaphragm muscle, we investigated whether loss of the Sema3-Npn-1 signaling pathway affects phrenic axon targeting to the PPF during early embryonic development. Due to the severity of axon defasciculation in the brachial plexus of both mutant embryos at E10.5, a reliable determination of PNs was barred (Huber et al., 2005; Huettl et al., 2011). Therefore, we performed immunohistochemistry on whole-mount preparations of E11.5 embryos, when the PNs project towards the PPFs (Figure 4.2 A, arrow head), and at E12.5, when the PNs have reached the developing diaphragm (Figure 4.2 A', arrows) and is starting to branch and innervate newly formed myofibers and fibroblasts of the PPF (Merrell et al., 2015). In addition, heterozygote *Npn-1*$^{Sema-}$ embryos showed the same fasciculated innervation pattern as wildtype mice at developmental stages E11.5 and E12.5 (Figure 7.1 A, B).

Upon systemic ablation of the Sema3-Npn-1 signaling pathway by mutating the Sema3 binding site of *Npn-1* at E11.5, we observed severe defasciculation within the brachial plexus (Figure 4.2 B, asterisk), however, PN axons fasciculated to one specific branch right after leaving the plexus region (Figure 4.2 B, arrow head). By E12.5, the PN have reached the PPF in a fasciculated manner and initially forming dorsal and ventral projections of the PN on the developing diaphragm muscles are comparable to wildtype littermates (Figure 4.2 B', arrow heads).

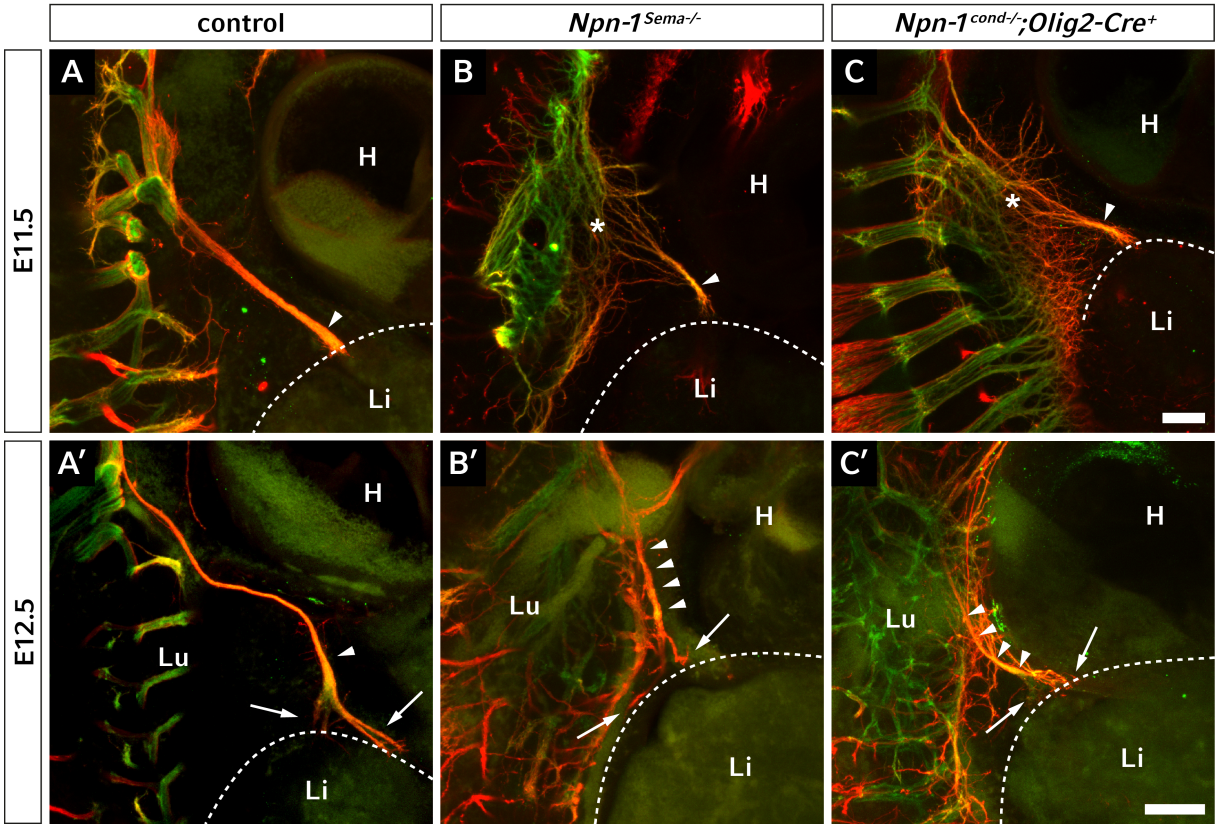

Figure 4.2: Whole-mount staining of the brachial plexus during diaphragm targeting.

Whole-mount immunohistochemistry against *Hb9::eGFP* (somatic motor projections, green) and neurofilament (motor and sensory axons, red) at stage E11.5 (A-C) and E12.5 (A'-C'). Control embryos show fasciculated phrenic projections after the brachial plexus at E11.5 (A, arrowhead). At the same stage, *Npn-1*$^{Sema-}$ (B) and *Npn-1*$^{cond-/-}$*;Olig2-Cre*$^{+}$ mutant embryos (C) expose mildly disorganized projections of the phrenic nerve at brachial levels (asterisks). Interestingly, PN axons reach the developing diaphragm as a fasciculated nerve branch regardless of the genotype (A-C, arrow heads). The PN faithfully targets the primordial developing diaphragm and starts to branch dorsally and ventrally at E12.5 (A'-C', arrows). H: Heart, L: Liver, Lu: Lung. Scale bar: 200 µm.

To elucidate whether Npn-1 is responsible for early fasciculation of the PNs in a cell autonomous manner, we selectively eliminated *Npn-1* from all somatic motor neurons in *Npn-1$^{cond-/-}$;Olig2-Cre^{+}* mutant embryos. Axons were defasciculated within the plexus region (Figure 4.2 C, asterisk), however, distinct PN projections were formed that targeted the primordial diaphragm (Figure 4.2 C, arrow heads). During the initial branching within the costal muscle at E12.5, no obvious alterations were observed in *Npn-1$^{cond-/-}$;Olig2-Cre^{+}* mutant embryos when compared to control littermates (Figure 4.2 C', arrows).

Hence, although spinal nerves that contribute to the brachial plexus and intercostal nerves are strongly defasciculated in both *Npn-1^{Sema-}* and *Npn-1$^{cond-/-}$;Olig2-Cre^{+}* mutant embryos (Huber et al., 2005; Huettl et al., 2011), Sema3-Npn-1 signaling has no effect on specific branch formation and initial guidance of the PN axons towards the PPFs, even when proper fasciculation within the brachial plexus is diminished.

4.3 Npn-1 cell-autonomously governs PN fasciculation within the diaphragm muscles

The PPFs, which are fully developed by E12.5 in wildtype mice, are positioned medially at the lateral cervical body wall, and mark the primordial diaphragm where MPCs that have migrated there from the cervical dermomyotome start to accumulate and finally fuse to myofibers (Babiuk et al., 2003). During developmental progression of the diaphragm, MPCs migrate ventrally on the septum transversum and liver. Overall muscle pattering of the costal and crural parts of the diaphragm is completed by E16.5, when migrating myoblasts have reached the early cartilaginous sternum and finished the first wave of fusion to myofibers (Allan and Greer, 1998; Merrell et al., 2015; Messina and Cossu, 2009).

To investigate whether the loss of Sema3-Npn-1 signaling affects PN fasciculation and targeting during the innervation of the newly formed myofibers of the developing diaphragm, we stained whole diaphragms of E16.5 embryos. In control embryos, phrenic motor axons enter the diaphragm at the left and right hemisphere at the height of the

vena cava (Figure 4.3 A, A', arrows) and form three distinct projections, one of which targets the crural muscle, and two branches which innervate the ventral and dorsal proportion of the costal musculature (Figure 4.3 A, A', arrow heads) with distinct branching patterns in each hemisphere. In addition, some thin axon bundles leave their normal track and project towards the crural muscle of the diaphragm in wildtype embryos (Figure 4.3 A, A', empty arrow head). Heterozygote *Npn-1*$^{Sema+/-}$ embryos largely copied the appearance of wildtype animals at E16.5, while the innervation pattern of the right CoM suggests a slight different axon branching (Figure 7.1 A, B, empty arrow heads). In contrast, systemic (Figure 4.3 B, B', empty arrow heads) or conditional ablation of the Sema3-Npn-1 signaling pathway in somatic MNs (Figure 4.3 C, C', empty arrow heads) lead to severe defasciculation of phrenic motor projections within both costal and crural musculature. Interestingly, the PN entry point was deviated *Npn-1*$^{Sema-}$ and *Npn-1*$^{cond-/-}$*;Olig2-Cre*$^{+}$ mutant diaphragms in some rare cases when compared to wildtype littermates (Figure 4.3 C', left arrow).

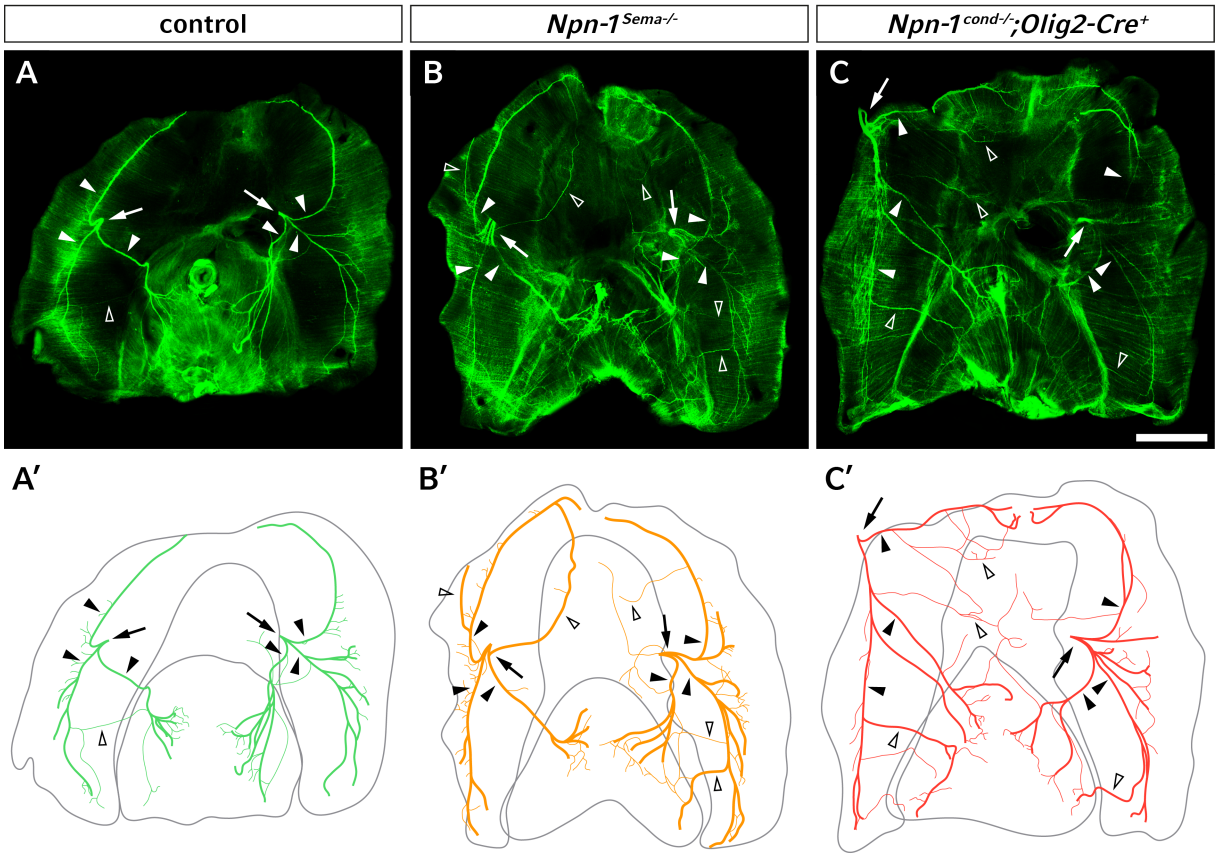

Figure 4.3: Whole-mount staining of control and mutant diaphragm.

Whole-diaphragm staining against neurofilament and synaptophysin (green). At E16.5, the PN forms three distinct branches (arrowheads) after the PN entry point (arrow) and a tight innervation at the midline of costal myofibers (A, A'), while *Npn-1*$^{Sema-}$ and *Npn-1*$^{cond-/-}$*;Olig2-Cre*$^{+}$ mutant embryos reveal a severely defasciculated innervation pattern (B, B', C, C', open arrowheads). Fluorescence images were redrawn for a better visualization of PN innervation pattern of the diaphragm muscles at developmental stage E16.5 (A'-C'). Note that PN branching is not similar between both costal hemispheres (A', A'). Scale bar: 1 mm.

To quantify these branching abnormalities within the costal muscles, we performed a Sholl analysis with concentrical circles every 50 µm around the PN entry point and counted axon intersections with each ring (compare Figure 10 B). Quantification of heterozygote *Npn-1*$^{Sema+/-}$ embryos revealed no difference of PN branching in the left CoM hemisphere, however, bifurcation of the PN was significant differently in the right CoM hemisphere ($p \leq 0.05$, Figure 7.2 B).

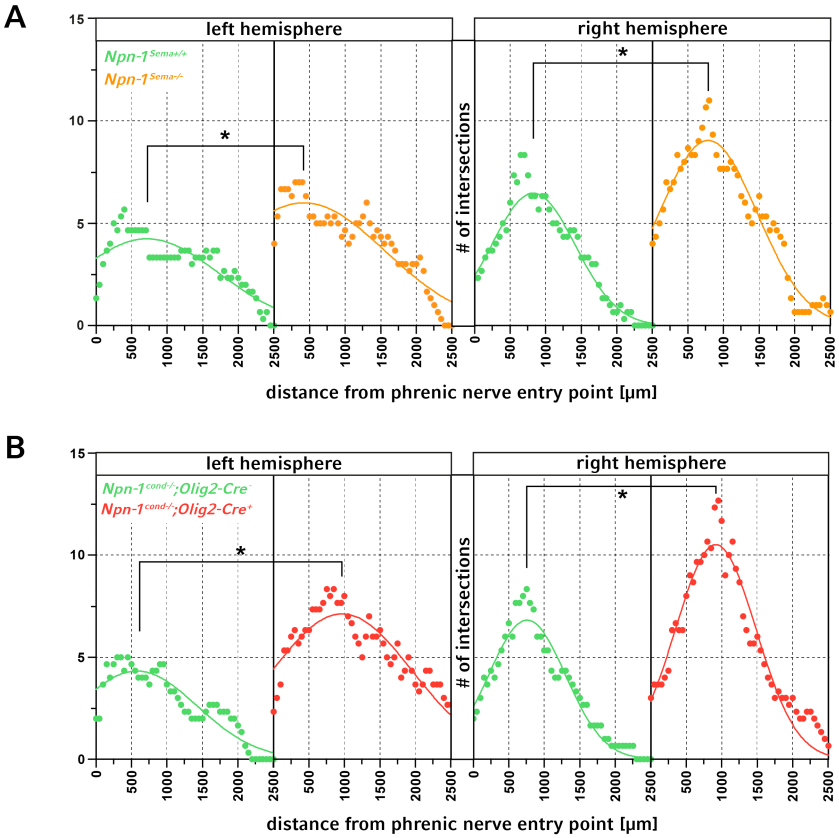

Figure 4.4: Sholl analysis of PN axon branching within the diaphragm.

Branching of the right and left PN within the costal muscles during development of the diaphragm was quantified by Sholl analysis centered at the PN entry point. At E16.5 (A), when the diaphragm is completely muscularized, the PN of *Npn-1*$^{Sema-}$ wildtype embryos branched significantly less on both costal muscle hemispheres compared to their mutant littermates (left: 4.24 ± 0.17 intersections (int) vs. 6.00 ± 0.18 int; right: 6.47 ± 0.15 int vs. 9.04 ± 0.21 int; $n = 3$, $p \leq 0.05$). Specific ablation of *Npn-1* from PN motor neurons (B) revealed a similar significant higher branching of the PN between control and mutant embryos (left: 4.37 ± 0.16 int vs. 7.12 ± 0.19 int; right: 6.82 ± 0.17 int vs. 10.50 ± 0.26 int, $n = 3$, $p \leq 0.05$). Significance levels: * equals $p \leq 0.05$.

In contrast, costal muscles are morphologically fully developed and innervated by PN branches, nerve intersections with Sholl rings have significantly increased by approximately 42 % in the left and 40 % in the right costal muscle hemisphere in *Npn-1*$^{Sema-}$ mutant embryos when compared to wildtype controls at developmental stage E16.5 (Figure 4.4 A). Additionaly, conditional ablation of *Npn-1* in all somatic MNs also showed a significant increase to 63 % of aberrant costal nerve branching of the PN in the left hemisphere, and 54 % in the right hemisphere of mutant diaphragms (Figure 4.4 B), which is very reminiscent of what we observed upon systemic ablation of Sema3-Npn-1

signaling.

We further analyzed costal diaphragm innervation at earlier developmental stages in *Npn-1*$^{Sema-}$ and *Npn-1*^{cond}*;Olig2-Cre* mouse lines by adding up all PN intersections with Sholl circles (sum of intersections, SOI) until the end of axonal innervation. We could not detect any significant difference of the SOI when comparing *Npn-1*$^{Sema+/-}$ heterozygote embryos to wildtype controls (Figure 7.2 C). However, while the SOI was not consistently significant for both costal hemispheres at E13.5 when costal and crural nerves start bifurcating, PN branching was significantly higher from E14.5 onwards, with an approximate increase of 78 % in the left and 55 % in the right hemisphere in both mutant mouse lines when compared to control littermates (Figure 4.5 A, B).

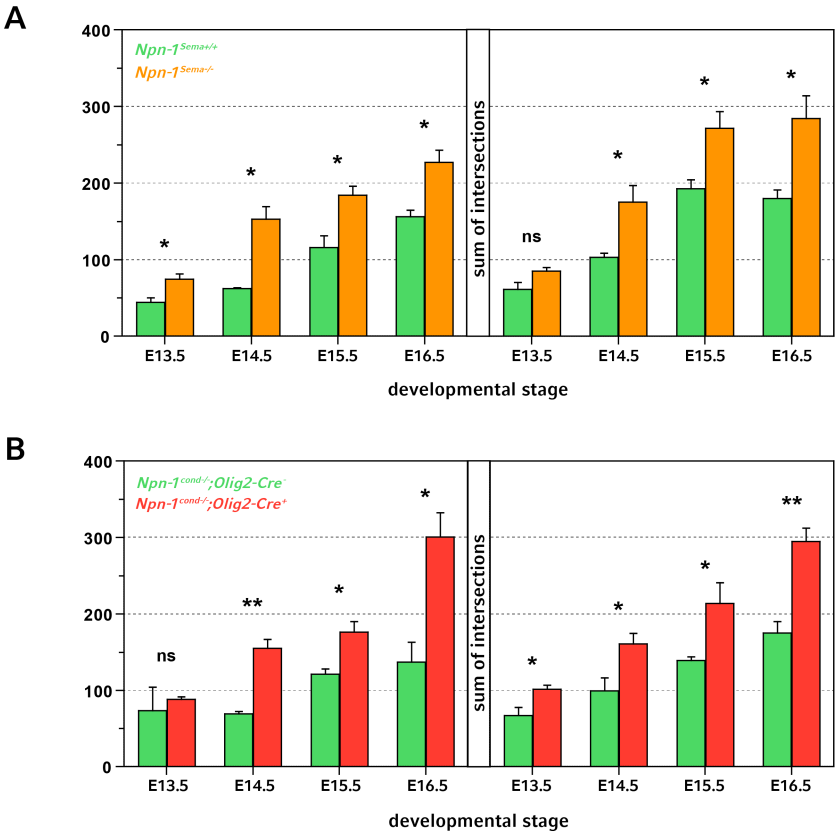

Figure 4.5: Quantification of PN branching within the diaphragm during development.

Entire defasciculation of the PN during E13.5 to E16.5 is shown by the sum of all intersections (SOI, A, B). Comparison of the SOI between *Npn-1*$^{Sema+/+}$ and *Npn-1*$^{Sema-/-}$ embryos showed a significant difference in all observed stages in the left costal hemisphere, while the right costal hemisphere was significant different from developmental stage E14.5 onwards. *Npn-1*$^{cond-/-}$*;Olig2-Cre*$^{+}$ mutants showed tantamount results when compared to control embryos. Despite branching in the left costal hemisphere at E13.5, PN branching was significant higher in mutant animals from E13.5 to E16.5. Data represents mean & SEM. Significance levels: * equals $p \leq 0.05$, ** equals $p \leq 0.01$, ns: not significant. *Npn-1*$^{Sema+/+}$ vs. *Npn-1*$^{Sema-/-}$: left hemisphere - E13.5: 44.00 ± 5.86 SOI, $n = 3$ vs. 74.50 ± 7.03 SOI, $n = 4$, $p \leq 0.05$; E14.5: 62.33 ± 0.88 SOI vs. 152.70 ± 16.70 SOI, $n = 3$, $p \leq 0.05$; E15.5: 116.00 ± 15.31 SOI vs. 184.00 ± 11.85 SOI, $n = 3$, $p \leq 0.05$; E16.5: 156.00 ± 8.51 SOI, $n = 3$ vs. 227.00 ± 16.05 SOI, $n = 4$, $p \leq 0.05$ and right hemisphere - E13.5: 61.00 ± 9.45 SOI, $n = 3$ vs. 85.25 ± 4.55 SOI, $n = 4$, $p = 0.052$; E14.5: 103.00 ± 5.51 SOI vs. 175.30 ± 21.37 SOI, $n = 3$, $p \leq 0.05$; E15.5: 192.7 ± 11.62 SOI vs. 271.70 ± 21.40 SOI, $n = 3$, $p \leq 0.05$; E16.5: 179.70 ± 11.20 SOI, $n = 3$ vs. 284.00 ± 29.68 SOI, $n = 4$, $p \leq 0.05$. *Npn-1*$^{cond-/-}$*;Olig2-Cre*$^{-}$ vs. *Npn-1*$^{cond-/-}$*;Olig2-Cre*$^{+}$: left hemisphere - E13.5: 73.50 ± 30.50 SOI vs. 88.00 ± 3.51 SOI, $n = 3$, $p = 0.7191$; E14.5: 69.33 ± 2.91 SOI vs. 155.00 ± 11.59 SOI, $n = 3$, $p \leq 0.01$, E15.5: 121.00 ± 7.10 SOI vs. 176.00 ± 13.80 SOI, $n = 3$, $p \leq 0.05$; E16.5: 137.00 ± 25.79 SOI vs. 295.00 ± 17.21 SOI, $n = 3$, $p \leq 0.01$ and right hemisphere - E13.5: 67.00 ± 10.79 SOI vs. 101.70 ± 5.18 SOI, $n = 3$, $p \leq 0.05$; E14.5: 99.33 ± 17.07 SOI, $n = 3$ vs. 161.00 ± 13.74 SOI, $n = 4$, $p \leq 0.05$; E15.5: 139.30 ± 4.41 SOI vs. 217.30 ± 23.39 SOI, $n = 3$, $p \leq 0.05$; E16.5: 175.00 ± 15.01 SOI vs. 295.00 ± 17.21 SOI, $n = 3$, $p \leq 0.01$.

Our results thus show that, first, Sema3-Npn-1 signaling cell autonomously governs PN fasciculation and branching during innervation of the costal muscles of the diaphragm and, second, the left costal muscle hemisphere is more affected than the right one.

4.4 Misprojecting PN axons innervate ectopic muscles in the CTR of the diaphragm

The CTR of the diaphragm is a tendinous tissue which provides functional force transduction between both costal muscle hemispheres. Normally, this region is free of muscles and/or nerve endings, and harbors only veins and arteries in close proximity to the medial part of the costal muscles (Stuelsatz et al., 2012). Remarkably, we observed a significant 8.7-fold increase in the number of misprojecting axons into the CTR of *Npn-1*$^{Sema-}$ mutants when compared to control embryos (Figure 4.3 B and Figure 4.6 A, arrowheads) already during initial innervation of the diaphragm at E13.5. During progression of diaphragm development, misprojected axons remain elevated in *Npn-1*$^{Sema-}$ mutants, however, the quantity of misguided axons did not change significantly over developmental stages (Figure 4.6 B). Intriguingly, upon closer investigation of the CTR, we observed ectopically formed muscle patches in embryos where Sema3-Npn-1 signaling was abolished systemically. Interestingly, nearly all of these EMs were innervated by misprojected axons (97.66 ± 1.05 % SEM), while approximately one tenth (12.25 ± 2.56 % SEM) of the misprojected axons did not innervate EMs (Figure 4.6 A, A'), which were evident from E15.5 onwards until late adulthood. Similar to *Npn-1*$^{Sema-}$ wildtype animals, *Npn-1*$^{Sema+/-}$ diaphragms revealed a similar average low incidence of approximately 0.82 ± 0.29 SEM misprojecting axons into the CTR and 0.79 ± 0.18 SEM EMs over all developmental stages (Figure 7.3 B, C).

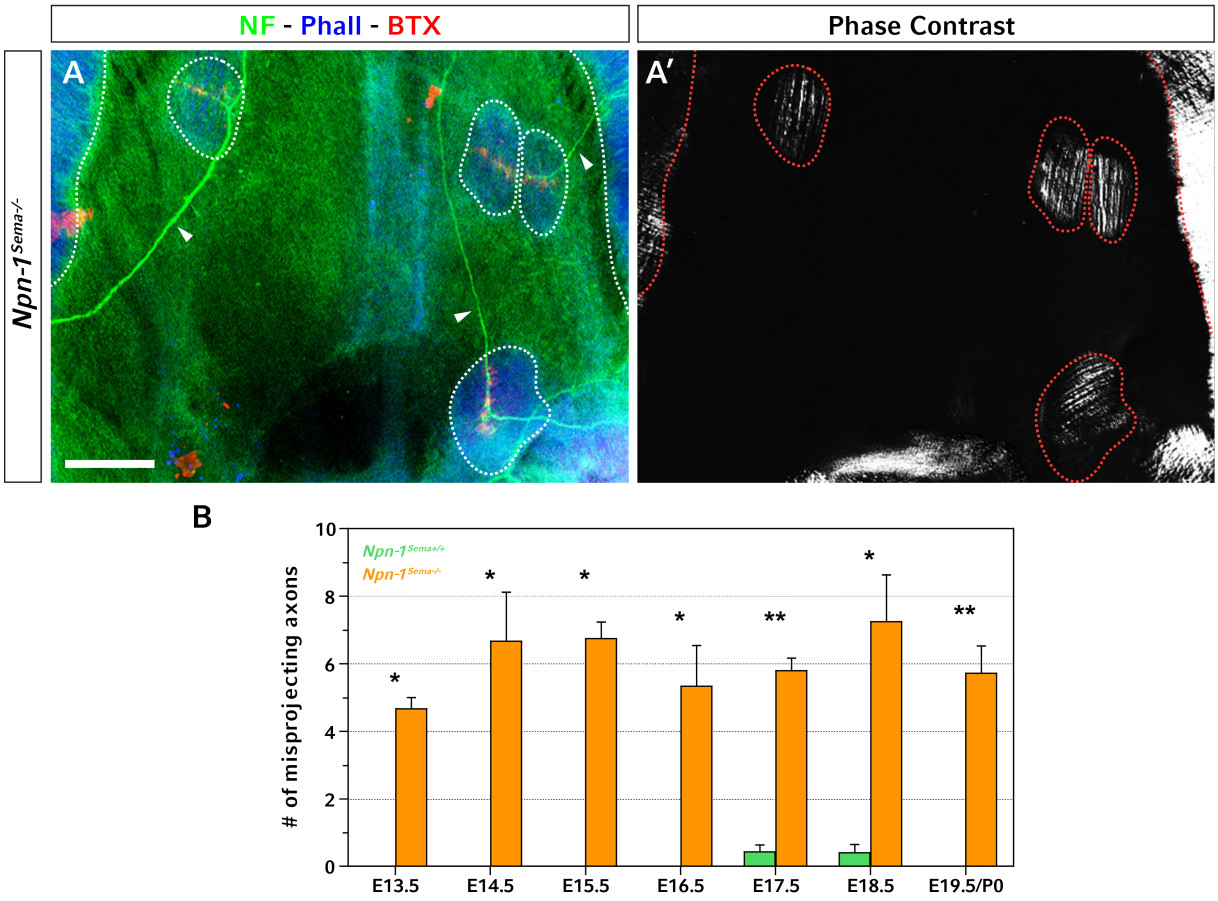

Figure 4.6: PN axons misproject into the CTR after systemic ablation of Sema3-Npn-1 signaling.

Whole-mount diaphragm staining against neurofilament (green), actin (blue) and acetylcholine receptors at neuromuscular junctions (red) revealed some misprojecting axons into the CTR of *Npn-1*$^{Sema-/-}$ (A, arrowheads), which is normally free of axons in wildtype embryos. At E16.5, the majority of these misprojecting axons innervate ectopic muscles in the CTR (A, dotted lines). Phase contrast microscopy showed a typical aligned myofiber orientation which was comparable to native costal muscles of the diaphragm, but did not have a specific orientation (A'). Misprojection of PN axons into the CTR is observed as early as E13.5, directly after nerve division into three distinct branches. Quantification revealed significantly more axons that misproject into the CTR in *Npn-1*$^{Sema-/-}$ (B) mutant embryos when compared to control embryos over the whole diaphragm development. *Npn-1*$^{Sema+/+}$ vs. *Npn-1*$^{Sema-/-}$ - E13.5: 0.00 ± 0.00, $n = 4$ vs. 4.67 ± 0.33, $n = 3$, $p \leq 0.05$; E14.5: 0.00 ± 0.00, $n = 4$ vs. 6.67 ± 1.45, $n = 3$, $p \leq 0.05$; E15.5: 0.00 ± 0.00, $n = 3$ vs. 6.75 ± 0.48, $n = 4$, $p \leq 0.05$; E16.5: 0.00 ± 0.00, $n = 4$ vs. 5.33 ± 1.20, $n = 3$, $p \leq 0.05$; E17.5: 0.43 ± 0.20, $n = 7$ vs. 5.80 ± 0.37, $n = 5$, $p \leq 0.01$; E18.5: 0.40 ± 0.00, $n = 5$ vs. 7.25 ± 1.38, $n = 4$, $p \leq 0.05$; E19.5/P0: 0.00 ± 0.00, $n = 4$ vs. 5.71 ± 0.81, $n = 7$, $p \leq 0.01$. Data represents the mean & SEM. Significance levels: * equals $p \leq 0.05$, ** equals $p \leq 0.01$. Scale bar: 200 μm.

As Sema3-Npn-1 signaling is involved in a variety of developmental processes such as the upregulation of the muscle-specific transcription factor MyoG in satellite cells, syndecan-dependend cell-autonomous upregulation of Sema3A in myoblasts, or development of lyphatic valves (Bouvrée et al., 2012; Do et al., 2015; Suzuki et al., 2013), Sema3-Npn-1 signaling in MPCs might be responsible for misguidance of PN axons into the CTR and subsequent EM formation. Therefore, we performed qPCR for Sema3A in addition to its binding partners and downstream signaling receptors, respectively. We showed that *Npn-1* (red), together with the Plexin A co-receptors (orange), is highly upregulated in cells of the costal musculature when compared to its expression level of cells in the CTR (Figure 4.7). Furthermore, Sema3A is even higher expressed in cells of the CoM when compared to its receptors (Figure 4.7, green).

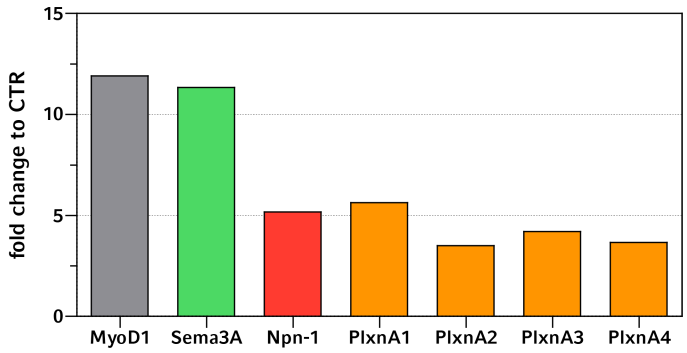

Figure 4.7: Sema3A and its signaling receptors are express in myoblasts of the CoM during diaphragm development.

Quantitative PCR revealed that Sema3A, Npn-1 and Plexin A are highly expressed in cells of the CoM when compared to cells from the CTR at E16.5. The muscle specific transcription factor MyoD1 served as positive control. Fold-increase CoM vs. CTR: MyoD1 – 11.91, Sema3A – 11.33, Npn-1 – 5.18, PlexA1 – 5.63, PlexA2 – 3.51, PlexA3 – 4.21, PlexA4 – 3.67. Data represents one qPCR with four pooled diaphragms.

Consequently, Sema3-Npn-1 signaling might affect ectopic myofiber formation in the CTR and therefore, we utilized conditional ablation of Npn-1 in all somatic motor neurons, including pMNs, to analyze whether mismigration of MPCs into the CTR is caused by systemic loss of Sema3-Npn-1 signaling or by an additional mechanism. *Npn-1*$^{cond-/-}$*;Olig2-Cre*$^{+}$ mutant embryos showed a very similar pattern of misprojecting axons towards the CTR when compared to *Npn-1*$^{Sema-}$ mutants, with no clear favor of a specific part of the CTR (Figure 4.8 A, arrowheads). Intriguingly, removal of *Npn-1* from somatic MNs revealed the same innervated EMs with a striated muscle fiber pattern as

systemic ablation of Sema3-Npn-1 signaling (Figure 4.8 A'). Quantification of misguided axons showed a significant average 9.3-fold increase of misprojecting axons into the CTR (Figure 4.8 B) in *Npn-1$^{cond-/-}$;Olig2-Cre^{+}* mutant embryos when compared to Cre^{-} control embryos. Misprojecting axons and EMs quantity did not change significantly during later development in *Npn-1$^{cond-/-}$;Olig2-Cre^{+}* animals.

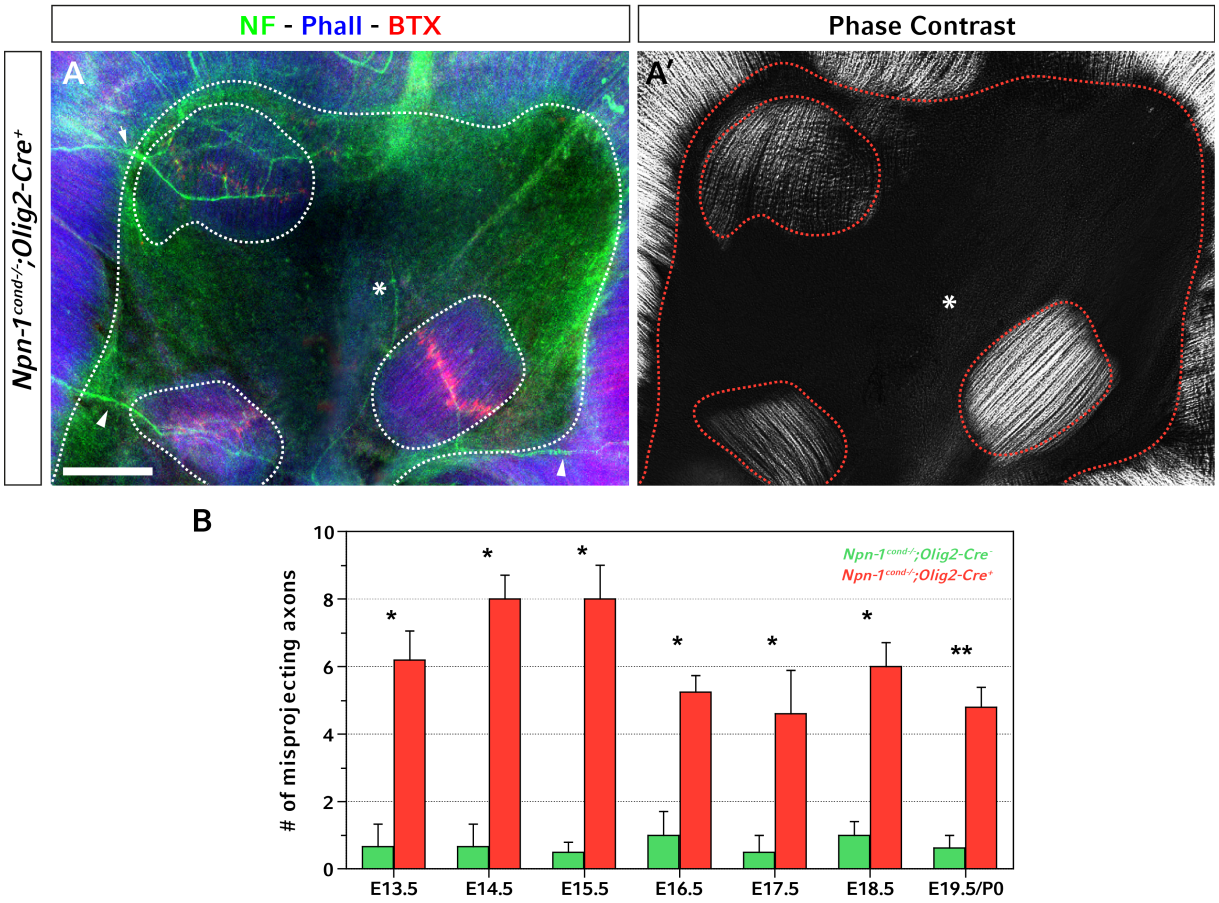

Figure 4.8: Quantification of misprojecting axons into the CTR during development after conditional ablation *Npn-1* in somatic MNs.

Whole-mount diaphragm staining against neurofilament (green), actin (blue) and acetylcholine receptors at motor endplates (red) revealed the same misprojecting axons into the CTR as shown for *Npn-1*$^{Sema-}$ mutant animals (A, arrowheads), while some axons occasionally did not innervate striated EMs (A, asterisk, A'). The majority of these misprojecting axons innervate ectopic muscles in the CTR (A, dotted lines). Quantification revealed significantly more axons that misproject into the CTR *Npn-1*$^{cond-/-}$*;Olig2-Cre*$^{+}$ mutant embryos when compared to control embryos over the whole diaphragm development (B). *Npn-1*$^{cond-/-}$*;Olig2-Cre*$^{-}$ vs. *Npn-1*$^{cond-/-}$*;Olig2-Cre*$^{+}$ - E13.5: 0.67 ± 0.67, $n = 3$ vs. 6.20 ± 0.86, $n = 5$, $p \leq 0.05$; E14.5: 0.67 ± 0.67, $n = 3$ vs. 8.00 ± 0.71, $n = 4$, $p \leq 0.05$; E15.5: 0.50 ± 0.29, $n = 4$ vs. 8.00 ± 1.00, $n = 3$, $p \leq 0.05$; E16.5: 1.00 ± 0.71, $n = 4$ vs. 5.25 ± 0.48, $n = 4$, $p \leq 0.05$; E17.5: 0.50 ± 0.50, $n = 4$ vs. 4.60 ± 1.29, $n = 5$, $p \leq 0.05$; E18.5: 1.00 ± 0.41, $n = 4$ vs. 6.00 ± 0.71, $n = 4$, $p \leq 0.05$; E19.5/P0: 0.63 ± 0.38, $n = 8$ vs. 4.80 ± 0.58, $n = 5$, $p \leq 0.01$). Data represents the mean & SEM. Significance levels: * equals $p \leq 0.05$, ** equals $p \leq 0.01$.

Furthermore, we quantified the number of EMs by counting clearly visible striated muscles patches within the CTR from developmental stage E15.5 onwards. Although we occasionally observed EMs in wildtype or control animals, EM formation was signif-

icantly increased in *Npn-1*$^{Sema-}$ or *Npn-1*$^{cond-/-}$*;Olig2-Cre*$^{+}$ mutant embryos when compared to control littermates (Figure 4.9 A, B). To assess the mean spatial location of EMs within the CTR, we divided the whole the CTR in 16 fields and summed up EMs in each field by pooling all developmental stages of *Npn-1*$^{Sema-}$ or *Npn-1*^{cond}*;Olig2-Cre* diaphragms. Interestingly, myocyte fusion was higher in the left side of the CTR when compared to the right side. However, EMs also formed in all other areas of the CTR (Figure 4.9 C).

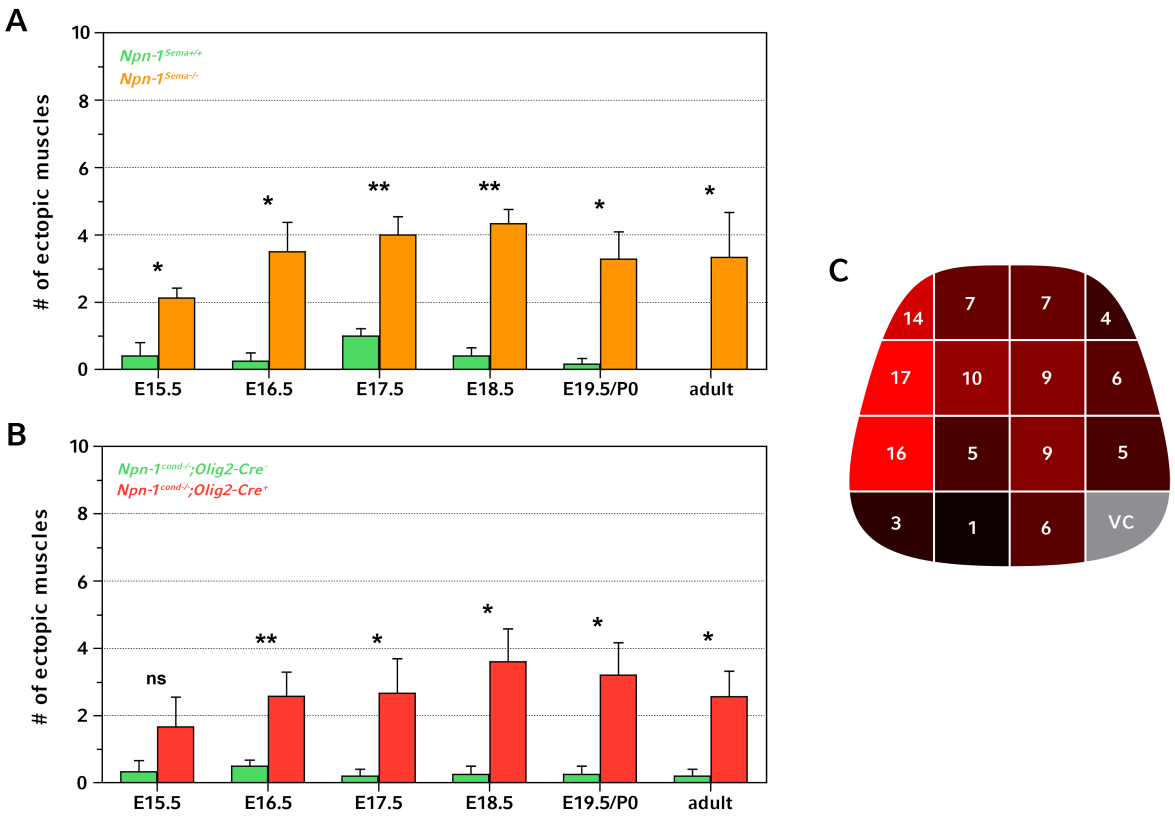

Figure 4.9: Quantification of EMs within the CTR during development and adulthood.

Quantification of EMs in *Npn-1*$^{Sema-}$ (A) and *Npn-1*^{cond}*;Olig2-Cre* (B) mouse lines revealed a slight, but not significant, increase of ectopic muscles from E15.5 till the beginning of muscle hypertrophy at E16.5/E17.5 (secondary myogenic wave), which slightly decreased during adulthood. EMs preferentially developed on the left side of the CTR (C). Ectopic muscles: *Npn-1*$^{Sema+/+}$ vs. *Npn-1*$^{Sema-/-}$ - E15.5: 0.40 ± 0.40, $n = 5$ vs. 2.13 ± 0.30, $n = 8$, $p \leq 0.05$; E16.5: 0.25 ± 0.25, $n = 4$ vs. 3.50 ± 0.87, $n = 4$, $p \leq 0.05$; E17.5: 1.00 ± 0.22, $n = 7$ vs. 4.00 ± 0.53, $n = 7$, $p \leq 0.01$; E18.5: 0.40 ± 0.25, $n = 5$ vs. 4.33 ± 0.42, $n = 6$, $p \leq 0.01$; E19.5/P0: 0.17 ± 0.17, $n = 6$ vs. 3.29 ± 0.81, $n = 7$, $p \leq 0.05$; adult: 0.00 ± 0.00, $n = 4$ vs. 3.33 ± 1.33, $n = 3$, $p \leq 0.05$ and *Npn-1*$^{cond-/-}$*;Olig2-Cre*$^{-}$ vs. *Npn-1*$^{cond-/-}$*;Olig2-Cre*$^{+}$ - E15.5: 0.33 ± 0.33, $n = 3$ vs. 1.67 ± 0.88, $n = 3$, $p = 0.36$; E16.5: 0.50 ± 0.17, $n = 14$ vs. 2.57 ± 0.72, $n = 7$, $p \leq 0.01$; E17.5: 0.20 ± 0.20, $n = 5$ vs. 4.00 ± 0.91, $n = 4$, $p \leq 0.05$; E18.5: 0.25 ± 0.25, $n = 4$ vs. 3.60 ± 0.98, $n = 5$, $p \leq 0.05$; E19.5/P0: 0.33 ± 0.33, $n = 3$ vs. 4.00 ± 0.71, $n = 4$, $p \leq 0.05$; adult: 0.20 ± 0.20, $n = 5$ vs. 2.56 ± 0.77, $n = 9$, $p \leq 0.05$). EM location: 119 muscles of 34 animals. Data represents the mean & SEM. Significance levels: * equals $p \leq 0.05$, ** equals $p \leq 0.01$, ns: not significant. Abbreviation: vc - vena cava.

4.5 Somatic motor neurons are not involved in normal muscle development but essential for EM formation

We next analyzed whether misprojected PN axons are the basis for EM formation. Therefore, we analyzed Olig2-Cre homozygote mutants at E16.5 that lack all somatic MNs due the replacement of exon 2 with the coding sequence for Cre recombinase (Dessaud et al., 2007). Whole-mount staining showed the absence of PN axons in Olig2$^{-/-}$ mutant animals when compared to wildtype littermates (Figure 4.10 A, B, arrow). Furthermore, the NMJ band at the midline within CoM is broadened (Figure 4.10 A', B'). Interestingly, costal diaphragm muscles are morphologically normal developed and span the entire thoracic cave (Figure 4.10 C, D). Nevertheless, CoM thickness of Olig2$^{-/-}$ mutant embryos is considerably reduced when compared to heterozygous control embryos (Figure 4.10 C', D'). This muscle thinning in mutant animals is accompanied by the loss of a muscle surrounding collagenous ECM (red), namely the epimysium (Figure 4.10 C', D'; arrow heads). The collagen rich epimysium normally provides a passive mechanical force at high muscle strains (Gao et al., 2008). However, we never observed EMs in the CTR of Olig2$^{-/-}$ mutant animals (n = 8).

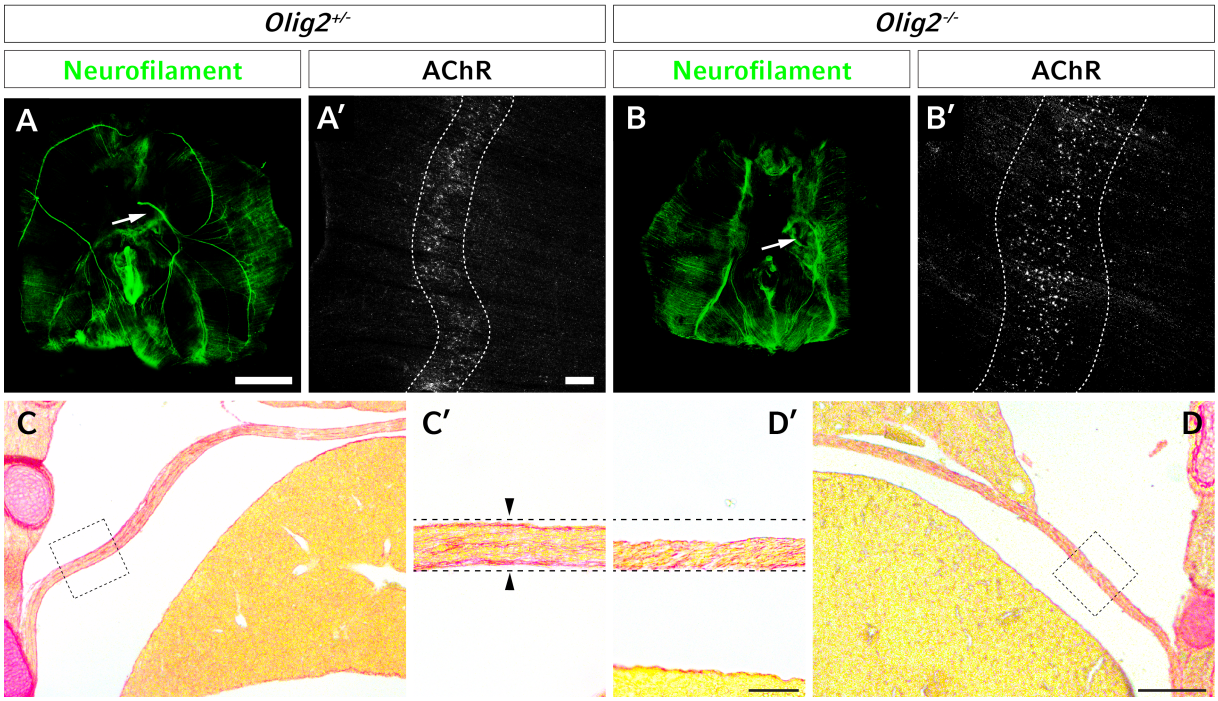

Figure 4.10: Complete removal of somatic MNs affects muscle development of the diaphragm.

Staining against neurofilament (A', B') and AChR (A', B') revealed the absence of PN axons in Olig2$^{-/-}$ mutant animals (B) leads to a broadening of the NMJ band (B') when compared to wildtype controls (A, A'). Picrosirius Red staining of frontal paraffin sections revealed a profound reduction of diaphragm muscle thickness in Olig2-Cre homozygote animals (D, D') when compared heterozygote controls (C, C'). Furthermore, wildtype diaphragms form a normal collagen rich epimysium (D', arrowheads), while mutant diaphragm do not. Scale bar: A, B - 1 mm; C, D - 500 µm; A', B', C', D' - 50 µm.

Thus, even if diaphragm muscles can form after ablation of somatic MNs, hypertrophy of myofibers is reduced. However, we did not observe any EMs in Olig2$^{-/-}$ mutant animals, which underlines the importance of misprojecting axons for ectopic MPC fusion within the CTR.

4.6 Ectopic muscles are likely to develop from muscle rather than transdifferentiation of tendon progenitor cells

To assess the underlying reason for EM formation, we investigated the localization of ectopic muscles within the CTR of the diaphragm. On the one hand, trans-differentiation of PPF fibroblasts, which migrate on the septum transversum and later form the CTR during development (Merrell et al., 2015), might cause EMs that are embedded within the CTR. On the other hand, migrating myoblasts may result in EMs, which lie directly on top of the CTR. Indeed, Picrosirius Red (PR) staining on frontal paraffin sections of mutant diaphragms at E16.5 indicates that newly formed muscles are located on top of the CTR (Figure 21A, B, arrow heads and dashed line, respectively), thus arguing for the latter. Polarization light microscopy on PR stained diaphragm sections furthermore revealed thick collagen I fibers below ectopic muscles (Figure 21A', B'; yellow-orange birefringence) which mark the highly organized collagenous CTR.

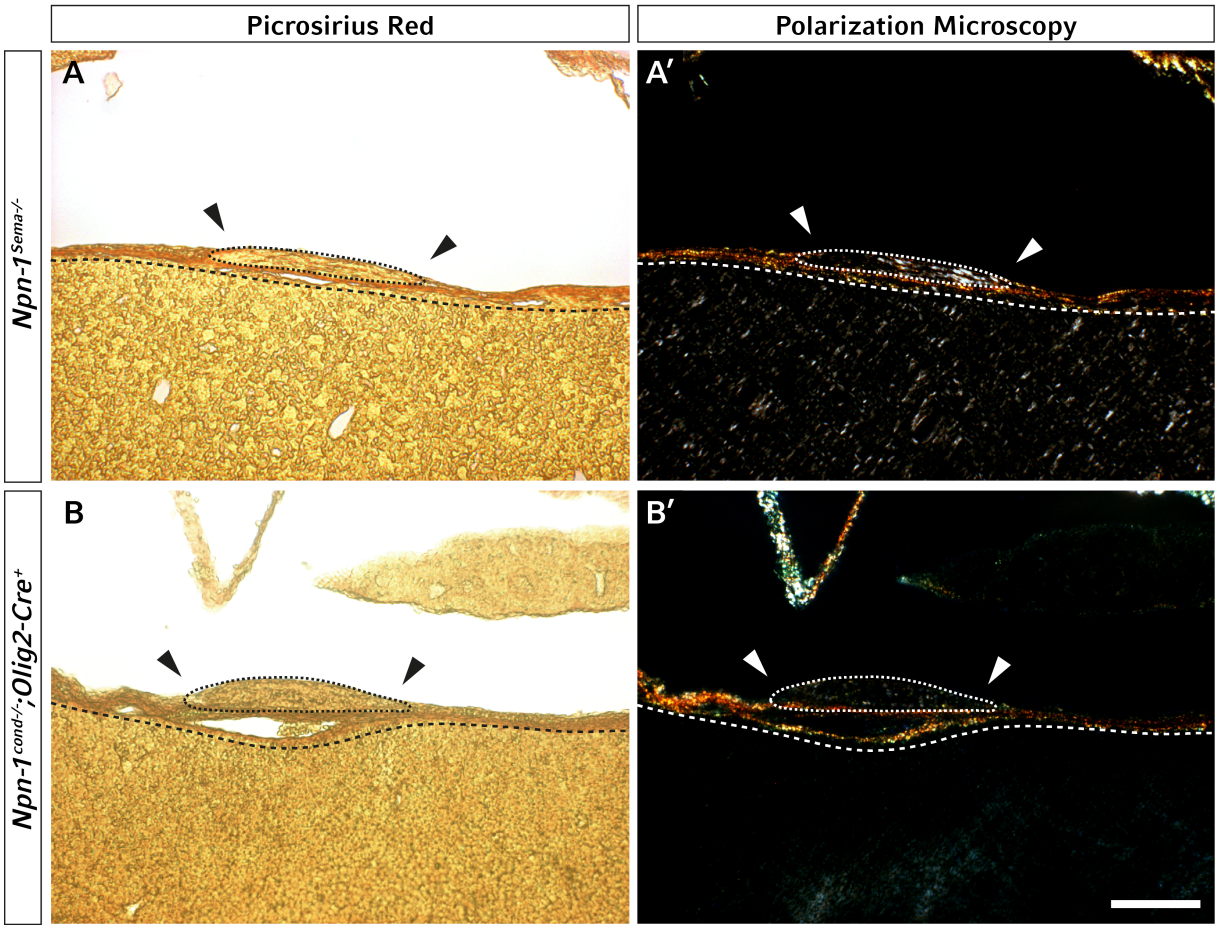

Figure 4.11: Rostral-caudal localization of EMs within the CTR.

Picrosirius Red staining (A, B) on frontal section of E16.5 *Npn-1*$^{Sema-}$ (A) and *Npn-1*^{cond}*;Olig2-Cre* (B) mutant embryos shows that ectopic muscles (dotted lines) are lying on top of the CTR (dashed lines) and are not surrounded by collagenous ECM (arrow heads). Polarization microscopy further underpinnes the results, as they stretch on top of birefringent collagen fibers of the CTR. Scale bar: 100 µm.

Taken together, PN axons are misguided at a significantly higher rate into the CTR of the diaphragm upon either systemic or motor neuron specific ablation of the Sema3-Npn-1 signaling pathway and innervate EMs which are formed in the CTR. These ectopic muscles appear to derive from MPCs that are mismigrating on top of tendinous tissue of the CTR. Given the fact, that ectopic muscles are also established upon motor neuron specific elimination of *Npn-1*, a direct effect of Sema3-Npn-1 signaling on migrating myoblasts appears unlikely and thus secondary effects of axons mismigrating into the CTR may cause EM formation.

4.7 Slits and Robo are expressed in pMN and myoblasts that will form costal muscles, respectively, during diaphragm development

Recent findings revealed a direct effect of Slit-Robo signaling not only on phrenic nerve fasciculation (Jaworski and Tessier-Lavigne, 2012), but Slit proteins which are released by the sclerotome, which is the source for later bones, were also shown to repel pioneering myoblasts during early embryonic development (Halperin-Barlev and Kalcheim, 2011). At later stages, migrating pioneering myoblasts are attracted by Slit proteins released by the tendon to guide them to their final destination (Kramer, 2001). We hypothesized that Slit-Robo signaling between motor neuron growth cones and pioneering and/or migrating myoblasts might be the underlying origin of ectopic muscle formation in *Npn-1*$^{Sema-}$ and *Npn-1*$^{cond-/-}$*;Olig2-Cre*$^{+}$ mutant mice.

To analyze whether Slit and Robo are expressed during the phase of diaphragm muscle generation and axon guidance, we performed *in situ* hybridization on spinal cord sections and the costal muscle during critical developmental time points. During diaphragm innervation, Slit2 (Figure 4.12 A”-D”) is strongly expressed in the majority of Scip^{+}/Isl1^{+} MNs in the phrenic nucleus between E10.5 to E12.5 and E15.5 (Figure 4.12 A-D). We also performed *in situ* hybridization against Slit1, which is strongly expressed in the floor plate but showed no noticeable expression in the ventral horn (data not shown).

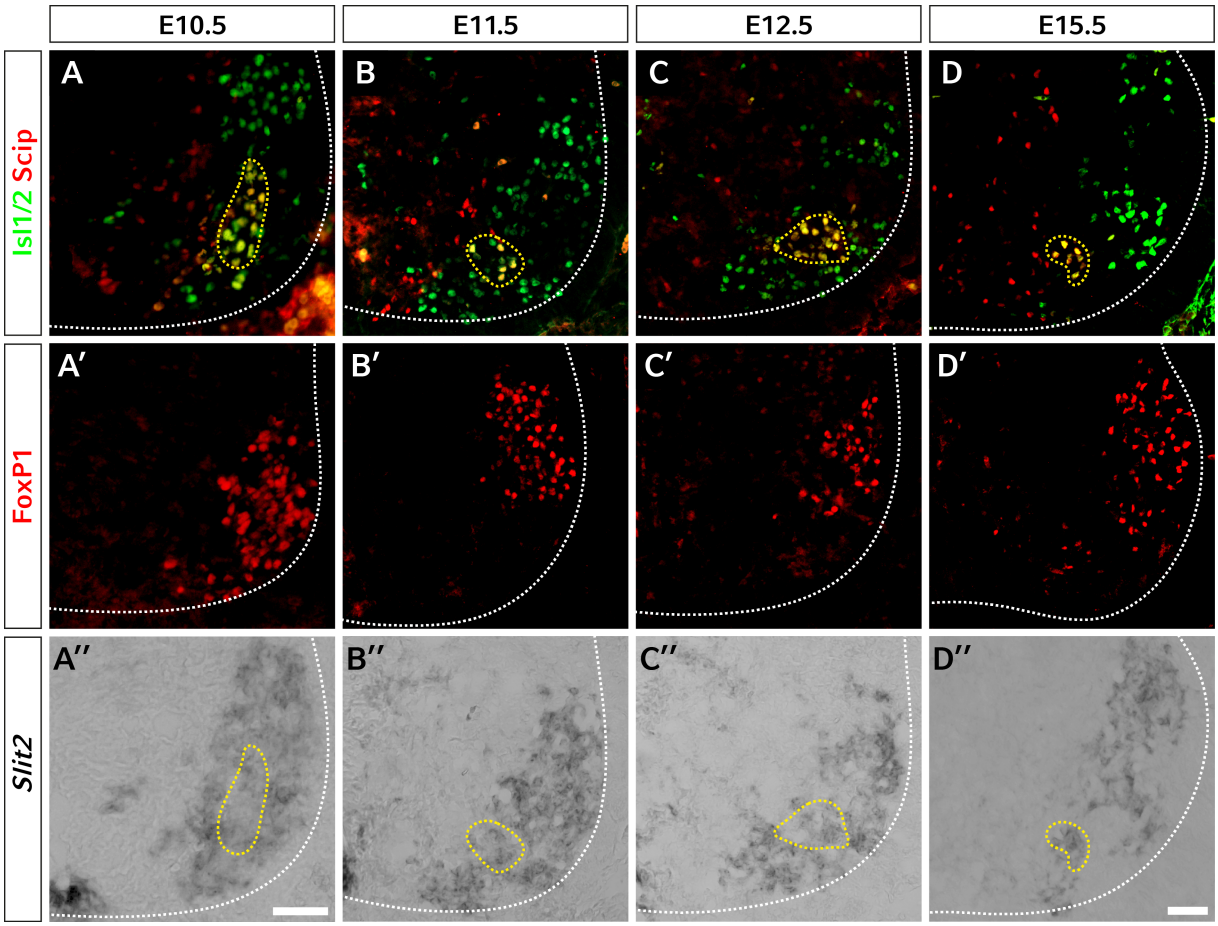

Figure 4.12: Expression of *Slit2* in the phrenic nucleus in the cervical spinal cord during targeting and innervation of the thoracic diaphragm.

ISH against *Slit2* (A" to D") and IHC against pMN (yellow dashed line) specific marker Isl1/2 and Scip (A-D) revealed a strong expression of *Slit2* during PN targeting (E10.5 and E11.5) and innervation of the thoracic diaphragm (E12.5 and E15.5). IHC against FoxP1 (A' to D'), a marker for limb innervating MNs of the LMC, was used to further specify the PMC. Scale bar: 200 µm.

Correspondingly, the Slit receptor *Robo1* (Figure 4.13 A') is expressed in Desmin$^+$ MPCs (Figure 4.13 A) at the developmental stage E15.5, when MPCs migrate and fuse on the septum transversum. In contrast, *in situ* hybridization against *Robo2* (Figure 4.13 B') showed no expression in Desmin$^+$ cells (Figure 4.13 B) of the costal diaphragm muscle, but a weak expression in the intermediate zone between the diaphragm muscle and the liver. *Robo* expression in costal diaphragm cells was further validated by qPCR on whole costal diaphragm RNA isolation at E14.5, which revealed an approximately 2-fold increased expression of *Robo1* when compared to *Robo2* (Figure 4.13 C).

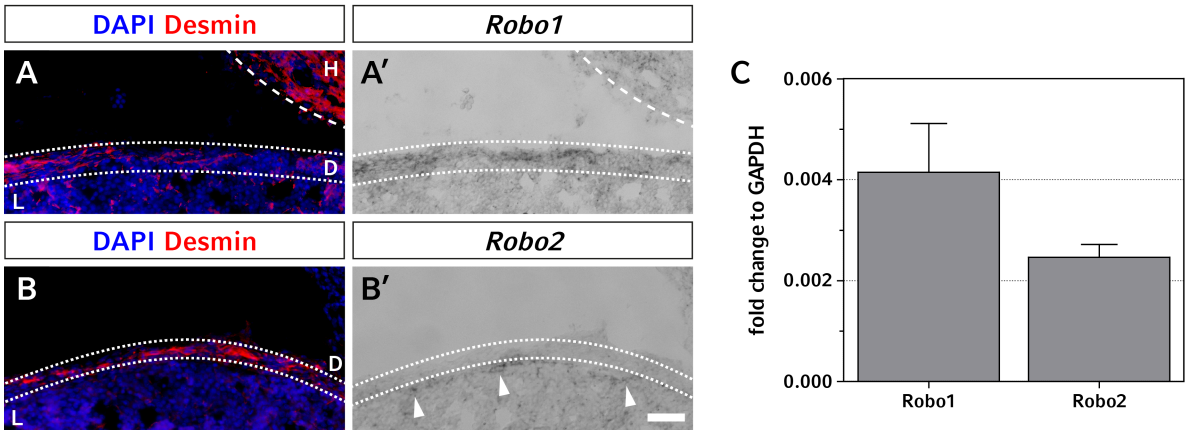

Figure 4.13: Expression of *Robo1* and *Robo2* in MPCs of the diaphragm during development.

ISH against *Robo1* and *Robo2* and IHC against Desmin$^+$ MPCs of the costal diaphragm muscle showed that *Robo1* (A') is expressed within the Desmin$^+$ cells of the CoM of the diaphragm (A). In contrast, *Robo2* (B') is expressed within cells of the intermediate zone between the diaphragm and the liver (B, B', arrow heads). *Robo* expression within MPCs of the CoM was further validated with qPCR and showed approximately 2-fold higher expression of *Robo1* when compared to *Robo2* (0.0042 ± 0.00056 vs. 0.0025 ± 0.00014; $n = 3$; p 0.05; Mean & SEM). H: heart, D: diaphragm, L: liver. Scale bar: 200 µm.

Thus, *Slit* and *Robo* mRNA is present in pMNs and myoblasts, respectively, at the time when EMs are generated, and might contribute to the formation of EMs in the CTR upon misguidance of phrenic axons into the CTR.

4.8 A subpopulation of primary MPCs is attracted by Slit1 and Slit2

To test our hypothesis of an attractive effect of Slit on MPCs, we performed chemotaxis experiments in vitro with freshly isolated primary MPCs from the CoM of the diaphragm in a transwell and 3D collagen matrix respectively. Purity of obtained costal muscle MPCs was validated by the muscle specific marker Desmin and quantification by FACS analysis showed that the majority of isolated pMPCs of E14.5 embryos were positive for Desmin (Figure 4.14 A, B).

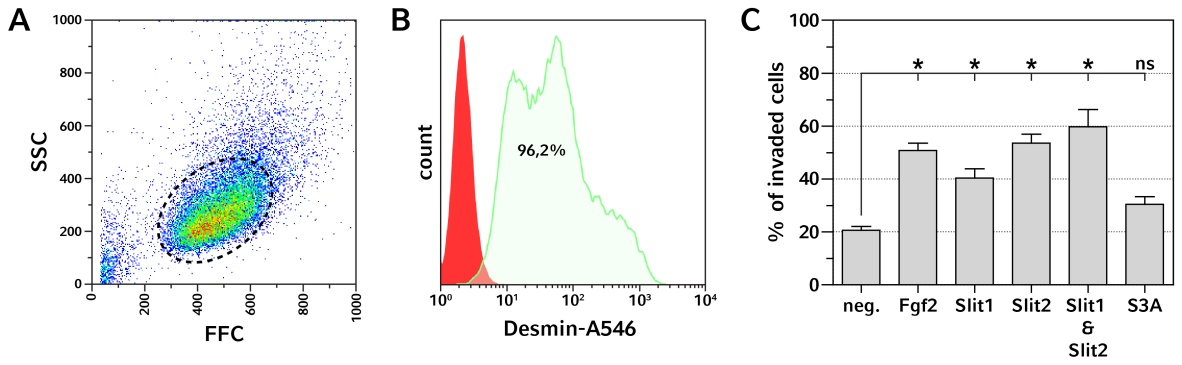

Figure 4.14: Characterization of primary MPCs and its response to chemokines.

Primary MPCs were tested by FACS analysis for Desmin$^+$ cells in isolated cells. Primary MPCs had a relatively homogenous size (A) and the majority of obtained cells were positive for the myogenic marker Desmin (B'). A transwell migration assay showed that Slit1 and Slit2, as well as the combination of both, are strongly attractive when compared to the negative control without any ligand. In contrast, Sema3A had no attractive effect of MPCs of the costal diaphragm muscle. FGF2, a known MPCs attractant served as a positive control (C). Percent of invaded cells: negative - 20.64 $\pm$ 1.50 %, Fgf2 - 50.80 $\pm$ 2.82 %, Slit1 - 40.39 $\pm$ 3.52 %, Slit2 - 53.53 $\pm$ 3.48 %, Slit1 and Slit2 - 59.79 $\pm$ 6.48 %; all $p \leq 0.05$; and Sema3A - 30.50 $\pm$ 2.80 %, $p = 0.057$; $n = 4$ for all experiments. Data represents the mean & SEM. Significance levels: * equals $p \leq 0.05$, ns: not significant.

To further analyze the functional effect of Slit ligands on MPCs, we carried out chemotaxis experiments in a 3D collagen I matrix. Primary MPCs which were not exposed to a chemotaxis gradient, did not show a high migration potential (Figure 4.15 A). Fgf2, a well-known attractant for myogenic cell lines (Bischoff, 1997; Corti et al., 2001), attracted 53 % of all cells, while 46 % of the cells did not show a repulsive or attractive response (Figure 4.15 B). Treatment with either Slit1 (Figure 4.15 C) or Slit2 (Figure 4.15 D) resulted in an increase to 29 % and 26 % of attracted cells, respectively. The combination of Slit1 and Slit2 further raised the proportion of attracted primary cells to 49 %. Intriguingly, a fraction of primary MPCs (pMPCs) is repelled by the combination of Slit1/2 (21 %) when compared to Slit1 (7 %) or Slit2 (0 %) alone (Figure 4.15 E). Interestingly, Sema3A did not lead to attraction of MPCs as already shown in transwell experiments, it moreover strongly repelled the majority (59 %) of primary MPCs (Figure 4.15 F).

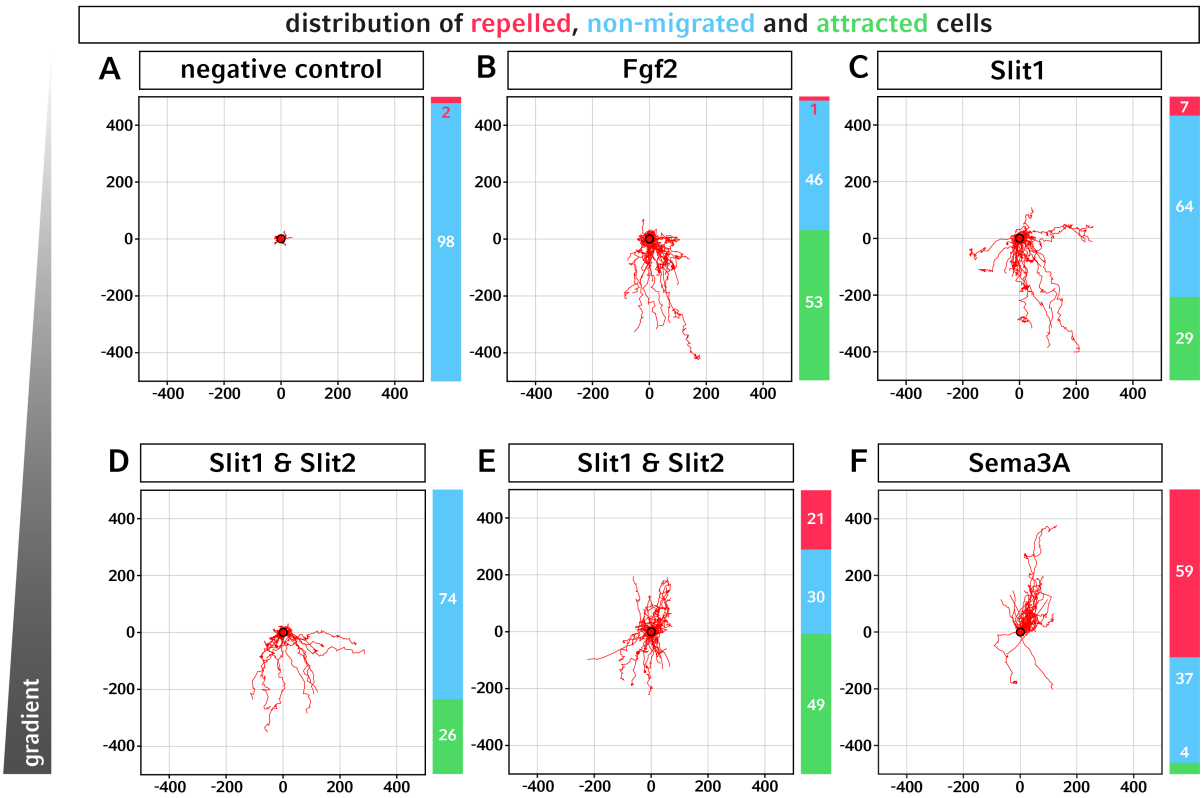

Figure 4.15: Chemotaxis assay of pMPCs in a 3D collagen matrix.

Chemotaxis assays with primary costal muscle MPCs of the diaphragm in a collagen I matrix reveals that approximately half of all cells are attracted by FGF2 (B) while cells without any chemo-kine are hardly attracted (A). In contrast, Slit1 (C) and Slit2 (D) attracted almost one third of MPCs. Exposure of primary cells to a combination of Slit1 & Slit2 further enhanced the attractive effect, while roughly one fifth turned towards repulsion (E). Interestingly, confronting MPCs to Sema3A strongly repelled the majority of cells (F). Scale bar in μm. Black centric circles illustrate non-migrated cells.

In addition, we calculated the forward migration index (FMI) (Figure 4.16 A) and the center of mass (COM) (Figure 4.16 B) of all cells after 24 h to quantify the direction of migration. While cells, which were not exposed to a gradient, showed a non-directed migration, FGF2 treatment strongly attracted pMPCs. Slit1 or Slit2 copied the attractive effect on migration of MPCs to a lesser extent, while combined exposure of Slit1 and Slit2 showed a non-directed migration for the whole cell population comparable to the negative control. Furthermore, quantification of the FMI and COM of Sema3A exposed pMPCs showed an even more drastic repellent effect.

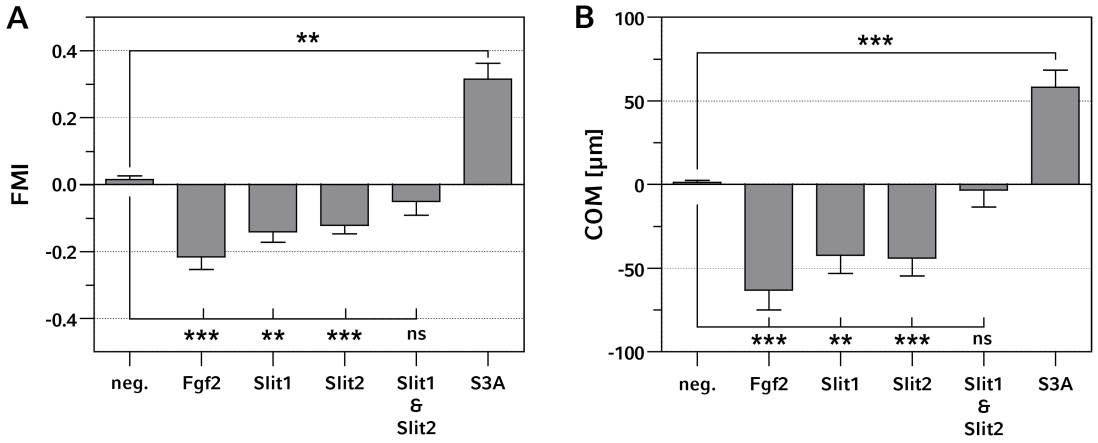

Figure 4.16: Quantification of FMI and COM of pMPCs during chemotaxis by soluble ligands.

Quantification of migrating cell efficiency and direction by determining the FMI (A) and COM (B) showed that FGF2, as well as Slit1 and Slit2 significantly attracted MPCs, while the FMI or COM did not change with the combination of both Slit proteins. Remarkably, Sema3A had a solid repulsive effect on MPCs in a 3D collagen matrix. FMI: negative - 0.015 ± 0.012, 45 cells; Fgf2 - -0.216 ± 0.039, 70 cells, $p \leq 0.001$; Slit1 - -0.141 ± 0.032, 75 cells, $p \leq 0.01$; Slit2 - -0.121 ± 0.026, 76 cells, $p \leq 0.001$; Slit1 and Slit2 - -0.050 ± 0.042, 67 cells, ns; Sema3A - 0.315 ± 0.047, 76 cells, $p \leq 0.001$. COM: negative - 1.41 ± 1.11; Fgf2 - -60.1 ± 11.8, $p \leq 0.001$; Slit1 - -42.4 ± 10.7, $p \leq 0.01$; Slit2 - -43.9 ± 10.8, $p \leq 0.001$; Slit1 and Slit2 - -3.2 ± 10.3, ns; Sema3A - 58.2 ± 10.3, $p \leq 0.001$; same cells numbers as FMI. Data represents the mean & SEM of four independent experiments. Significance levels: ** equals $p \leq 0.01$, *** equals $p \leq 0.001$, ns: not significant.

Taken together, a subpopulation of primary MPCs from E14.5 costal diaphragm muscles are attracted by Slit1 and Slit2, and the combination of both ligands results in a cumulative attractive effect, while Sema3A strongly repelled pMPCs.

4.9 *Npn-1^{Sema-}* and *Npn-1$^{cond-/-}$;Olig2-Cre^{+}* mutant neonates show increased lethality

In contrast to the moderate phenotype prior to diaphragm innervation and targeting, mutants of both used mouse lines revealed a severe increase of axon branching over the whole period of diaphragm development. Interestingly, both mouse lines are born in a normal Mendelian inheritance, however, only approximately 60 % of *Npn-1^{Sema-}* and 70 % of *Npn-1$^{cond-/-}$;Olig2-Cre^{+}* mutant embryos survive the first postnatal weeks (Gu

et al., 2003; Söllner, 2012). As deceased neonates appeared cyanotic, it might be possible that proper innervation of the diaphragm is not established during development. One indication of misdevelopment of correct synapse innervation is the broadening of the NMJ band at the midline of muscle, which could be shown in ETS related protein (Erm) or Agrin (Arg) mutant mice (Hippenmeyer et al., 2007; Tezuka et al., 2014). Therefore, we stained NMJs of costal diaphragm muscles with α-bungarotoxin at developmental stage E16.5 and determined the NMJ band width (Figure 4.17). Interestingly, even though we could observe a severe defasciculation of PN axons in the diaphragm, measurement of NMJ band width of *Npn-1*$^{Sema-}$ and *Npn-1*$^{cond-/-}$*;Olig2-Cre*$^{+}$ mutant embryos revealed no significant difference, when compared to control littermates.

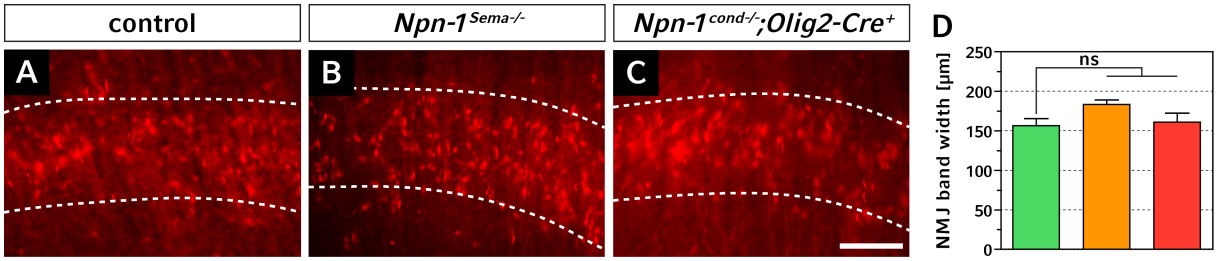

Figure 4.17: Manipulation of Sema3-Npn-1 signaling is not affecting NMJ band width in the CoM of the diaphragm.

α-bungarotoxin staining of NMJs within the center of costal diaphragm muscles at E16.5 revealed a similar patterning of NMJ bands of *Npn-1*$^{Sema-}$ (B) and *Npn-1*$^{cond-/-}$*;Olig2-Cre*$^{+}$ (C) mutant embryos when compared to control littermates (A). Measurement of the NMJ band width revealed no significant broadening of the NMJ band of both mutant mouse lines (*Npn-1*$^{Sema-}$: orange; *Npn-1*$^{cond-/-}$*;Olig2-Cre*$^{+}$: red) when compared to control embryos (D, green, $p>0.05$). Scale bar: 200 µm.

Thus, broadening of the central NMJ band within CoM of the diaphragm is arguably not the reason for neonatal death. Another possibility might be that the size or the length of EMs is affecting normal physiological contraction of the diaphragm in mutant animals. Therefore, we measured the area of EMs over all developmental stages and in adult mice.

Even though wildtype animals have significant less ectopic muscles when compared to *Npn-1*$^{Sema-}$ and *Npn-1*$^{cond-/-}$*;Olig2-Cre*$^{+}$ mutant embryos (compare Figure 4.9), quantification of the size showed no significant difference between mutant EMs and the very rarely occurring EMs in control embryos at the same stage (Figure 4.18 A, B). Although

EM size decreased significantly in *Npn-1*$^{Sema-}$ mutants during adulthood, EMs were still present, while we could not observe any EMs in adult wildtype animals (Figure 4.18 A). Furthermore, the length of muscle fibers is decisive for the total contractile magnitude, as the mean sarcomere length is varying around 1.6 and 2.6 µm depending of the current status of muscle contraction (Edman, 1979; Gordon et al., 1966). Consequently, we also measured the myofiber length of EMs in the midline and pooled the data of all developmental stages. We could not see any significant difference between *Npn-1*$^{Sema-}$ and *Npn-1*$^{cond-/-}$*;Olig2-Cre*$^{+}$ mutant embryos and their control animals concerning the length of EM myofibers (Figure 4.18 C).

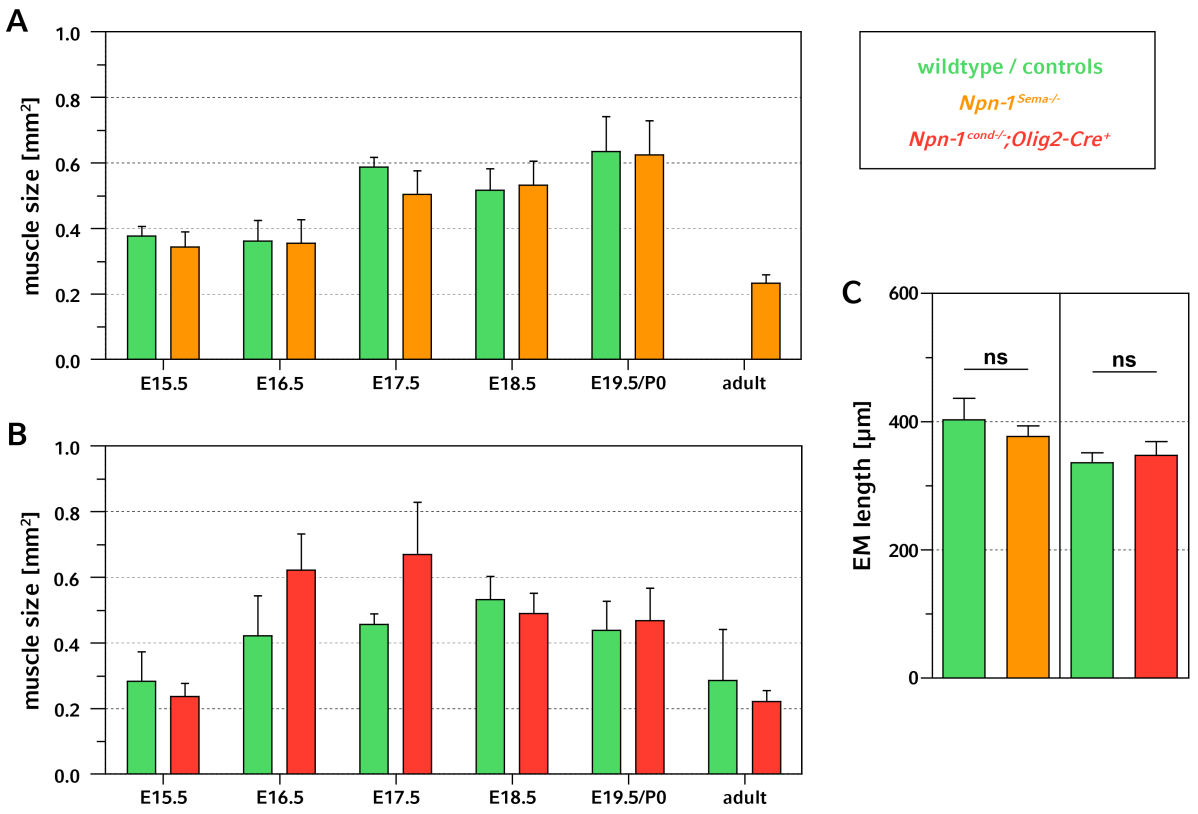

Figure 4.18: No difference of EM size and length between mutant and control embryos.

Even if EM were a very rare event in wildtype mice, comparison of EM size between wildtype animals was not different when compared to *Npn-1*$^{Sema-}$ (A) and *Npn-1*$^{cond-/-}$*;Olig2-Cre*$^{+}$ (B) mutants. *Npn-1*$^{Sema+/+}$ vs. *Npn-1*$^{Sema-/-}$: E15.5 - 0.377 ± 0.029 mm^2, n = 3 vs. 0.344 ± 0.046 mm^2, n = 4; E16.5 - 0.361 ± 0.063 mm^2, n = 4 vs. 0.354 ± 0.073 mm^2, n = 3; E17.5 - 0.587 ± 0.029 mm^2, n = 4 vs. 0.504 ± 0.071 mm^2, n = 23; E18.5 - 0.517 ± 0.065 mm^2, n = 3 vs. 0.532 ± 0.072 mm^2, n = 16; E19.5/P0 - 0.635 ± 0.107 mm^2, n = 3 vs. 0.625 ± 0.104 mm^2, n = 17; adult - 0 EMs, n = 3 vs. 0.233 ± 0.025 mm^2, n = 6. *Npn-1*$^{cond-/-}$*;Olig2-Cre*$^{-}$ vs. *Npn-1*$^{cond-/-}$*;Olig2-Cre*$^{+}$: E15.5 - 0.283 ± 0.090 mm^2, n = 3 vs. 0.236 ± 0.040 mm^2, n = 4; E16.5 - 0.421 ± 0.122 mm^2, n = 4 vs. 0.622 ± 0.111 mm^2, n = 6; E17.5 - 0.456 ± 0.032 mm^2, n = 5 vs. 0.670 ± 0.032 mm^2, n = 9; E18.5 - 0.532 ± 0.072 mm^2, n = 3 vs. 0.490 ± 0.063 mm^2, n = 15; E19.5/P0 - 0.438 ± 0.089 mm^2, n = 7 vs. 0.467 ± 0.099 mm^2, n = 13; adult - 0.286 ± 0.155 mm^2, n = 4 vs. 0.222 ± 0.033 mm^2, n = 16. Furthermore, EM length revealed no significant difference between mutant embryos of both mouse lines and their littermate controls. *Npn-1*$^{Sema+/+}$ vs. *Npn-1*$^{Sema-/-}$: 402.8 ± 33.4 µm, n = 7 vs. 376.9 ± 16.7 µm, n = 72 and *Npn-1*$^{cond-/-}$*;Olig2-Cre*$^{-}$ vs. *Npn-1*$^{cond-/-}$*;Olig2-Cre*$^{+}$: 335.8 ± 15.5 µm, n = 21 vs. 347.6 ± 21.17 µm, n = 50. Data represents the mean & SEM. $p > 0.05$ for all developmental stages, ns: not significant.

Although individual EM size and length of individual EMs was not different between *Npn-1*$^{Sema-}$ and *Npn-1*$^{cond-/-}$*;Olig2-Cre*$^{+}$ mutant and control embryos, the total EM area that occupies the CTR might be differing. We therefore calculated the cumulative EM area of each animal, by summing up all EM area values, and compared mutant to control

embryos. As the quantity of EMs for individual animals did not change significantly over the time course of development, we pooled all animals from stage E15.5 to E19.5/P0. Quantification of the cumulative EM area showed an approximate 2.4-fold increase for *Npn-1*$^{Sema-}$ and an 2.1-fold increase for *Npn-1*$^{cond-/-}$*;Olig2-Cre*$^{+}$ mutants when compared to their wildtype or control embryos (Figure 4.19).

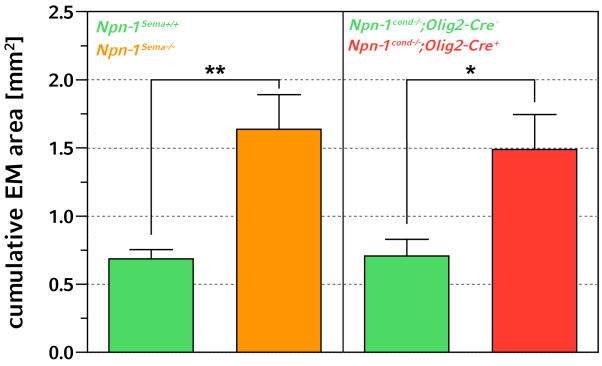

Figure 4.19: Mutant animals of both mouse lines have an increased cumulative EM area.

Quantification of the cumulative EM area of each animal revealed a significant increase of total EM area in *Npn-1*$^{Sema-}$ and *Npn-1*$^{cond-/-}$*;Olig2-Cre*$^{+}$ mutant embryos when compared to their control embryos. *Npn-1*$^{Sema+/+}$ vs. *Npn-1*$^{Sema-/-}$: $0.687 \pm 0.667\,mm^2$, n = 6 vs. $1.636 \pm 0.255\,mm^2$, n = 23, $p \leq 0.01$. N*Npn-1*$^{cond-/-}$*;Olig2-Cre*$^{-}$ vs. *Npn-1*$^{cond-/-}$*;Olig2-Cre*$^{+}$: $0.708 \pm 0.121\,mm^2$, n = 12 vs. $1.488 \pm 0.278\,mm^2$, n = 16, $p \leq 0.05$. Data represents the mean & SEM. Significance levels: * equals $p \leq 0.05$, ** equals $p \leq 0.01$.

Since not only the length or area of EMs, but also their orientation within the CTR in regard to the CoM of the diaphragm might influence successful force transmission of the diaphragm (Steffen et al., 2007), we measured the angle between native CoM fibers and ectopic myofibers. The results show that the majority of EM is orientated in an approximate 45° angle to diaphragm muscle fibers (Figure 4.20 A, B) of both *Npn-1*$^{Sema-}$ and *Npn-1*$^{cond-/-}$*;Olig2-Cre*$^{+}$ mutant embryos. Nevertheless, some EMs either aligned more or less in the direction of native CoMs or even adjusted an orthogonal position compared to CoM myofibers in both mutant mouse lines.

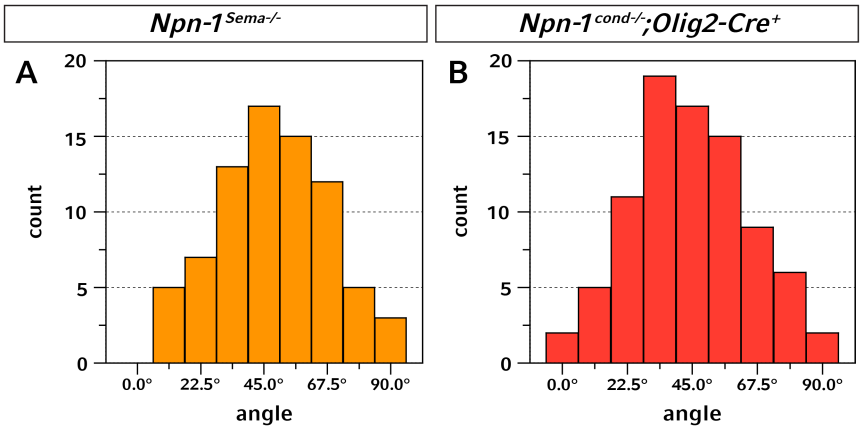

Figure 4.20: The majority of EMs show a nonlinear alignment towards CoM fibers.

Measurement of the relative orientation revealed, that the majority of EMs in both mutant mouse lines adapt approximately an 45° angle to costal muscle fibers (A, B). All developmental stages were pooled for quantification. *Npn-1*$^{Sema-}$: $48.56 \pm 2.17°$, n = 77 and *Npn-1*$^{cond-/-}$*;Olig2-Cre*$^{+}$: $44.32 \pm 2.21°$, n = 86; mean & SEM.

Taken together, *Npn-1*$^{Sema-}$ and *Npn-1*$^{cond-/-}$*;Olig2-Cre*$^{+}$ mutant embryos show no alteration of NMJ patterning at the midline of CoMs when compared to control embryos. Furthermore, EM size and myofiber length is not different between mutants of both mouse lines and the rarely occurring EMs in control animals. Nevertheless, due to the higher number of EMs in specific animals, mutant embryos show a significantly higher EM area than their controls. Furthermore, the orientation of EMs in correlation to CoM fibers is severely shifted and thus might be the reason for diaphragm disfunction in mutant animals.

4.10 Systemic ablation of Robo1 and Robo2 showed no ectopic muscle formation, but a severe misalignment of muscle fibers in the diaphragm

The Robo receptors 1 and 2 were shown to act redundantly during development of a plentitude of different tissues, e.g. the vascularization of the retina, pioneering longitudinal axons, or separation of cells during the formation of the foregut (Domyan et al., 2013; Farmer et al., 2008; Rama et al., 2015). Furthermore, Robo1/2 double

knockout animals have a reduced PN fasciculation and an impaired innervation of the thoracic diaphragm (Jaworski and Tessier-Lavigne, 2012). Therefore, we performed whole-mount IHC staining against Neurofilament and Actin on Robo1$^{+/+}$/Robo2$^{+/+}$ and Robo1$^{-/-}$/Robo2$^{-/-}$ diaphragms at developmental stage E16.5. Diaphragms of Robo1/2 wildtype animals showed normal innervation of the CoM at the midline of myofibers and myocyte fusion arrived at the sternum (Figure 4.21 A, A', arrow), though some PN axons that normally innervate the costal musculature branch into the CrM. In contrast, Robo1/2 mutant embryos revealed the mild defasciculation of PN axons that innervate costal myofibers that were already shown by Jaworski A. (Jaworski and Tessier-Lavigne, 2012). Furthermore, we could not observe any misprojecting axons into the CTR, but also no EM formation. Interestingly, however, the ventral proportion of the CoM was not fully developed at E16.5 (Figure 4.21 B, B', arrow).

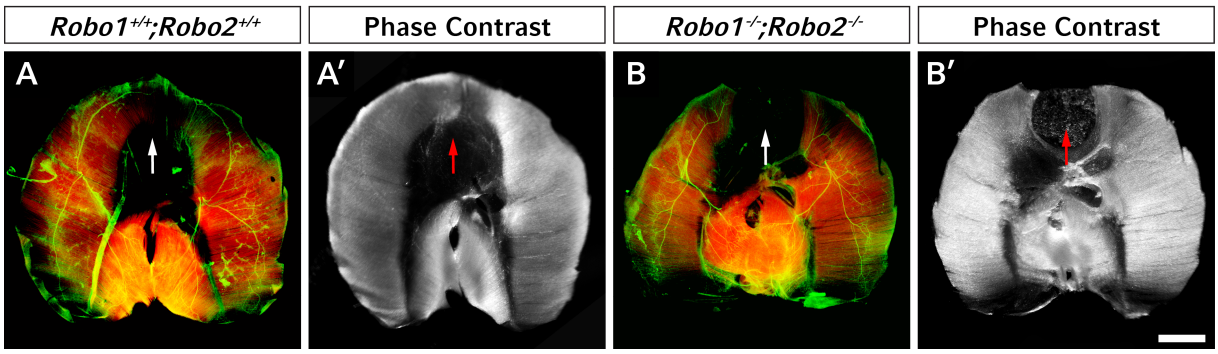

Figure 4.21: Robo1/Robo2 mutants have no misprojecting axons into the CTR, but also no ectopic muscle formation.

Whole-mount staining against Neurofilament and Synaptophysin (green) as well as Actin (red). At E16.5, wildtype diaphragm showed normal innervation and formation of the musculature (A, A', arrow). In contrast, diaphragms of Robo1/2$^{-/-}$ double mutant animals revealed a slightly different innervation pattern and, contrary to the wildtype situation, a misdevelopment of the ventral CoM (B, B', arrow). Robo1$^{+/+}$/Robo2$^{+/+}$: n = 3; Robo1$^{-/-}$/Robo2$^{-/-}$: n = 4. Scale bar: 1 mm.

It has been shown previously that the manipulation of Slit-Robo signaling has a severe effect on myoblast migration and subsequent myocyte fusion in Drosophila (Kramer, 2001; Steigemann et al., 2004). Nonetheless, no similar results have been reported for mammalian muscle development. Therefore, we took a closer look at myofiber organization within the musculature. Interestingly, Robo1/2 double mutant embryos (Figure 4.22 B', arrowheads) had a severe misalignment of myofibers when compared to their littermate controls (Figure 4.22 A', arrow heads). However, innervation of these

myofibers by PN axons seemed to be normal 4.22 A, B, asterisk).

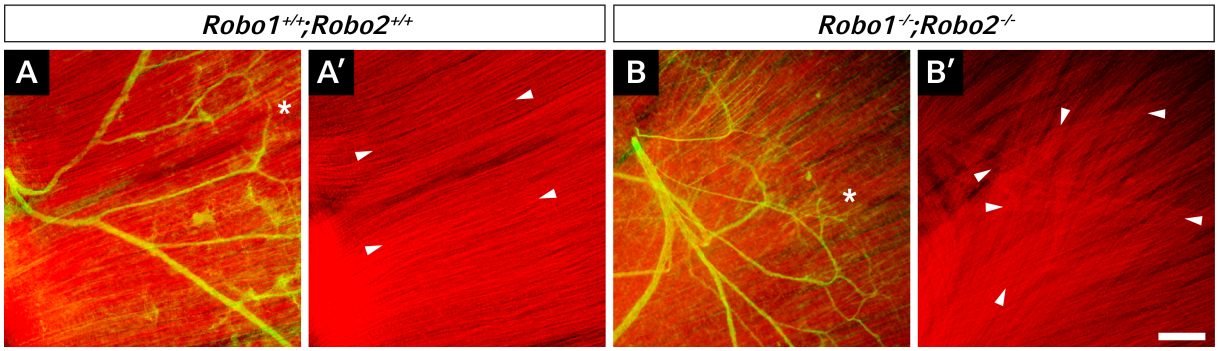

Figure 4.22: Robo1/Robo2 ablation leads to misalignment of CoM fibers.

Whole-mount staining against Neurofilament and Synaptophysin (green) as well as Actin (red). Diaphragm of wildtype animals have a normal alignment of muscle fibers (A', arrow head), while double mutant animals for Robo1/2 have a substantial unorganized myofiber appearance (B', arrow head). However, wildtype and mutant embryos showed a normal innervation by PN axons (A, B, asterisk). Robo1$^{+/+}$/Robo2$^{+/+}$: n=3, B'). Robo1$^{-/-}$/Robo2$^{-/-}$: n=4. Scale bar: 200 µm.

Thus, systemic ablation of Robo1 and Robo2 leads to significant increase of PN defasciculation within the thoracic diaphragm, but no axons are misguided into the CTR and as a consequence, also no EMs are formed. However, myofibers of the CoM are rigorously misaligned.

Chapter 5

Discussion

Development and maturation of neuronal circuits are pivotal for functional innervation of muscles and thereby the viability of any organism. Uncovering the underlying mechanisms of peripheral nerve pathfinding during development thus ultimately may be beneficial for treatment of various self-acquired or genetic deficits, such as paraplegia or nerve-muscle related diseases like amyotrophic lateral sclerosis (ALS) or progressive muscular atrophy (PMA), which also result in impairment of breathing due to the loss of motor innervation and subsequent degeneration of the thoracic diaphragm. Understanding the complete genetic fundament of phrenic nerve and diaphragm development is thus crucial to establish treatments for developmental or postnatal degenerative diseases. Therefore, we employed two different genetic approaches to uncover the influence of Sema3-Npn-1 signaling on PN targeting of the PPF and branching within the diaphragm. Intriguingly, phrenic axons not only misprojected into the CTR, but, unexpectedly, also innervated ectopic musculature, thus raising questions concerning the primary mechanisms for (ectopic) muscle formation.

5.1 Sema3-Npn-1 signaling is not involved in early targeting of the PPF

Prevention of functional signaling between class 3 Semaphorins and its receptor Npn-1 leads to premature ingrowth into the developing limb bud, defasciculation of limb innervating sensory and motor projections, and axon pathfinding defects during the development of neuronal circuits (Huber et al., 2005; Huettl et al., 2011). We show here that a

proportion of somatic motor neurons of the phrenic nucleus express *Npn-1* during axon targeting towards the brachial plexus, their stopover at the PPF and the final branching within the developing diaphragm musculature. Systemic or motor neuron specific elimination of Sema3-Npn-1 signaling causes a slight defasciculation of all spinal nerves, most likely also axons of both phrenic nerves, within the brachial plexus region, however, it does not affect fasciculation of the PN to one distinct branch or targeted growth towards the PPF. Nonetheless, we could not quantify defasciculation of PN projections due to the impossibility to clearly distinguish PN axons from other axonal tracks within the brachial plexus. Modern three dimensional reconstruction of high resolution confocal microscopy images might allow the discrimination of brachial and phrenic nerves.

Our data indicates that PN axons utilize different guidance mechanisms than projections of the LMC in the brachial plexus to avoid a black-out or an intermixture of axon tracts of both respiratory and locomotor systems upon loss of one peripheral axon guidance system. Interestingly, systemic deletion of the homebox transcription factor Hb9, for example, leads to a severe misprojection of various classes of somatic MNs at brachial levels, including pMNs. In Hb9 knockout embryos, PN axons might be redirected into the limb bud during early development (Arber et al., 1999; Thaler et al., 1999). However, pMNs might even not be specified, as Hb9 is mainly expressed in motor neuron progenitor cells and acts as an important transcription factor for MN migration and settling in the ventral horn of the spinal cord (Arber et al., 1999). Furthermore, hypomorphic embryos for the transcription factor Isl1 phenocopy the reduction of MNs of the MMC, and possibly of the PMC, which results in misguidance of LMC neurons and, intrestingly, a complete absence of PN projections (Liang et al., 2011). In contrast, the columnar organization of somatic MNs also influences directed target innervation, as systemic deletion of the transcription factor FoxP1 leads to an extensive increase of neurons within the MMC, including neurons of the PMC, which ultimately leads to an increase of phrenic nerve thickness due to an excess of pMNs (Rousso et al., 2008). Similar PN guidance defects into the limb or epiaxial mesenchyme in *Npn-1*$^{Sema-}$ and *Npn-1*$^{cond-/-}$*;Olig2-Cre*$^{+}$ mutants cannot be completely excluded. Such guidance defects might be uncovered by the combination of retrograde tracings of limb/epaxial projecting axons and specific neuronal markers of the phrenic nucleus in combination with the comparison of axon count of both PNs (Helmbrecht et al., 2015). One mechanism that

might possibly govern early fasciculation and/or targeting of the PN is the interaction of the transmembrane glycoprotein Alcam (activated leukocyte cell adhesion molecule) as it is specifically expressed at brachial levels in motor neurons of the phrenic nucleus (Philippidou et al., 2012). However, mice with systemic deletion of Alcam have only a mild defasciculation of axons, including intercostal nerves, and are viable, which renders the function of Alcam as a specific PN guidance mechanism unlikely (Dillon et al., 2005; Weiner et al., 2004).

Thus, PN axons are not affected like axons originating from the LMC that innervate limb musculature in *Npn-1*$^{Sema-}$ and *Npn-1*$^{cond-/-}$*;Olig2-Cre*$^{+}$ mutant mice (Huber et al., 2005; Huettl et al., 2011). As Sema3-Npn-1 signaling is not involved in guidance of PN axons towards the PPF, unbiased experiments that compare the level of gene expression between limb mesenchym and PPFs, in combination with retrograde labeling of pMNs, by microarray or next generation sequencing might uncover promising candidate genes that are involved in axon guidance, and are not affecting cell specification and/or neuron survival.

5.2 Systemic and MN-specific ablation of Sema3-Npn-1 signaling shows a severe effect during innervation of the diaphragm musculature

In contrast to the moderate phenotype prior to diaphragm innervation and targeting, mutants of both used mouse lines revealed a severe increase of axon branching over the whole period of diaphragm development. Interestingly, both mouse lines are born in a normal Mendelian inheritance, however, a high percentage of mutant embryos do not survive the first postnatal week (Gu et al., 2003; Söllner, 2012), which provides evidence for a neonatal and not a developmental effect. The high incidence of neonatal lethality might indicate that the degree of defasciculation and therewith myofiber innervation might have an effect on neonatal survival. For example, in animals where the transcription factor Hox5 or the receptor Unc5c (Unc-5 homolog C (C. elegans)) were mutated, a substantial reduction of costal muscle innervation of the diaphragm was observed, which leads to neonatal cyanosis (Burgess et al., 2006; Philippidou et al.,

2012). Interestingly, other members of the netrin signaling pathways, such as Deleted in colorectal cancer (Dcc), Neogenin (Neo1) and Netrin1 (Ntn1), also seem to have an effect on PN branching within the diaphragm (Burgess et al., 2006). Furthermore, systemic ablation of erbB2, a receptor tyrosine kinase results in a similar defasciculation of the PN during innervation of both diaphragm muscles. In contrast to *Npn-1*$^{Sema-}$ and *Npn-1*$^{cond-/-}$*;Olig2-Cre*$^{+}$ mutant embryos, however, deletion of erbB2 leads to a degeneration of NMJs from E14.5 onwards due to the complete loss of NMJ stabilizing Schwann cells and thus results in neonatal death (Lin et al., 2000; Morris et al., 1999). Intriguingly, conditional gain-of-function experiments with early (Myo-Cre^{+}) or later (HSA-Cre^{+}) muscle specific stabilization of β-catenin showed a likewise strong increase of PN branching which is related to a broadening of the centered NMJ band (Liu et al., 2012; Wu et al., 2012). It is unlikely that neonatal death of *Npn-1*$^{Sema-}$ and *Npn-1*$^{cond-/-}$*;Olig2-Cre*$^{+}$ mutants is caused by such NMJ destabilization and band broadening, as the majority of both neonatal mutant pups are vital and did not show any NMJ defects. In contrast to an apparent increase of PN branching within the diaphragm musculature after ablation of systemic or MN specific Npn-1 signaling, double knock-out of the receptor tyrosine phosphatases D and S (PTPRD and PTPRS) in mice also show normal PPF targeting but completely lack initial branching and therewith later innervation of diaphragm muscles (Uetani, 2006). Interestingly, this lack of myofiber innervation by PN axons resulted in a similar thinning of costal diaphragm muscles observed in Olig2 mutant embryos and therefore underlines the independence of primary muscle development from functional innervation by MN axons.

Thus, Sema3-Npn-1 signaling acts cell-autonomously during diaphragm innervation on PN axon branching throughout diaphragm development while NMJ formation is normal. Furthermore, neonatal lethality of both investigated mouse lines is more likely caused by another effect, most likely diaphragm disfunction caused by ectopic muscle formation.

5.3 Ectopic muscles in the CTR of the diaphragm are innervated by misrouted axons of the PN after ablation of Sema3-Npn-1 signaling

Diaphragm misdevelopment causes e.g. hernias, which in turn cause neonatal lethality due to the inability to breathe and a displacement of abdominal organs to the thoracic cave (Merrell et al., 2015). Interestingly, while we found no hernias in our mutant embryos, we observed significantly higher numbers of PN axons that occasionally projected into the CTR, and the majority of these misguided axons innervated EMs. One explanation for the lack of ectopic myocyte fusion might be that cells in the periphery of ectopic growth cones are either not mitotically active or initially to few to provide a sufficient cell density and thereby cell-cell contact for myocyte fusion. It has been reported that fusion of myocytes, at least *in vitro*, depend on cell density and a variety of extracellular released molecules (Konigsberg, 1971; Tanaka et al., 2011). It would be interesting, if ectopic growth cones without maturated myofibers are at least surrounded by MPCs during development of the diaphragm CTR. However, it can be assumed that misprojected axons that don't innervate EMs later degenerate due to a missing trophic support (Luo and O'Leary, 2005). Furthermore, EM size is significantly reduced in adult wildtype as well as mutant animals. This might have two underlying possibilities: First, more myofibers are formed that can't be functionally innervated by ectopic axons or second, all ectopically fused myofibers are initially innervated but NMJs are not stabilized neonatally. Both mechanisms would lead to a muscle atrophy during adulthood (Glass, 2005; Jackman, 2004). Nevertheless, the majority of EM patches were maintained until late adulthood, which implies a functional innervation by the PN.

This formation of EMs raises the question whether misguided axons or mismigrated MPCs initiate the process of EM formation? The development of these EMs might have different causes: First, transdifferentiation of tendon progenitor cells or fibroblasts of the PPF to MPCs or directly into myoblasts caused by yet unknown secreted cues of the misprojected growth cones. Second, another possible reason is the attraction and/or condensation of migrating myoblasts towards the growth cones of misguided PN axons and a following cellular fusion to myofibers.

The current opinion of diaphragm muscle development consists of pioneering myoblasts that delaminate from the ventrolateral lip of the dermomyotome and migrate to their final mesenchymal compartment to provide a target point for following mitotically active myoblasts which then will fuse to myofibers (Babiuk et al., 2003; Dietrich et al., 1999; Merrell et al., 2015). Furthermore, recent findings revealed the importance of GATA4^{+} PPF fibroblasts for normal development of the diaphragm, by supporting proliferation and suppressing apoptosis of MPCs (Merrell et al., 2015).

We favor a migratory mechanism of MPCs due to the position of EMs on top of the CTR. It might be possible, that this mismigration of MPCs is caused by the lack of Sema3-Npn-1 signaling in *Npn-1*$^{Sema-}$ mutant embryos. Considering that tissue-specific ablation of Npn-1 receptors in pMNs mimics both aberrant projections into the CTR and EM formation of systemically abolished Sema3-Npn-1 signaling, the direct involvement of this pathway in MPC migration is, however, doubtful. Therefore, a secondary mechanism, which is independent of Sema3-Npn-1 signaling, might be the reason for mismigration of MPCs into the CTR and subsequent myocyte fusion. This signaling could be mediated by secreted ligands or by direct interaction of growth cones and MPCs during innervation of developing (ectopic) muscles.

One possibility for secreted ligands by phrenic growth cones would be Sema3A, as *in vitro* experiments with mouse myoblasts cell lines indicated that Sema3A can upregulate Myogenin (Suzuki et al., 2013), which is an indispensable transcription factor during skeletal muscle development (Nabeshima et al., 1993). Sema3A is also expressed in the phrenic nucleus (data not shown) and its secretion from misprojecting growth cones into the CTR might induce myogenesis in PPF fibroblasts within the CTR by the induction of a similar myogenic pathway. Contrary, chemotaxis assays with recombinant Sema3A revealed a strongly repulsive effect on Npn-1 expressing MPCs and therefore condensation of MPCs around misproject growth cones is implausible.

Contact mediated fusion of myocytes that is initialized by the interaction with MN growth cones is another possibility. Even if a direct ligand-receptor system that stimulates myocyte fusion is currently unknown, conditional stabilization of β-catenin in skele-

tal muscle cells interestingly results not only in an increased branching of the PN along the costal muscles of the diaphragm, but also in establishment of EMs in the CTR that formed NMJ bands and were innervated by misprojecting axons from the PN (Wu et al., 2012). The authors postulated that newly formed EMs attract misprojecting axons during development of the diaphragm from E14.5 onwards. In contrast, we observed misprojecting axons as early as E13.5, before fused myofibers were visible at E15.5. This discrepancy illustrates that the sequence of muscle development and its innervation has to be further elucidated.

To this end, our results demonstrate that a cell-autonomous effect of Sema3-Npn-1 signaling governs PN fasciculation during diaphragm muscle innervation, while a direct involvement of Npn-1 in EM formation is rendered highly unlikely. Nevertheless, the specific function of Sema3-Npn-1 signaling during muscle development is currently unknown.

5.4 Diaphragm myoblasts from costal muscles are attracted by Slits

Due to a cell-autonomous effect of Sema3-Npn-1 signaling in PN branching and ectopic muscle formation in the diaphragm, we hypothesize a secondary, underlying mechanism that causes misguided myoblast migration and later fusion. The tight interaction of migrating pMN growth cones and myoblasts provides a tightly specified microenvironment and therefore can also influence myoblast migration. This delamination and migration of pMPCs from the dermomyotome (DM) to their final targets is crucial for the correct patterning of the musculoskeletal system. Disturbance of native guidance signals, such as SF/HGF-c-Met signaling, or ablation of its upstream transcription factors like Pax3 or Lbx1, lead to severely impaired skeletal muscle phenotypes (Brohmann et al., 2000; Dietrich et al., 1999; Swartz et al., 2001), and therewith also perturb diaphragms formation (Babiuk et al., 2003; Babiuk and Greer, 2002).

Recent findings revealed a direct effect of Slit-Robo signaling not only on phrenic nerve fasciculation (Jaworski and Tessier-Lavigne, 2012), but sclerotome-released Slit

proteins were also shown to repel pioneering myoblasts during early embryonic development (Halperin-Barlev and Kalcheim, 2011). At later stages, migrating pioneering myoblasts are attracted by Slit proteins released by the tendon to guide them to their final destination (Kramer, 2001). We hypothesized that Slit-Robo signaling between motor neuron growth cones and pioneering and/or migrating myoblasts might be the underlying origin of ectopic muscle formation in *Npn-1*$^{Sema-}$ and *Npn-1*$^{cond-/-}$*;Olig2-Cre*$^{+}$ mutant mice. In wildtype animals, migrating myoblasts might be attracted by Slit that is potentially released from the myotendinous junction between the CTR and costal muscles. In addition, Slit, secreted by motor neuron growth cones during muscle innervation concentrates at the NMJ band (Figure 5.1 A) and may act as a migration target for secondary myogenesis, as *Olig2* mutants, in which all somatic motor neurons and their projections are absent, show a significantly thinned diaphragm muscle. In contrast, misprojecting PN axons into the CTR in embryos with systemic or motor neuron specific ablation of Sema3-Npn-1 signaling may continue to release a high level of Slit proteins which subsequently might pull some myoblasts out of the developing costal muscles as axons aberrantly invade the tendon region. Within the newly formed microenvironment, which is composed of MN growth cones and myoblasts, ectopic muscles are formed by myoblast fusion due to autocrine signaling between neighboring myoblasts and/or paracrine trophic support provided by ectopic growth cones of the PN (Figure 5.1 B). Nonetheless, verification of spatial expression of Slit proteins is mandatory. However, available antibodies against Slit1 or Slit2 did not bind on embryonic cryosections and ISH against Slits is not feasible as transcripts are mostly located within the soma. Possible methods that could visualize Slit expression would include direct fluorescence tagging by creating fusion proteins or indirectly by ALP-tagged purified Robo receptors.

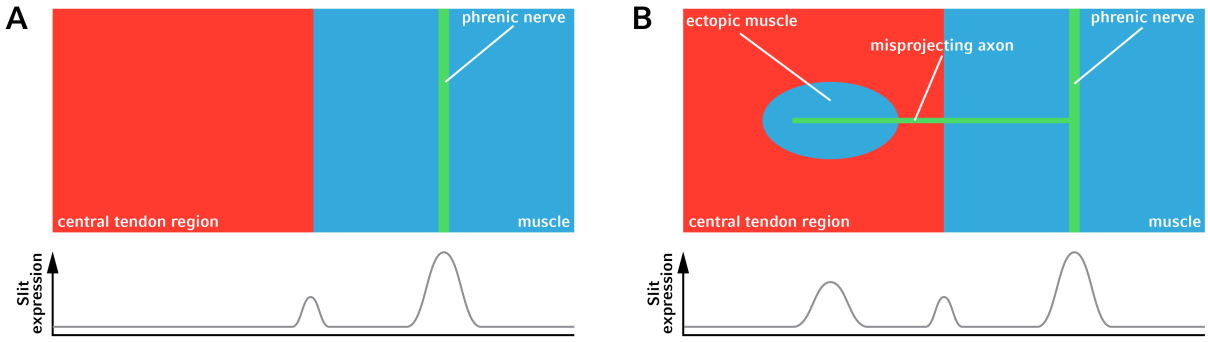

Figure 5.1: Hypothesis of EM formation in the CTR of the diaphragm.

Schematic view of hypothetical phrenic nerve and myoblast interaction during diaphragm development. In wildtype embryos, Slit is released from cells of the PPF at the border between CTR and premature muscle. In addition, Slit is also accumulated in the proximity of PN growth cones at the midline of newly formed costal muscles where it attracts resident MPCs (A). In *Npn-1*$^{Sema-}$ and *Npn-1*$^{cond-/-}$*;Olig2-Cre*$^{+}$ mutant animals, axons that misproject into the CTR continue to release Slit and pull out some resident MPCs, which later fuse to striated myofibers (B).

We could provide a first indication that Slit1 and Slit2 have an attractive effect on *in vitro* cultured pMPCs of the developing costal diaphragm muscles. Beside our postulated mechanism of MPC guidance by MN growth cones *in vivo*, axonal-derived Slit2 could also be involved in NMJ stabilization, as muscle intrinsic Slit2 can compensate NMJ formation when β-catenin is deleted in a skeletal actin background (Wu et al., 2015). Therefore, Slit2 might be essential for anterograde as well as retrograde signaling between axonal tips and myocytes.

Interestingly, some primary cells turn towards repulsion when Slit1 and Slit2 proteins are combined, which possibly relies on receptor complex formation of Robo and their coreceptors and therewith modification of downstream signaling (reviewed in (Ypsilanti et al., 2010)). Nevertheless, it is unlikely that axonal-derived Slit1 has a major role *in vivo*, as it is not expressed in the ventral horn of the spinal cord during innervation of the diaphragm (Jaworski and Tessier-Lavigne, 2012). In contrast, Slit, which is released from the midline in Drosophila, is involved in early repulsion of MPCs (Kramer, 2001). Furthermore, it seems that Slit-mediated repulsion during delamination of MPCs from the dermomyotome is phylogenetically conserved, as Slit1 directs the migration in a somite-intrinsic manner in avian (Halperin-Barlev and Kalcheim, 2011). Remarkably, initial Slit-mediated repulsion of MPCs turns towards attraction at the future MAS. The

main source of Slit during myocyte attraction in later development seems to be cells in the MASs, likely tendon progenitor cells (Kramer, 2001).

Therefore, Robo^{+} MPCs might be initially repulsed from the DM by sclerotome-released Slit1 and subsequently captured by Slit2-releasing MN growth cones that project towards their final targets. It is unlikely that axonal Slit affects guidance of MPCs during the primary myogenic wave, as ablation of all motor neurons, by deletion of its Olig2^{+} progenitors, is not affecting overall diaphragm muscle formation, even though costal diaphragm muscles are weakened, which favors the involvement of MN axons in muscle hypertrophy. Remarkably, muscle formation was altogether normal when Robo1/Robo2 or Slit2 were systemically abled, while PN axons were severely defasciculated (personal communication with Alexander Jaworski and (Jaworski and Tessier-Lavigne, 2012)). Nevertheless, MPCs might be especially sensitive to extracellular Slit signals during the secondary wave of myogenesis and misguided PN axons into the CTR by disturbance of Sema3-Npn-1 signaling is responsible for EM formation. However, only Slit2 ablation in MNs or deletion of Robo1/2 in MPCs, in combination with axon guidance disturbance, can elucidate the underlying mechanisms of Slit-Robo signaling *in vivo*.

5.5 Ectopic muscles might be the cause of neonatal lethality after manipulation of Sema3-Npn-1 signaling

Approximately 40 % of *Npn-1*$^{Sema-}$ and 30 % of *Npn-1*$^{cond-/-}$*;Olig2-Cre*$^{+}$ mutants die neonatally, which might be caused by EMs that impair normal diaphragm muscle function (Söllner, 2012; Gu et al., 2003). If EMs are the reason of neonatal lethality it is most likely due to the misalignment of EM fibers to costal myofibers that can decrease the overall contractibility of the diaphragm and therewith total available lung volume. Furthermore, the majority of EMs develop on the left side of the CTR and the cumulative EM area is significant higher in both mutant mouse lines when compared to wildtype mice.

An indirect method to detect affected breathing possibly caused by EMs in mutant animals would be a lung functionality test to compare lung volumes of mutant and wildtype animals. However, another potential approach would be the simulation of diaphragm contraction by a finite element model, where EMs could be inserted as disturbance elements. Additionally, electromyography and electroneuronography on single muscle fiber and misprojecting PN axons, which would be a challenging experimental setup due to the small size and frailty of the tissues, could provide evidence for functionality. Nevertheless, it might be the combination of EMs and misinnervation of the costal muscle proportion which provoke neonatal death.

Chapter 6

Conclusion & Outlook

Taken together, Sema3-Npn1 signaling plays only a minor role during early PN targeting of the PPF, while systemic or motor neuron specific deletion of this signaling pathway lead to severe defasciculation of phrenic nerve branches during sophisticated innervations of the diaphragm musculature. Furthermore, *Npn-1*$^{Sema-}$ or *Npn-1*$^{cond-/-}$*;Olig2-Cre*$^{+}$ mutants reveal that several PN axons misproject into the CTR and innervate EMs which are observed until late adulthood. As Sema3-Npn1 signaling is not disturbed in myoblasts of conditional mutants, we provide first evidence that a secondary axon guidance mechanism, namely Slit-Robo signaling, may have an attractive effect on a subpopulation of primary *in vitro* cultured MPCs. Future comprehensive understanding of the close interaction between motor neuron growth cones and myoblasts/myofibers during development, adulthood and various muscle related diseases will help to develop cures for novel therapeutic treatments. Future experiments should include the following approaches to verify our hypothesis *in vivo*:

1. Conditional ablation of Slit2 and Npn-1 in an Olig2-Cre or Hb9-Cre background should lead to a similar or even higher, caused by the additional loss of interaxonal Slit-Robo signaling, defasciculation of PN axons and therewith misprojection into the CTR. However, as Robo expressing MPCs are not exhibited to Slit2 molecules that are released by misguided as well as normal innervating PN growth cones, we do not expect MPC migration into the CTR and subsequent EM formation.

2. Conditional ablation of Robo1 and Robo2 receptors in long-range migrating MPCs by crossing with an early (Pax3-Cre) or a late (Lbx1-Cre) in combination with MN

specific removal of Npn-1 should lead to comparable results as conditional ablation of Slit2 in pMNs, as migrating MPCs cannot bind anymore to axonal-derived or any other source of Slit2 (and Slit1).

3. Furthermore, we observed a severe disorganization of myofibers after systemic loss of Robo1/2 dependend signaling. It would be interesting, if this misalignment is caused by the loss of axon-derived signals or alternative sources, presumably TPCs. Therefore, TPC-specific ablation (Scx-Cre) of Slit ligands could uncover the mechanism.

4. However, no distinct ligand-receptor signaling pathway is currently identified that guides bilateral PNs towards the PPF during development. A promising approach would be the dissection of PPFs at different development stages right before growth cones of PNs have reached the PPFs and subsequent next-generation sequencing (NGS) to uncover ligands that are involved in axon pathfinding. Additionally, retrograde tracing of phrenic MNs by fluorescence labeled dextrans with successive fluorescent activated cell sorting and NGS could reveal corresponding receptors.

5. The high number of EMs in *Npn-1*$^{Sema-}$ and *Npn-1*$^{cond-/-}$*;Olig2-Cre*$^{+}$ mutants animals or the intercrossing of myofibers in Robo1/Robo2 double mutant embryos might affect normal physiological function. As electrophysiological recordings are very challenging during embryonic development, the establishment of a basic computational model using the finite element method (FEM) for diaphragm contraction and therewith lung volume changes during breathing of healthy wildtype mice. Such model could be calibrated on on available experimental data to simulate how EMs in the diaphragm are affecting the overall force generation and the lung volume change.

Chapter 7

Supplementary data

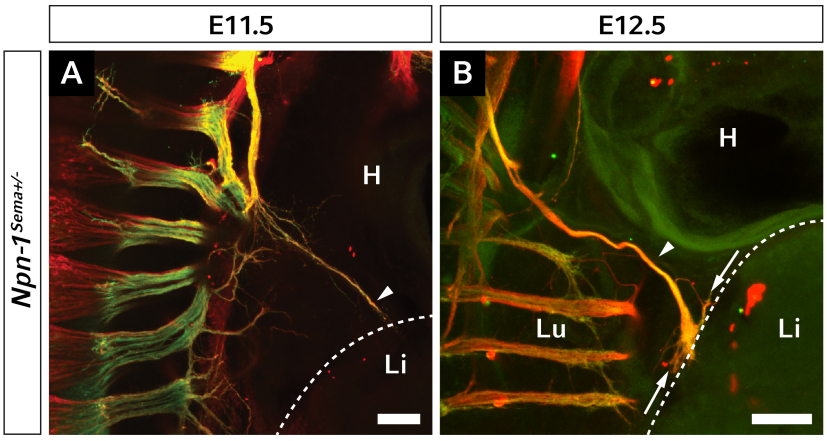

Figure 7.1: Whole mount staining of *Npn-1*$^{Sema-}$ heterozygote embryos.

Whole mount immunohistochemistry against *Hb9::eGFP* (somatic motor projections, green) and neurofilament (motor and sensory axons, red) at stage E11.5 (A) and E12.5 (B). *Npn-1*$^{Sema-}$ heterozygote embryos are indistinguishable from wildtype embryos (Figure 12A, A') during diaphragm targeting by the PNs and show a fasciculated phrenic projections after the brachial plexus at E11.5 (A, B, arrowheads). One day later, at E12.5, PN axons reach the developing diaphragm as a fasciculated nerve branch (B, arrow heads). The PN faithfully targets the primordial developing diaphragm and starts to branch dorsally and ventrally at E12.5 (A'-C', arrows). H: Heart, L: Liver, Lu: Lung. Scale bar: 200 µm.

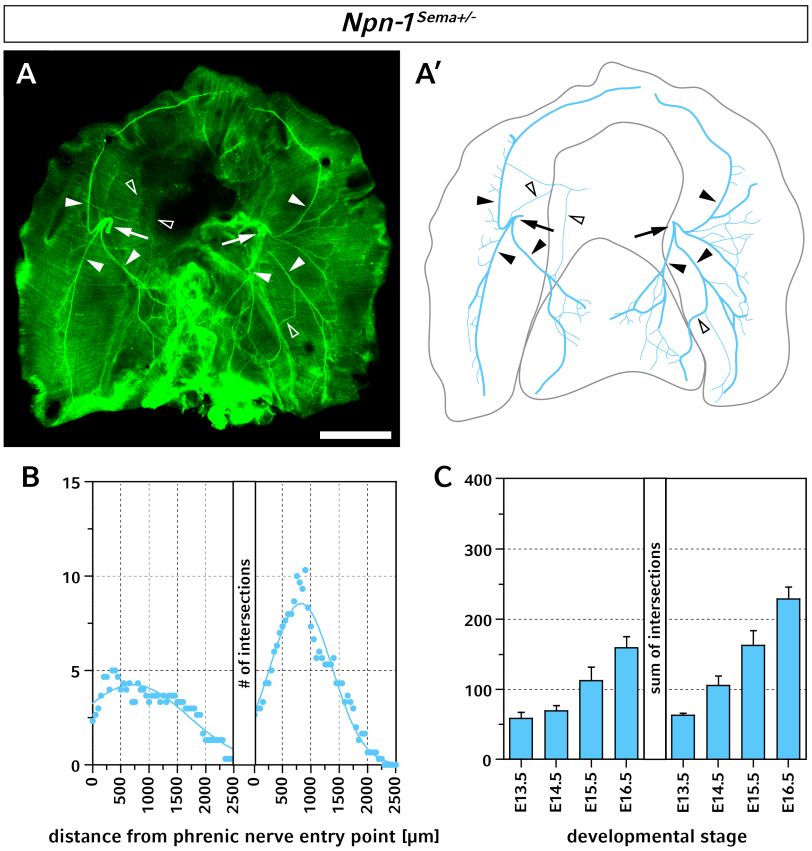

Figure 7.2: Whole mount staining of *Npn-1*$^{Sema-}$ and quantification of defasciculation.

Whole diaphragm staining against neurofilament and synaptophysin (green). Diaphragms of *Npn-1*$^{Sema+/-}$ animals establish three distinct branches (arrow heads) after the PN entry point (arrow), which is comparable to wildtype embryos (A, A') Schematic representations of PN innervation of the diaphragm at E16.5 (A'). Scale bar: 1 ,mm. Quantification by a Sholl analysis revealed analogous results for axonal branching in the left CoM hemisphere, while, interestingly, defasciculation in the right CoM hemisphere is more comparable to the situation in mutant animals (B). (left: 4.28 ± 0.12 intersections (int), $p \geq 0.05$; right: 8.55 ± 0.20 int; $n = 3$, $p \leq 0.05$). Entire defasciculation of the PN during E13.5 to E16.5 is shown by the sum of all intersections (SOI, C). The SOI of *Npn-1*$^{Sema+/-}$ embryos never showed a significant difference in all observed stages when compared to littermate controls. Data represents mean & SEM. Significance levels: * equals $p \leq 0.05$, ns: not significant. Left hemisphere - E13.5: 58.50 ± 8.50 SOI; E14.5: 69.00 ± 7.57 SOI; E15.5: 112.00 ± 19.55 SOI; E16.5: 159.00 ± 15.83 SOI and right hemisphere - E13.5: 63.00 ± 2.65 SOI; E14.5: 105.30 ± 13.67 SOI; E15.5: 162.3 ± 21.06 SOI; E16.5: 228.3,$\pm$ 17.27 SOI. All values: $n = 3$ and $p \geq 0.05$ when compared to wildtype embryos.

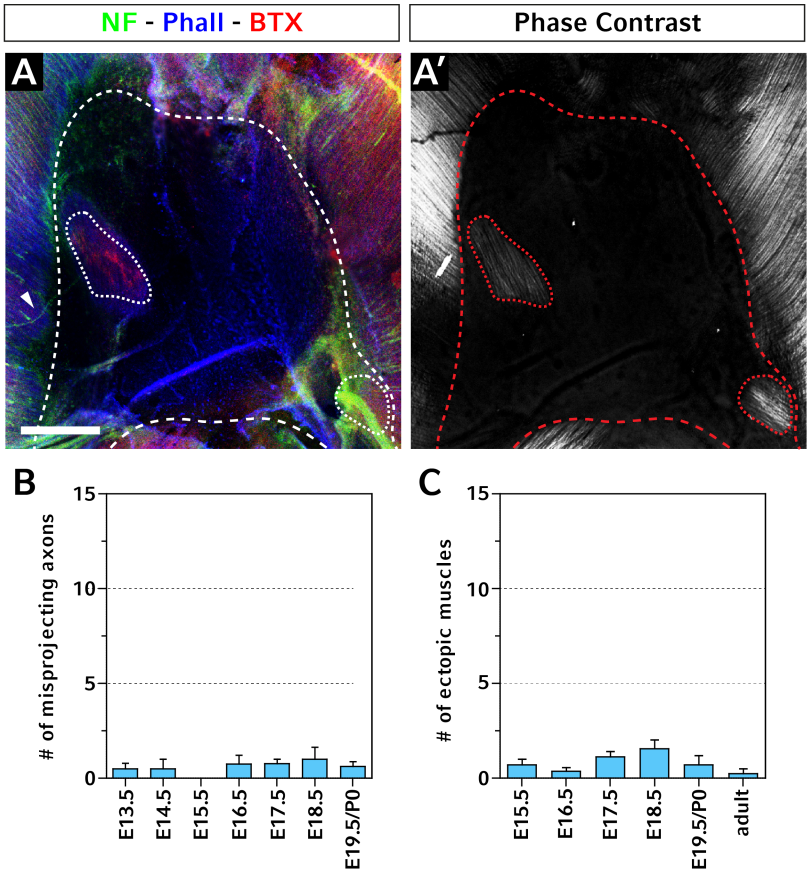

Figure 7.3: Quantification of EM formation and misprojecting axons of *Npn-1*$^{Sema+/-}$ embryos.

Whole mount diaphragm staining against neurofilament (green), actin (blue) and neuromuscular junctions (NMJs, red) revealed some misprojecting axons into the CTR (A, arrow heads), which innervated ectopic muscles in the CTR (A, A', dotted lines). Quantification of misguided axons and EM formation revealed no significant difference when compared to wildtype embryos (B, C) over the whole diaphragm development. Scale bar: 200 µm. Misprojecting axons: E13.5: 0.50 ± 0.29, $n = 4$; E14.5: 0.50 ± 0.50, $n = 4$; E15.5: 0.00 ± 0.00, $n = 4$; E16.5: 0.75 ± 0.48, $n = 4$; E17.5: 0.78 ± 0.22, $n = 9$; E18.5: 2.60 ± 0.68, $n = 5$; E19.5/P0: 0.63 ± 0.26, $n = 8$. Ectopic muscles: E15.5: 0.71 ± 0.29, $n = 7$; E16.5: 0.38 ± 0.18, $n = 8$; E17.5: 1.14 ± 0.26, $n = 7$; E18.5: 1.56 ± 0.47, $n = 9$; E19.5/P0: 0.71 ± 0.47, $n = 7$, adult: 0.25 ± 0.25, $n = 4$. Data represents the mean & SEM.

Bibliography

Ackerman, K. G., Herron, B. J., Vargas, S. O., Huang, H., Tevosian, S. G., Kochilas, L., Rao, C., Pober, B. R., Babiuk, R. P., Epstein, J. a., Greer, J. J. and Beier, D. R. (2005). Fog2 is required for normal diaphragm and lung development in mice and humans. *PLoS genetics* **1**, 58–65.

Alheid, G. F., Jiao, W. and McCrimmon, D. R. (2011). Caudal nuclei of the rat nucleus of the solitary tract differentially innervate respiratory compartments within the ventrolateral medulla. *Neuroscience* **190**, 207–227.

Alheid, G. F. and McCrimmon, D. R. (2008). The chemical neuroanatomy of breathing. *Respiratory Physiology and Neurobiology* **164**, 3–11.

Allan, D. W. and Greer, J. J. (1997). Embryogenesis of the phrenic nerve and diaphragm in the fetal rat. *Journal of Comparative Neurology* **382**, 459–468.

Allan, D. W. and Greer, J. J. (1998). Polysialylated ncam expression during motor axon outgrowth and myogenesis in the fetal rat. *Journal of Comparative Neurology* **391**, 275–292.

Amthor, H., Christ, B. and Patel, K. (1999). A molecular mechanism enabling continuous embryonic muscle growth - a balance between proliferation and differentiation. *Development (Cambridge, England)* **126**, 1041–53.

Arber, S., Han, B., Mendelsohn, M., Smith, M., Jessell, T. M. and Sockanathan, S. (1999). Requirement for the homeobox gene hb9 in the consolidation of motor neuron identity. *Neuron* **23**, 659–674.

Asahina, K., Zhou, B., Pu, W. T. and Tsukamoto, H. (2011). Septum transversum-derived mesothelium gives rise to hepatic stellate cells and perivascular mesenchymal cells in developing mouse liver. *Hepatology (Baltimore, Md.)* **53**, 983–95.

Audouard, E., Schakman, O., René, F., Huettl, R. E., Huber, A. B., Loeffler, J. P., Gailly, P. and Clotman, F. (2012). The onecut transcription factor hnf-6 regulates in motor neurons the formation of the neuromuscular junctions. *PLoS ONE* **7**.

Babiuk, R. P. and Greer, J. J. (2002). Diaphragm defects occur in a cdh hernia model independently of myogenesis and lung formation. *American journal of physiology. Lung cellular and molecular physiology* **283**, L1310–L1314.

Babiuk, R. P., Zhang, W., Clugston, R., Allan, D. W. and Greer, J. J. (2003). Embryological origins and development of the rat diaphragm. *The Journal of comparative neurology* **455**, 477–487.

Ballanyi, K., Panaitescu, B. and Ruangkittisakul, A. (2010). Control of breathing by "nerve glue". *Science signaling* **3**, pe41.

Baum, P. D. and Garriga, G. (1997). Neuronal migrations and axon fasciculation are disrupted in ina-1 integrin mutants. *Neuron* **19**, 51–62.

Bautista, T. G. and Dutschmann, M. (2014). Inhibition of the pontine kölliker-fuse nucleus abolishes eupneic inspiratory hypoglossal motor discharge in rat. *Neuroscience* **267**, 22–9.

Beckett, K. and Baylies, M. K. (2007). 3d analysis of founder cell and fusion competent myoblast arrangements outlines a new model of myoblast fusion. *Developmental Biology* **309**, 113–125.

Benarroch, E. E. (2007a). Brainstem respiratory chemosensitivity: new insights and clinical implications. *Neurology* **68**, 2140–3.

Benarroch, E. E. (2007b). Brainstem respiratory control: Substrates of respiratory failure of multiple system atrophy. *Movement Disorders* **22**, 155–161.

Bendall, a. J., Ding, J., Hu, G., Shen, M. M. and Abate-Shen, C. (1999). Msx1 antagonizes the myogenic activity of pax3 in migrating limb muscle precursors. *Development (Cambridge, England)* **126**, 4965–4976.

Bentzinger, C. F., Wang, Y. X. and Rudnicki, M. A. (2012). Building muscle: molecular regulation of myogenesis. *Cold Spring Harbor Perspectives in Biology* **4**, a008342–a008342.

Berger, A. J. (1977). Dorsal respiratory group neurons in the medulla of cat: Spinal projections, responses to lung inflation and superior laryngeal nerve stimulation. *Brain Research* **135**, 231–254.

Bermingham, J. R., Scherer, S. S., O'Connell, S., Arroyo, E., Kalla, K. a., Powell, F. L. and Rosenfeld, M. G. (1996). Tst-1/oct-6/scip regulates a unique step in peripheral myelination and is required for normal respiration. *Genes and Development* **10**, 1751–1762.

Bianchi, A. L., Denavit-Saubié, M. and Champagnat, J. (1995). Central control of breathing in mammals: neuronal circuitry, membrane properties, and neurotransmitters. *Physiological reviews* **75**, 1–45.

Birchmeier, C. and Gherardi, E. (1998). Developmental roles of hgf/sf and its receptor, the c-met tyrosine kinase. *Trends in cell biology* **8**, 404–10.

Bischoff, R. (1997). Chemotaxis of skeletal muscle satellite cells. *Developmental dynamics : an official publication of the American Association of Anatomists* **208**, 505–15.

Bladt, F., Riethmacher, D., Isenmann, S., Aguzzi, A. and Birchmeier, C. (1995). Essential role for the c-met receptor in the migration of myogenic precursor cells into the limb bud. *Nature* **376**, 768–771.

Bober, E., Franz, T., Arnold, H. H., Gruss, P. and Tremblay, P. (1994). Pax-3 is required for the development of limb muscles: a possible role for the migration of dermomyotomal muscle progenitor cells. *Development (Cambridge, England)* **120**, 603–612.

Boiten, F. a. (1994). Emotions and respiratory patterns: Review and critical analysis. *International Journal of Psychophysiology* **17**, 103–128.

Bonanomi, D. and Pfaff, S. L. (2010). Motor axon pathfinding.

Bonis, J. M., Neumueller, S. E., Marshall, B. D., Krause, K. L., Qian, B., Pan, L. G., Hodges, M. R. and Forster, H. V. (2011). The effects of lesions in the dorsolateral pons on the coordination of swallowing and breathing in awake goats. *Respiratory physiology & neurobiology* **175**, 272–82.

Boppart, M. D., Volker, S. E., Alexander, N., Burkin, D. J. and Kaufman, S. J. (2008). Exercise promotes alpha7 integrin gene transcription and protection of skeletal muscle. *American journal of physiology. Regulatory, integrative and comparative physiology* **295**, R1623–R1630.

Bouvrée, K., Brunet, I., Del Toro, R., Gordon, E., Prahst, C., Cristofaro, B., Mathivet, T., Xu, Y., Soueid, J., Fortuna, V., Miura, N., Aigrot, M. S., Maden, C. H., Ruhrberg, C., Thomas, J. L. and Eichmann, A. (2012). Semaphorin3a, neuropilin-1, and plexina1 are required for lymphatic valve formation. *Circulation Research* **111**, 437–445.

Brainerd, E. L. (1999). New perspectives on the evolution of lung ventilation mechanisms in vertebrates. *Experimental Biology Online* **4**, 1–28.

Brand-Saberi, B., Müller, T. S., Wilting, J., Christ, B. and Birchmeier, C. (1996). Scatter factor/hepatocyte growth factor (sf/hgf) induces emigration of myogenic cells at interlimb level in vivo. *Developmental biology* **179**, 303–8.

Brandau, O., Meindl, A., Fässler, R. and Aszódi, A. (2001). A novel gene, tendin, is strongly expressed in tendons and ligaments and shows high homology with chondromodulin-i. *Developmental Dynamics* **221**, 72–80.

Bray, M. A., Sheehy, S. P. and Parker, K. K. (2008). Sarcomere alignment is regulated by myocyte shape. *Cell Motility and the Cytoskeleton* **65**, 641–651.

Brent, A. E., Schweitzer, R. and Tabin, C. J. (2003). A somitic compartment of tendon progenitors. *Cell* **113**, 235–248.

Brohmann, H., Jagla, K. and Birchmeier, C. (2000). The role of lbx1 in migration of muscle precursor cells. *Development (Cambridge, England)* **127**, 437–445.

Brose, K., Bland, K. S., Wang, K. H., Arnott, D., Henzel, W., Goodman, C. S., Tessier-Lavigne, M. and Kidd, T. (1999). Slit proteins bind robo receptors and have an evolutionarily conserved role in repulsive axon guidance. *Cell* **96**, 795–806.

Brown, R. P. and Gerbarg, P. L. (2009). Yoga breathing, meditation, and longevity. *Annals of the New York Academy of Sciences* **1172**, 54–62.

Brown, T. G. (1914). On the nature of the fundamental activity of the nervous centres; together with an analysis of the conditioning of rhythmic activity in progression, and a theory of the evolution of function in the nervous system. *The Journal of physiology* **48**, 18–46.

Brownlee, E. M., Howatson, A. G., Davis, C. F. and Sabharwal, A. J. (2009). The hidden mortality of congenital diaphragmatic hernia: a 20-year review. *Journal of pediatric surgery* **44**, 317–20.

Burden, S. J. (1998). The formation of neuromuscular synapses. *Genes and Development* **12**, 133–148.

Burgess, R. W., Jucius, T. J. and Ackerman, S. L. (2006). Motor axon guidance of the mammalian trochlear and phrenic nerves: dependence on the netrin receptor unc5c and modifier loci. *The Journal of neuroscience : the official journal of the Society for Neuroscience* **26**, 5756–66.

Butera, R. J., Rinzel, J. and Smith, J. C. (1999a). Models of respiratory rhythm generation in the pre-bötzinger complex. i. bursting pacemaker neurons. *Journal of neurophysiology* **82**, 382–97.

Butera, R. J., Rinzel, J. and Smith, J. C. (1999b). Models of respiratory rhythm generation in the pre-bötzinger complex. ii. populations of coupled pacemaker neurons. *Journal of neurophysiology* **82**, 398–415.

Caton, a., Hacker, A., Naeem, A., Livet, J., Maina, F., Bladt, F., Klein, R., Birchmeier, C. and Guthrie, S. (2000). The branchial arches and hgf are growth-promoting and chemoattractant for cranial motor axons. *Development (Cambridge, England)* **127**, 1751–66.

Chédotal, a., Del Rio, J. a., Ruiz, M., He, Z., Borrell, V., de Castro, F., Ezan, F., Goodman, C. S., Tessier-Lavigne, M., Sotelo, C. and Soriano, E. (1998). Semaphorins iii and iv repel hippocampal axons via two distinct receptors. *Development (Cambridge, England)* **125**, 4313–4323.

Chen, J.-F., Tao, Y., Li, J., Deng, Z., Yan, Z., Xiao, X. and Wang, D.-Z. (2010). microrna-1 and microrna-206 regulate skeletal muscle satellite cell proliferation and differentiation by repressing pax7. *The Journal of cell biology* **190**, 867–79.

Conover, J. C., Doetsch, F., Garcia-Verdugo, J. M., Gale, N. W., Yancopoulos, G. D. and Alvarez-Buylla, a. (2000). Disruption of eph/ephrin signaling affects migration and proliferation in the adult subventricular zone. *Nature neuroscience* **3**, 1091–1097.

Corti, S., Salani, S., Del Bo, R., Sironi, M., Strazzer, S., D'Angelo, M. G., Comi, G. P., Bresolin, N. and Scarlato, G. (2001). Chemotactic factors enhance myogenic cell migration across an endothelial monolayer. *Experimental cell research* **268**, 36–44.

Cremer, H., Chazal, G., Goridis, C. and Represa, A. (1997). Ncam is essential for axonal growth and fasciculation in the hippocampus. *Molecular and cellular neurosciences* **8**, 323–35.

Crist, C. G., Montarras, D., Pallafacchina, G., Rocancourt, D., Cumano, A., Conway, S. J. and Buckingham, M. (2009). Muscle stem cell behavior is modified by microrna-27 regulation of pax3 expression. *Proceedings of the National Academy of Sciences of the United States of America* **106**, 13383–13387.

Crone, S. A., Viemari, J.-C., Droho, S., Mrejeru, A., Ramirez, J.-M. and Sharma, K. (2012). Irregular breathing in mice following genetic ablation of v2a neurons. *The Journal of neuroscience : the official journal of the Society for Neuroscience* **32**, 7895–906.

Cserjesi, P., Brown, D., Ligon, K. L., Lyons, G. E., Copeland, N. G., Gilbert, D. J., Jenkins, N. a. and Olson, E. N. (1995). Scleraxis: a basic helix-loop-helix protein that prefigures skeletal formation during mouse embryogenesis. *Development (Cambridge, England)* **121**, 1099–1110.

Dasen, J. S., De Camilli, A., Wang, B., Tucker, P. W. and Jessell, T. M. (2008). Hox repertoires for motor neuron diversity and connectivity gated by a single accessory factor, foxp1. *Cell* **134**, 304–316.

Davis-Dusenbery, B. N., Williams, L. a., Klim, J. R. and Eggan, K. (2014). How to make spinal motor neurons. *Development (Cambridge, England)* **141**, 491–501.

De, O., van den Hoogen, B. G., de Jong, J. C., Groen, J., Kuiken, T., de Groot, R., Fouchier, R. A. and Osterhaus, A. D. (2001). A newly discovered human pneumovirus isolated from young children with respiratory tract disease. *Nature medicine* **7**, 719–724.

DeChiara, T. M., Bowen, D. C., Valenzuela, D. M., Simmons, M. V., Poueymirou, W. T., Thomas, S., Kinetz, E., Compton, D. L., Rojas, E., Park, J. S., Smith, C., DiStefano, P. S., Glass, D. J., Burden, S. J. and Yancopoulos, G. D. (1996). The receptor tyrosine kinase musk is required for neuromuscular junction formation in vivo. *Cell* **85**, 501–512.

Dessaud, E., Yang, L. L., Hill, K., Cox, B., Ulloa, F., Ribeiro, A., Mynett, A., Novitch, B. G. and Briscoe, J. (2007). Interpretation of the sonic hedgehog morphogen gradient by a temporal adaptation mechanism. *Nature* **450**, 717–720.

Dey, B. K., Gagan, J. and Dutta, A. (2011). mir-206 and -486 induce myoblast differentiation by downregulating pax7. *Molecular and cellular biology* **31**, 203–14.

Dietrich, S., Abou-Rebyeh, F., Brohmann, H., Bladt, F., Sonnenberg-Riethmacher, E., Yamaai, T., Lumsden, a., Brand-Saberi, B. and Birchmeier, C. (1999). The role of sf/hgf and c-met in the development of skeletal muscle. *Development (Cambridge, England)* **126**, 1621–1629.

Dillon, A. K., Fujita, S. C., Matise, M. P., Jarjour, A. A., Kennedy, T. E., Kollmus, H., Arnold, H.-H., Weiner, J. A., Sanes, J. R. and Kaprielian, Z. (2005). Molecular control of spinal accessory motor neuron/axon development in the mouse spinal cord. *The Journal of neuroscience : the official journal of the Society for Neuroscience* **25**, 10119–30.

Do, M.-k. Q., Shimizu, N., Suzuki, T., Ohtsubo, H., Mizunoya, W., Nakamura, M., Sawano, S., Furuse, M., Ikeuchi, Y., Anderson, J. E. and Tatsumi, R. (2015). Transmembrane proteoglycans syndecan-2, 4, receptor candidates for the impact of hgf and fgf2 on semaphorin 3a expression in early-differentiated myoblasts. *Physiological reports* **3**, e12553.

Docheva, D., Popov, C., Alberton, P. and Aszodi, A. (2014). Integrin signaling in skeletal development and function. *Birth defects research. Part C, Embryo today : reviews* **102**, 13–36.

Domyan, E. T., Branchfield, K., Gibson, D. A., Naiche, L., Lewandoski, M., Tessier-Lavigne, M., Ma, L. and Sun, X. (2013). Roundabout receptors are critical for foregut separation from the body wall. *Developmental Cell* **24**, 52–63.

Dubrulle, J. and Pourquie, O. (2003). Welcome to syndetome: a new somitic compartment. *Developmental cell* **4**, 611–612.

Dutschmann, M. and Herbert, H. (2006). The kolliker-fuse nucleus gates the postinspiratory phase of the respiratory cycle to control inspiratory off-switch and upper airway resistance in rat. *European Journal of Neuroscience* **24**, 1071–1084.

Ebens, A., Brose, K., Leonardo, E. D., Hanson, M. G., Bladt, F., Birchmeier, C., Barres, B. a. and Tessier-Lavigne, M. (1996). Hepatocyte growth factor/scatter factor is an axonal chemoattractant and a neurotrophic factor for spinal motor neurons. *Neuron* **17**, 1157–72.

Edelstein, P. H. (1982). Comparative study of selective media for isolation of legionella pneumophila from potable water. *Journal of clinical microbiology* **16**, 697–9.

Edman, K. A. (1979). The velocity of unloaded shortening and its relation to sarcomere length and isometric force in vertebrate muscle fibres. *The Journal of Physiology* **291**, 143–159.

Epstein, J. A., Shapiro, D. N., Cheng, J., Lam, P. Y. and Maas, R. L. (1996). Pax3 modulates expression of the c-met receptor during limb muscle development. *Proceedings of the National Academy of Sciences of the United States of America* **93**, 4213–8.

Ericson, J., Morton, S., Kawakami, A., Roelink, H. and Jessell, T. M. (1996). Two critical periods of sonic hedgehog signaling required for the specification of motor neuron identity. *Cell* **87**, 661–673.

Fallon, J. F., López, a., Ros, M. a., Savage, M. P., Olwin, B. B. and Simandl, B. K. (1994). Fgf-2: apical ectodermal ridge growth signal for chick limb development. *Science (New York, N.Y.)* **264**, 104–7.

Fan, C., Lee, C. and Tessier-Lavigne, M. (1997). A role for wnt proteins in induction of dermomyotome. *Developmental biology* **191**, 160–5.

Farmer, W. T., Altick, A. L., Nural, H. F., Dugan, J. P., Kidd, T., Charron, F. and Mastick, G. S. (2008). Pioneer longitudinal axons navigate using floor plate and slit/robo signals. *Development* **135**, 3643–3653.

Feng, G., Laskowski, M. B., Feldheim, D. A., Wang, H., Lewis, R., Frisen, J., Flanagan, J. G. and Sanes, J. R. (2000). Roles for ephrins in positionally selective synaptogenesis between motor neurons and muscle fibers. *Neuron* **25**, 295–306.

Flanagan, J. G. and Vanderhaeghen, P. (1998). The ephrins and eph receptors in neural development. *Annual review of neuroscience* **21**, 309–345.

Fortier, M., Comunale, F., Kucharczak, J., Blangy, a., Charrasse, S. and Gauthier-Rouvière, C. (2008). Rhoe controls myoblast alignment prior fusion through rhoa and rock. *Cell death and differentiation* **15**, 1221–1231.

Frisén, J., Yates, P. a., McLaughlin, T., Friedman, G. C., O'Leary, D. D. M. and Barbacid, M. (1998). Ephrin-a5 (al-1/rags) is essential for proper retinal axon guidance and topographic mapping in the mammalian visual system. *Neuron* **20**, 235–243.

Fujiwara, M., Ghazizadeh, M. and Kawanami, O. (2006). Potential role of the slit/robo signal pathway in angiogenesis. *Vascular medicine (London, England)* **11**, 115–121.

Fukuda, T., Takeda, S., Xu, R., Ochi, H., Sunamura, S., Sato, T., Shibata, S., Yoshida, Y., Gu, Z., Kimura, A., Ma, C., Xu, C., Bando, W., Fujita, K., Shinomiya, K., Hirai, T., Asou, Y., Enomoto, M., Okano, H., Okawa, A. and Itoh, H. (2013). Sema3a regulates bone-mass accrual through sensory innervations. *Nature* **497**, 490–3.

Galli, L. M., Willert, K., Nusse, R., Yablonka-Reuveni, Z., Nohno, T., Denetclaw, W. and Burrus, L. W. (2004). A proliferative role for wnt-3a in chick somites. *Developmental Biology* **269**, 489–504.

Gao, Y., Kostrominova, T. Y., Faulkner, J. A. and Wineman, A. S. (2008). Age-related changes in the mechanical properties of the epimysium in skeletal muscles of rats. *Journal of Biomechanics* **41**, 465–469.

Gara, R. K., Kumari, S., Ganju, A., Yallapu, M. M., Jaggi, M. and Chauhan, S. C. (2015). Slit/robo pathway: a promising therapeutic target for cancer. *Drug discovery today* **20**, 156–164.

Gerety, S. S., Wang, H. U., Chen, Z. F. and Anderson, D. J. (1999). Symmetrical mutant phenotypes of the receptor ephb4 and its specific transmembrane ligand ephrin-b2 in cardiovascular development. *Molecular Cell* **4**, 403–414.

Gibson, D. A., Tymanskyj, S., Yuan, R. C., Leung, H. C., Lefebvre, J. L., Sanes, J. R., Chédotal, A. and Ma, L. (2014). Dendrite self-avoidance requires cell-autonomous slit/robo signaling in cerebellar purkinje cells. *Neuron* **81**, 1040–1056.

Glass, D. J. (2005). Skeletal muscle hypertrophy and atrophy signaling pathways. *The International Journal of Biochemistry & Cell Biology* **37**, 1974–1984.

Glass, D. J., Bowen, D. C., Stitt, T. N., Radziejewski, C., Bruno, J., Ryan, T. E., Gies, D. R., Shah, S., Mattsson, K., Burden, S. J., DiStefano, P. S., Valenzuela, D. M., DeChiara, T. M. and Yancopoulos, G. D. (1996). Agrin acts via a musk receptor complex. *Cell* **85**, 513–523.

Glinka, Y. and Prud'homme, G. J. (2008). Neuropilin-1 is a receptor for transforming growth factor beta-1, activates its latent form, and promotes regulatory t cell activity. *Journal of leukocyte biology* **84**, 302–310.

Goldberg, D., Borojevic, R., Anderson, M., Chen, J. J., Gershon, M. D. and Ratcliffe, E. M. (2013). Slit/robo-mediated chemorepulsion of vagal sensory axons in the fetal gut. *Developmental Dynamics* **242**, 9–15.

Goodman, C., Kolodkin, A., Luo, Y., Püschel, A. and Raper, J. (1999). Unified nomenclature for the semaphorins/collapsins. *Cell* **97**, 551–552.

Gordon, A. M., Huxley, A. F. and Julian, F. J. (1966). The variation in isometric tension with sarcomere length in vertebrate muscle fibres. *The Journal of Physiology* **184**, 170–192.

Grandclement, C. and Borg, C. (2011). Neuropilins: a new target for cancer therapy. *Cancers* **3**, 1899–928.

Greer, J. J., Allan, D. W., Martin-Caraballo, M. and Lemke, R. P. (1999). An overview of phrenic nerve and diaphragm muscle development in the perinatal rat. *Journal of applied physiology (Bethesda, Md. : 1985)* **86**, 779–86.

Greer, J. J., Cote, D., Allan, D. W., Zhang, W., Babiuk, R. P., Ly, L., Lemke, R. P. and Bagnall, K. (2000). Structure of the primordial diaphragm and defects associated with nitrofen-induced cdh. *Journal of applied physiology (Bethesda, Md. : 1985)* **89**, 2123–2129.

Grifone, R., Demignon, J., Houbron, C., Souil, E., Niro, C., Seller, M. J., Hamard, G. and Maire, P. (2005). Six1 and six4 homeoproteins are required for pax3 and mrf expression during myogenesis in the mouse embryo. *Development (Cambridge, England)* **132**, 2235–49.

Gros, J., Manceau, M., Thomé, V. and Marcelle, C. (2005). A common somitic origin for embryonic muscle progenitors and satellite cells. *Nature* **435**, 954–958.

Gross, M. K., Moran-Rivard, L., Velasquez, T., Nakatsu, M. N., Jagla, K. and Goulding, M. (2000). Lbx1 is required for muscle precursor migration along a lateral pathway into the limb. *Development (Cambridge, England)* **127**, 413–424.

Gu, C., Rodriguez, E. R., Reimert, D. V., Shu, T., Fritzsch, B., Richards, L. J., Kolodkin, A. L. and Ginty, D. D. (2003). Neuropilin-1 conveys semaphorin and vegf signaling during neural and cardiovascular development. *Developmental Cell* **5**, 45–57.

Halperin-Barlev, O. and Kalcheim, C. (2011). Sclerotome-derived slit1 drives directional migration and differentiation of robo2-expressing pioneer myoblasts. *Development (Cambridge, England)* **138**, 2935–45.

Hamasaki, H., Honda, H., Suzuki, S. O., Hokama, M., Kiyohara, Y., Nakabeppu, Y. and Iwaki, T. (2014). Down-regulation of met in hippocampal neurons of alzheimer's disease brains. *Neuropathology* **34**, 284–290.

Hayakawa, T., Takanaga, A., Tanaka, K., Maeda, S. and Seki, M. (2004). Ultrastructure of the rostral ventral respiratory group neurons in the ventrolateral medulla of the rat. *Brain Research* **1027**, 94–102.

Hayashi, M., Nakashima, T., Taniguchi, M., Kodama, T., Kumanogoh, A. and Takayanagi, H. (2012). Osteoprotection by semaphorin 3a.

He, Z. and Tessier-Lavigne, M. (1997). Neuropilin is a receptor for the axonal chemorepellent semaphorin iii. *Cell* **90**, 739–751.

Helmbacher, F., Schneider-Maunoury, S., Topilko, P., Tiret, L. and Charnay, P. (2000). Targeting of the epha4 tyrosine kinase receptor affects dorsal/ventral pathfinding of limb motor axons. *Development (Cambridge, England)* **127**, 3313–3324.

Helmbrecht, M. S., Soellner, H., Truckenbrodt, A. M., Sundermeier, J., Cohrs, C., Hans, W., de Angelis, M. H., Feuchtinger, A., Aichler, M., Fouad, K. and Huber, A. B. (2015). Loss of npn1 from motor neurons causes postnatal deficits independent from sema3a signaling. *Developmental Biology* **399**, 2–14.

Heymann, S., Koudrova, M., Arnold, H., Köster, M. and Braun, T. (1996). Regulation and function of sf/hgf during migration of limb muscle precursor cells in chicken. *Developmental biology* **180**, 566–78.

Hippenmeyer, S., Huber, R. M., Ladle, D. R., Murphy, K. and Arber, S. (2007). Ets transcription factor erm controls subsynaptic gene expression in skeletal muscles. *Neuron* **55**, 726–740.

Hirai, H., Maru, Y., Hagiwara, K., Nishida, J. and Takaku, F. (1987). A novel putative tyrosine kinase receptor encoded by the eph gene. *Science (New York, N.Y.)* **238**, 1717–20.

Hirasawa, T. and Kuratani, S. (2013). A new scenario of the evolutionary derivation of the mammalian diaphragm from shoulder muscles. *Journal of Anatomy* **222**, 504–517.

Holder, A., Klaassens, M., Tibboel, D., de Klein, A., Lee, B. and Scott, D. (2007). Genetic factors in congenital diaphragmatic hernia. *The American Journal of Human Genetics* **80**, 825–845.

Holzman, L. B., Marks, R. M. and Dixit, V. M. (1990). A novel immediate-early response gene of endothelium is induced by cytokines and encodes a secreted protein. *Molecular and cellular biology* **10**, 5830–8.

Hu, J. S., Olson, E. N. and Kingston, R. E. (1992). Heb, a helix-loop-helix protein related to e2a and itf2 that can modulate the dna-binding ability of myogenic regulatory factors. *Molecular and Cellular Biology* **12**, 1031–1042.

Huber, A. B., Kania, A., Tran, T. S., Gu, C., De Marco Garcia, N., Lieberam, I., Johnson, D., Jessell, T. M., Ginty, D. D. and Kolodkin, A. L. (2005). Distinct roles for secreted semaphorin signaling in spinal motor axon guidance. *Neuron* **48**, 949–64.

Huber, A. B., Kolodkin, A. L., Ginty, D. D. and Cloutier, J.-F. (2003). Signaling at the growth cone: ligand-receptor complexes and the control of axon growth and guidance. *Annual review of neuroscience* **26**, 509–63.

Huettl, R. E., Haehl, T. and Huber, A. B. (2012). Fasciculation and guidance of spinal motor axons in the absence of fgfr2 signaling. *PLoS ONE* **7**, 1–10.

Huettl, R. E., Soellner, H., Bianchi, E., Novitch, B. G. and Huber, A. B. (2011). Npn-1 contributes to axon-axon interactions that differentially control sensory and motor innervation of the limb. *PLoS Biology* **9**.

Ikeya, M. and Takada, S. (1998). Wnt signaling from the dorsal neural tube is required for the formation of the medial dermomyotome. *Development (Cambridge, England)* **125**, 4969–4976.

Jackman, R. W. (2004). The molecular basis of skeletal muscle atrophy. *AJP: Cell Physiology* **287**, C834–C843.

Jaegle, M., Mandemakers, W., Broos, L., Zwart, R., Karis, a., Visser, P., Grosveld, F. and Meijer, D. (1996). The pou factor oct-6 and schwann cell differentiation. *Science (New York, N.Y.)* **273**, 507–510.

Jagla, T., Bellard, F., Lutz, Y., Dretzen, G., Bellard, M. and Jagla, K. (1998). ladybird determines cell fate decisions during diversification of drosophila somatic muscles. *Development (Cambridge, England)* **125**, 3699–3708.

Janczewski, W. a. and Feldman, J. L. (2006). Distinct rhythm generators for inspiration and expiration in the juvenile rat. *The Journal of physiology* **570**, 407–420.

Jaworski, A. and Tessier-Lavigne, M. (2012). Autocrine/juxtaparacrine regulation of axon fasciculation by slit-robo signaling. *Nature Neuroscience* **15**, 367–369.

Jay, P. Y., Bielinska, M., Erlich, J. M., Mannisto, S., Pu, W. T., Heikinheimo, M. and Wilson, D. B. (2007). Impaired mesenchymal cell function in gata4 mutant mice

leads to diaphragmatic hernias and primary lung defects. *Developmental Biology* **301**, 602–614.

Jessell, T. M. (2000). Neuronal specification in the spinal cord: inductive signals and transcriptional codes. *Nature reviews. Genetics* **1**, 20–29.

Jordaens, K., Dillen, L. and Backeljau, T. (2007). Effects of mating , breeding system and parasites on reproduction in hermaphrodites : pulmonate gastropods (mollusca). *Animal Biology* **57**, 137–195.

Kahane, N., Cinnamon, Y., Bachelet, I. and Kalcheim, C. (2001). The third wave of myotome colonization by mitotically competent progenitors: regulating the balance between differentiation and proliferation during muscle development. *Development* **128**, 2187–2198.

Kahane, N., Ribes, V., Kicheva, A., Briscoe, J. and Kalcheim, C. (2013). The transition from differentiation to growth during dermomyotome-derived myogenesis depends on temporally restricted hedgehog signaling. *Development (Cambridge, England)* **140**, 1740–50.

Kassar-Duchossoy, L., Gayraud-Morel, B., Gomès, D., Rocancourt, D., Buckingham, M., Shinin, V. and Tajbakhsh, S. (2004). Mrf4 determines skeletal muscle identity in myf5:myod double-mutant mice. *Nature* **431**, 466–71.

Kassar-Duchossoy, L., Giacone, E., Gayraud-Morel, B., Jory, A., Gomès, D. and Tajbakhsh, S. (2005). Pax3/pax7 mark a novel population of primitive myogenic cells during development. *Genes & development* **19**, 1426–31.

Kawasaki, T., Kitsukawa, T., Bekku, Y., Matsuda, Y., Sanbo, M., Yagi, T. and Fujisawa, H. (1999). A requirement for neuropilin-1 in embryonic vessel formation. *Development (Cambridge, England)* **126**, 4895–4902.

Kidd, T., Bland, K. S. and Goodman, C. S. (1999). Slit is the midline repellent for the robo receptor in drosophila. *Cell* **96**, 785–794.

Kim, M., Fontelonga, T., Roesener, A. P., Lee, H., Gurung, S., Mendonca, P. R. F. and Mastick, G. S. (2015). Motor neuron cell bodies are actively positioned by slit/robo repulsion and netrin/dcc attraction. *Developmental biology* **399**, 68–79.

Klein, R. (2004). Eph/ephrin signaling in morphogenesis, neural development and plasticity. *Current opinion in cell biology* **16**, 580–9.

Kobayashi, H., Koppel, a. M., Luo, Y. and Raper, J. a. (1997). A role for collapsin-1 in olfactory and cranial sensory axon guidance. *The Journal of neuroscience : the official journal of the Society for Neuroscience* **17**, 8339–8352.

Koike, H., Ishida, A., Shimamura, M., Mizuno, S., Nakamura, T., Ogihara, T., Kaneda, Y. and Morishita, R. (2006). Prevention of onset of parkinson's disease by in vivo gene transfer of human hepatocyte growth factor in rodent model: a model of gene therapy for parkinson's disease. *Gene therapy* **13**, 1639–44.

Kolodkin, A. L., Levengood, D. V., Rowe, E. G., Tai, Y. T., Giger, R. J. and Ginty, D. D. (1997). Neuropilin is a semaphorin iii receptor. *Cell* **90**, 753–762.

Konigsberg, I. R. (1971). Diffusion-mediated control of myoblast fusion. *Developmental Biology* **26**, 133–152.

Koutsoulidou, A., Mastroyiannopoulos, N. P., Furling, D., Uney, J. B. and Phylactou, L. a. (2011). Expression of mir-1, mir-133a, mir-133b and mir-206 increases during development of human skeletal muscle. *BMC developmental biology* **11**, 34.

Kozlov, G., Perreault, A., Schrag, J. D., Park, M., Cygler, M., Gehring, K. and Ekiel, I. (2004). Insights into function of psi domains from structure of the met receptor psi domain. *Biochemical and Biophysical Research Communications* **321**, 234–240.

Kramer, S. G. (2001). Switching repulsion to attraction: Changing responses to slit during transition in mesoderm migration. *Science* **292**, 737–740.

Kubin, L., Alheid, G. F., Zuperku, E. J. and McCrimmon, D. R. (2006). Central pathways of pulmonary and lower airway vagal afferents. *Journal of applied physiology (Bethesda, Md. : 1985)* **101**, 618–627.

Kullander, K. and Klein, R. (2002). Mechanisms and functions of eph and ephrin signalling. *Nature reviews. Molecular cell biology* **3**, 475–86.

Kumanogoh, A. and Kikutani, H. (2003). Immune semaphorins: a new area of semaphorin research. *Journal of cell science* **116**, 3463–3470.

Lai, K. O. and Ip, N. Y. (2009). Synapse development and plasticity: roles of ephrin/eph receptor signaling. *Current Opinion in Neurobiology* **19**, 275–283.

Landmesser, L., Dahm, L., Schultz, K. and Rutishauser, U. (1988). Distinct roles for adhesion molecules during innervation of embryonic chick muscle. *Dev Biol* **130**, 645–670.

Laskowski, M. B. and Sanes, J. R. (1987). Topographic mapping of motor pools onto skeletal muscles. *The Journal of neuroscience : the official journal of the Society for Neuroscience* **7**, 252–60.

Laws, N. (2004). Progression of kyphosis in mdx mice. *Journal of Applied Physiology* **97**, 1970–1977.

Lee, H., Kim, M., Kim, N., Macfarlan, T., Pfaff, S. L., Mastick, G. S. and Song, M.-R. (2015). Slit and semaphorin signaling governed by islet transcription factors positions motor neuron somata within the neural tube. *Experimental neurology* **269**, 17–27.

Lee, K.-F., Li, E., Huber, L. J., Landis, S. C., Sharpe, A. H., Chao, M. V. and Jaenisch, R. (1992). Targeted mutation of the gene encoding the low affinity ngf receptor p75 leads to deficits in the peripheral sensory nervous system. *Cell* **69**, 737–749.

Lee, P., Wang, C. C. and Adamis, A. P. (1998). Ocular neovascularization: An epidemiologic review. *Survey of Ophthalmology* **43**, 245–269.

Legate, K. R., Wickström, S. a. and Fässler, R. (2009). Genetic and cell biological analysis of integrin outside-in signaling. *Genes & development* **23**, 397–418.

Leu, M., Bellmunt, E., Schwander, M., Farinas, I., Brenner, H. R. and Muller, U. (2003). Erbb2 regulates neuromuscular synapse formation and is essential for muscle spindle development. *Development* **130**, 2291–301.

Liang, X., Song, M.-R., Xu, Z., Lanuza, G. M., Liu, Y., Zhuang, T., Chen, Y., Pfaff, S. L., Evans, S. M. and Sun, Y. (2011). Isl1 is required for multiple aspects of motor neuron development. *Molecular and Cellular Neuroscience* **47**, 215–222.

Liem, K. F., Tremml, G., Roelink, H. and Jessell, T. M. (1995). Dorsal differentiation of neural plate cells induced by bmp-mediated signals from epidermal ectoderm. *Cell* **82**, 969–979.

Lin, W., Sanchez, H. B., Deerinck, T., Morris, J. K., Ellisman, M. and Lee, K. F. (2000). Aberrant development of motor axons and neuromuscular synapses in erbb2-deficient mice. *Proceedings of the National Academy of Sciences of the United States of America* **97**, 1299–304.

Liu, J., Zhang, L., Wang, D., Shen, H., Jiang, M., Mei, P., Hayden, P. S., Sedor, J. R. and Hu, H. (2003). Congenital diaphragmatic hernia, kidney agenesis and cardiac defects associated with slit3-deficiency in mice. *Mechanisms of Development* **120**, 1059–1070.

Liu, Y., Sugiura, Y., Wu, F., Mi, W., Taketo, M. M., Cannon, S., Carroll, T. and Lin, W. (2012). B-catenin stabilization in skeletal muscles, but not in motor neurons, leads to aberrant motor innervation of the muscle during neuromuscular development in mice. *Developmental Biology* **366**, 255–267.

Londhe, P. and Davie, J. K. (2011). Sequential association of myogenic regulatory factors and e proteins at muscle-specific genes. *Skeletal Muscle* **1**, 14.

Long, H., Sabatier, C., Ma, L., Plump, A., Yuan, W., Ornitz, D. M., Tamada, A., Murakami, F., Goodman, C. S. and Tessier-Lavigne, M. (2004). Conserved roles for slit and robo proteins in midline commissural axon guidance. *Neuron* **42**, 213–223.

Lu, Q., Sun, T., Zhu, Z., Ma, N., Garcia, M., Stiles, C. D. and Rowitch, D. H. (2002). Common developmental requirement for olig function indicates a motor neuron/oligodendrocyte connection. *Cell* **109**, 75–86.

Lu, W., van Eerde, A. M., Fan, X., Quintero-Rivera, F., Kulkarni, S., Ferguson, H., Kim, H.-G., Fan, Y., Xi, Q., Li, Q.-g., Sanlaville, D., Andrews, W., Sundaresan, V., Bi, W., Yan, J., Giltay, J. C., Wijmenga, C., de Jong, T. P. V. M., Feather, S. a., Woolf, A. S., Rao, Y., Lupski, J. R., Eccles, M. R., Quade, B. J., Gusella, J. F., Morton, C. C. and Maas, R. L. (2007). Disruption of robo2 is associated with urinary tract anomalies and confers risk of vesicoureteral reflux. *American journal of human genetics* **80**, 616–32.

Lundström, A., Gallio, M., Englund, C., Steneberg, P., Hemphälä, J., Aspenström, P., Keleman, K., Falileeva, L., Dickson, B. J. and Samakovlis, C. (2004). Vilse, a conserved rac/cdc42 gap mediating robo repulsion in tracheal cells and axons. *Genes & development* **18**, 2161–71.

Luo, L. and O'Leary, D. D. (2005). Axon retraction and degeneration in development and disease. *Annual Review of Neuroscience* **28**, 127–156.

Luo, Y., Raible, D. and Raper, J. a. (1993). Collapsin: a protein in brain that induces the collapse and paralysis of neuronal growth cones. *Cell* **75**, 217–227.

MacLarnon, A. M. and Hewitt, G. P. (1999). The evolution of human speech: the role of enhanced breathing control. *American journal of physical anthropology* **109**, 341–63.

Maden, M. (2007). Retinoic acid in the development, regeneration and maintenance of the nervous system. *Nature reviews. Neuroscience* **8**, 755–65.

Maina, F., Hilton, M. C., Ponzetto, C., Davies, A. M. and Klein, R. (1997). Met receptor signaling is required for sensory nerve development and hgf promotes axonal growth and survival of sensory neurons. *Genes & development* **11**, 3341–50.

Mantilla, C. B., Zhan, W. Z. and Sieck, G. C. (2009). Retrograde labeling of phrenic motoneurons by intrapleural injection. *Journal of Neuroscience Methods* **182**, 244–249.

Marder, E. and Bucher, D. (2001). Central pattern generators and the control of rhythmic movements. *Current Biology* **11**, 986–996.

Martin, B. L. and Harland, R. M. (2006). A novel role for lbx1 in xenopus hypaxial myogenesis. *Development (Cambridge, England)* **133**, 195–208.

Matsuo, K. and Otaki, N. (2012). Bone cell interactions through eph/ephrin: bone modeling, remodeling and associated diseases. *Cell adhesion & migration* **6**, 148–56.

Mayer, U., Saher, G., Fässler, R., Bornemann, a., Echtermeyer, F., von der Mark, H., Miosge, N., Pöschl, E. and von der Mark, K. (1997). Absence of integrin alpha 7 causes a novel form of muscular dystrophy. *Nature genetics* **17**, 318–323.

Meijering, E., Dzyubachyk, O. and Smal, I. (2012). Methods for cell and particle tracking. *Methods in enzymology* **504**, 183–200.

Mennerich, D., Schäfer, K. and Braun, T. (1998). Pax-3 is necessary but not sufficient for lbx1 expression in myogenic precursor cells of the limb. *Mechanisms of development* **73**, 147–58.

Menon, S. D., Osman, Z., Chenchill, K. and Chia, W. (2005). A positive feedback loop between dumbfounded and rolling pebbles leads to myotube enlargement in drosophila. *Journal of Cell Biology* **169**, 909–920.

Merrell, A. J., Ellis, B. J., Fox, Z. D., Lawson, J. a., Weiss, J. a. and Kardon, G. (2015). Muscle connective tissue controls development of the diaphragm and is a source of congenital diaphragmatic hernias. *Nature Genetics* **47**, 496–504.

Merrell, A. J. and Kardon, G. (2013). Development of the diaphragm - a skeletal muscle essential for mammalian respiration. *FEBS Journal* **280**, 4026–4035.

Merrill, E. G. and Fedorko, L. (1984). Monosynaptic inhibition of phrenic motoneurons: a long descending projection from bötzinger neurons. *The Journal of neuroscience : the official journal of the Society for Neuroscience* **4**, 2350–3.

Merrill, E. G., Lipski, J., Kubin, L. and Fedorko, L. (1983). Origin of the expiratory inhibition of nucleus tractus solitarius inspiratory neurones. *Brain Research* **263**, 43–50.

Messersmith, E. K., Leonardo, E. D., Shatz, C. J., Tessier-Lavigne, M., Goodman, C. S. and Kolodkin, a. L. (1995). Semaphorin iii can function as a selective chemorepellent to pattern sensory projections in the spinal cord. *Neuron* **14**, 949–959.

Messina, G. and Cossu, G. (2009). The origin of embryonic and fetal myoblasts: a role of pax3 and pax7. *Genes and Development* **23**, 902–905.

Ming, G. L., Song, H. J., Berninger, B., Holt, C. E., Tessier-Lavigne, M. and Poo, M. M. (1997). camp-dependent growth cone guidance by netrin-1. *Neuron* **19**, 1225–1235.

Mommersteeg, M. T. M., Yeh, M. L., Parnavelas, J. G. and Andrews, W. D. (2015). Disrupted slit-robo signalling results in membranous ventricular septum defects and bicuspid aortic valves. *Cardiovascular research* , cvv040–.

Morlot, C., Thielens, N. M., Ravelli, R. B. G., Hemrika, W., Romijn, R. A., Gros, P., Cusack, S. and McCarthy, A. a. (2007). Structural insights into the slit-robo complex. *Proc Natl Acad Sci USA* **104**, 14923–8.

Morris, J. K., Weichun, L., Hauser, C., Marchuk, Y., Getman, D. and Kuo-Fen, L. (1999). Rescue of the cardiac defect in erbb2 mutant mice reveals essential roles of erbb2 in peripheral nervous system development. *Neuron* **23**, 273–283.

Movshon, J. a., Nundy, S. and Crowley, J. C. (2003). Cyclic amp / gmp-dependent modulation of ca 21 channels sets the polarity of nerve growth-cone turning. *Cerebral Cortex* **423**, 990–995.

Murchison, N. D., Price, B. a., Conner, D. a., Keene, D. R., Olson, E. N., Tabin, C. J. and Schweitzer, R. (2007). Regulation of tendon differentiation by scleraxis distinguishes force-transmitting tendons from muscle-anchoring tendons. *Development (Cambridge, England)* **134**, 2697–2708.

Myster, F., Palmeira, L., Sorel, O., Bouillenne, F., DePauw, E., Schwartz-Cornil, I., Vanderplasschen, A. and Dewals, B. G. (2015). Viral semaphorin inhibits dendritic cell phagocytosis and migration but is not essential for gammaherpesvirus-induced lymphoproliferation in malignant catarrhal fever. *Journal of virology* **89**, 3630–47.

Nabeshima, Y., Hanaoka, K., Hayasaka, M., Esumi, E., Li, S., Nonaka, I. and Nabeshima, Y. (1993). Myogenin gene disruption results in perinatal lethality because of severe muscle defect. *Nature* **364**, 532–535.

Naidu, P. S., Ludolph, D. C., To, R. Q., Hinterberger, T. J. and Konieczny, S. F. (1995). Myogenin and mef2 function synergistically to activate the mrf4 promoter during myogenesis. *Molecular and cellular biology* **15**, 2707–18.

Neufeld, G. and Kessler, O. (2008). The semaphorins: versatile regulators of tumour progression and tumour angiogenesis. *Nature reviews. Cancer* **8**, 632–45.

Neufeld, G., Sabag, A. D., Rabinovicz, N. and Kessler, O. (2012). Semaphorins in angiogenesis and tumor progression. *Cold Spring Harbor perspectives in medicine* **2**, 1–13.

Nord, H., Nygård Skalman, L. and von Hofsten, J. (2013). Six1 regulates proliferation of pax7-positive muscle progenitors in zebrafish. *Journal of cell science* **126**, 1868–80.

Novitch, B. G., Chen, A. I. and Jessell, T. M. (2001). Coordinate regulation of motor neuron subtype identity and pan-neuronal properties by the bhlh repressor olig2. *Neuron* **31**, 773–789.

Novitch, B. G., Wichterle, H., Jessell, T. M. and Sockanathan, S. (2003). A requirement for retinoic acid-mediated transcriptional activation in ventral neural patterning and motor neuron specification. *Neuron* **40**, 81–95.

O'Leary, D. D. and Wilkinson, D. G. (1999). Eph receptors and ephrins in neural development. *Current Opinion in Neurobiology* **9**, 65–73.

O'Malley, A. M., Shanley, D. K., Kelly, A. T. and Barry, D. S. (2014). Towards an understanding of semaphorin signalling in the spinal cord. *Gene* **553**, 69–74.

Onimaru, H. and Homma, I. (2003). A novel functional neuron group for respiratory rhythm generation in the ventral medulla. *The Journal of neuroscience : the official journal of the Society for Neuroscience* **23**, 1478–1486.

Ordan, E., Brankatschk, M., Dickson, B., Schnorrer, F. and Volk, T. (2015). Slit cleavage is essential for producing an active, stable, non-diffusible short-range signal that guides muscle migration. *Development (Cambridge, England)* **142**, 1431–6.

Organ, S. L. and Tsao, M.-S. (2011). An overview of the c-met signaling pathway. *Therapeutic Advances in Medical Oncology* **3**, S7–S19.

Palmeirim, I., Henrique, D., Ish-Horowicz, D. and Pourquié, O. (1997). Avian hairy gene expression identifies a molecular clock linked to vertebrate segmentation and somitogenesis. *Cell* **91**, 639–648.

Palmer, A. and Klein, R. (2003). Multiple roles of ephrins in morphogenesis, neuronal networking, and brain function. *Genes and Development* **17**, 1429–1450.

Pasquale, E. B. (2010). Eph receptors and ephrins in cancer: bidirectional signalling and beyond. *Nature reviews. Cancer* **10**, 165–180.

Pasterkamp, R. J., Peschon, J. J., Spriggs, M. K. and Kolodkin, A. L. (2003). Semaphorin 7a promotes axon outgrowth through integrins and mapks. *Nature* **424**, 398–405.

Peixoto, F. O., Pereira-Terra, P., Moura, R. S., Carvalho-Dias, E., Correia-Pinto, J. and Nogueira-Silva, C. (2015). The role of ephrins-b1 and -b2 during fetal rat lung development. *Cellular Physiology and Biochemistry* **35**, 104–115.

Perry, S. F., Wilson, R. J. a., Straus, C., Harris, M. B. and Remmers, J. E. (2001). Which came first, the lung or the breath? *Comparative Biochemistry and Physiology - A Molecular and Integrative Physiology* **129**, 37–47.

Pfaff, S. L., Mendelsohn, M., Stewart, C. L., Edlund, T. and Jessell, T. M. (1996). Requirement for lim homeobox gene isl1 in motor neuron generation reveals a motor neuron– dependent step in interneuron differentiation. *Cell* **84**, 309–320.

Philippidou, P., Walsh, C. M., Aubin, J., Jeannotte, L. and Dasen, J. S. (2012). Sustained hox5 gene activity is required for respiratory motor neuron development. *Nature Neuroscience* **15**.

Pitulescu, M. E. and Adams, R. H. (2010). Eph/ephrin molecules–a hub for signaling and endocytosis. *Genes & development* **24**, 2480–92.

Pober, B. R., Lin, A., Russell, M., Ackerman, K. G., Chakravorty, S., Strauss, B., Westgate, M. N., Wilson, J., Donahoe, P. K. and Holmes, L. B. (2005). Infants with bochdalek diaphragmatic hernia: sibling precurrence and monozygotic twin discordance in a hospital-based malformation surveillance program. *American journal of medical genetics. Part A* **138A**, 81–8.

Polleux, F., Morrow, T. and Ghosh, a. (2000). Semaphorin 3a is a chemoattractant for cortical apical dendrites. *Nature* **404**, 567–573.

Pownall, M. E., Gustafsson, M. K. and Emerson, C. P. (2002). Myogenic regulatory factors and the specification of muscle progenitors in vertebrate embryos. *Annual review of cell and developmental biology* **18**, 747–83.

Prakash, N., Puelles, E., Freude, K., Trumbach, D., Omodei, D., Di Salvio, M., Sussel, L., Ericson, J., Sander, M., Simeone, A. and Wurst, W. (2009). Nkx6-1 controls the identity and fate of red nucleus and oculomotor neurons in the mouse midbrain. *Development* **136**, 2545–2555.

Prunotto, C., Crepaldi, T., Forni, P. E., Ieraci, A., Kelly, R. G., Tajbakhsh, S., Buckingham, M. and Ponzetto, C. (2004). Analysis of mlc-lacz met mutants highlights the essential function of met for migratory precursors of hypaxial muscles and reveals a role for met in the development of hyoid arch-derived facial muscles. *Developmental dynamics : an official publication of the American Association of Anatomists* **231**, 582–91.

Rama, N., Dubrac, A., Mathivet, T., Ní Chárthaigh, R.-A., Genet, G., Cristofaro, B., Pibouin-Fragner, L., Ma, L., Eichmann, A. and Chédotal, A. (2015). Slit2 signaling through robo1 and robo2 is required for retinal neovascularization. *Nature Medicine* **21**, 483–491.

Relaix, F., Rocancourt, D., Mansouri, A. and Buckingham, M. (2004). Divergent functions of murine pax3 and pax7 in limb muscle development. *Genes & development* **18**, 1088–105.

Ricardo, J. A. and Koh, E. T. (1978). Anatomical evidence of direct projections from the nucleus of the solitary tract to the hypothalamus, amygdala, and other forebrain structures in the rat. *Brain research* **153**, 1–26.

Rida, P. C. G., Le Minh, N. and Jiang, Y. J. (2004). A notch feeling of somite segmentation and beyond. *Developmental biology* **265**, 2–22.

Rochlin, K., Yu, S., Roy, S. and Baylies, M. K. (2010). Myoblast fusion: When it takes more to make one. *Developmental Biology* **341**, 66–83.

Rossi, J. M., Dunn, N. R., Hogan, B. L. and Zaret, K. S. (2001). Distinct mesodermal signals, including bmps from the septum transversum mesenchyme, are required in combination for hepatogenesis from the endoderm. *Genes & development* **15**, 1998–2009.

Rousso, D. L., Gaber, Z. B., Wellik, D., Morrisey, E. E. and Novitch, B. G. (2008). Coordinated actions of the forkhead protein foxp1 and hox proteins in the columnar organization of spinal motor neurons. *Neuron* **59**, 226–40.

Russell, M. K., Longoni, M., Wells, J., Maalouf, F. I., Tracy, A. A., Loscertales, M., Ackerman, K. G., Pober, B. R., Lage, K., Bult, C. J. and Donahoe, P. K. (2012). Congenital diaphragmatic hernia candidate genes derived from embryonic transcriptomes. *Proceedings of the National Academy of Sciences of the United States of America* **109**, 2978–2983.

Rutishauser, U. (1992). Ncam and its polysialic acid moiety: a mechanism for pull/push regulation of cell interactions during development? *Development (Cambridge, England). Supplement* , 99–104.

Saga, Y. and Takeda, H. (2001). The making of the somite: molecular events in vertebrate segmentation. *Nature reviews. Genetics* **2**, 835–845.

Sant'Ambrogio, G., Tsubone, H. and Sant'Ambrogio, F. B. (1995). Sensory information from the upper airway: Role in the control of breathing. *Respiration Physiology* **102**, 1–16.

Santiago, A. and Erickson, C. A. (2002). Ephrin-b ligands play a dual role in the control of neural crest cell migration. *Development (Cambridge, England)* **129**, 3621–32.

Scaal, M., Bonafede, a., Dathe, V., Sachs, M., Cann, G., Christ, B. and Brand-Saberi, B. (1999). Sf/hgf is a mediator between limb patterning and muscle development. *Development (Cambridge, England)* **126**, 4885–4893.

Scaal, M. and Christ, B. (2004). Formation and differentiation of the avian dermomyotome. *Anatomy and embryology* **208**, 411–24.

Schäfer, K. and Braun, T. (1999). Early specification of limb muscle precursor cells by the homeobox gene lbx1h. *Nature genetics* **23**, 213–216.

Schnorrer, F., Kalchhauser, I. and Dickson, B. J. (2007). The transmembrane protein kon-tiki couples to dgrip to mediate myotube targeting in drosophila. *Developmental Cell* **12**, 751–766.

Schwander, M., Leu, M., Stumm, M., Dorchies, O. M., Ruegg, U. T., Schittny, J. and Müller, U. (2003). B1 integrins regulate myoblast fusion and sarcomere assembly. *Developmental Cell* **4**, 673–685.

Schwander, M., Shirasaki, R., Pfaff, S. L. and Müller, U. (2004). Beta1 integrins in muscle, but not in motor neurons, are required for skeletal muscle innervation. *The Journal of neuroscience : the official journal of the Society for Neuroscience* **24**, 8181–91.

Schweitzer, R., Chyung, J. H., Murtaugh, L. C., Brent, a. E., Rosen, V., Olson, E. N., Lassar, a. and Tabin, C. J. (2001). Analysis of the tendon cell fate using scleraxis, a specific marker for tendons and ligaments. *Development (Cambridge, England)* **128**, 3855–3866.

Sentürk, A., Pfennig, S., Weiss, A., Burk, K. and Acker-Palmer, A. (2011). Ephrin bs are essential components of the reelin pathway to regulate neuronal migration. *Nature* **472**, 356–60.

Sholl, D. a. (1953). Dendritic organization in the neurons of the visual and motor cortices of the cat. *Journal of anatomy* **87**, 387–406.

Slovakova, J., Speicher, S., Sanchez-Soriano, N., Prokop, a. and Carmena, a. (2012). The actin-binding protein canoe/af-6 forms a complex with robo and is required for slit-robo signaling during axon pathfinding at the cns midline. *Journal of Neuroscience* **32**, 10035–10044.

Smith, J. C., Abdala, A. P. L., Borgmann, A., Rybak, I. A. and Paton, J. F. R. (2013). Brainstem respiratory networks: building blocks and microcircuits. *Trends in neurosciences* **36**, 152–62.

Smith, J. C., Ellenberger, H. H., Ballanyi, K., Richter, D. W. and Feldman, J. L. (1991). Pre-bötzinger complex: a brainstem region that may generate respiratory rhythm in mammals. *Science (New York, N.Y.)* **254**, 726–9.

Soker, S., Miao, H. Q., Nomi, M., Takashima, S. and Klagsbrun, M. (2002). Vegf165 mediates formation of complexes containing vegfr-2 and neuropilin-1 that enhance vegf165-receptor binding. *Journal of Cellular Biochemistry* **85**, 357–368.

Soker, S., Takashima, S., Miao, H. Q., Neufeld, G. and Klagsbrun, M. (1998). Neuropilin-1 is expressed by endothelial and tumor cells as an isoform-specific receptor for vascular endothelial growth factor. *Cell* **92**, 735–745.

Söllner, H. (2012). *Developmental wiring and adaptive plasticity of peripheral sensorimotor circuitry*. Ph.D. thesis.

Song, H.-j., Ming, G.-l. and Poo, M.-m. (1997). camp-induced switching in turning direction of nerve growth cones. *Nature* **388**, 275–279.

Steffen, L. S., Guyon, J. R., Vogel, E. D., Howell, M. H., Zhou, Y., Weber, G. J., Zon, L. I. and Kunkel, L. M. (2007). The zebrafish runzel muscular dystrophy is linked to the titin gene. *Developmental Biology* **309**, 180–192.

Steigemann, P., Molitor, A., Fellert, S., Jäckle, H. and Vorbrüggen, G. (2004). Heparan sulfate proteoglycan syndecan promotes axonal and myotube guidance by slit/robo signaling. *Current biology : CB* **14**, 225–30.

Stein, E. and Tessier-Lavigne, M. (2001). Hierarchical organization of guidance receptors: silencing of netrin attraction by slit through a robo/dcc receptor complex. *Science* **291**, 1928–1938.

Strittmatter, S. M., Fankhauser, C., Huang, P. L., Mashimo, H. and Fishman, M. C. (1995). Neuronal pathfinding is abnormal in mice lacking the neuronal growth cone protein gap-43. *Cell* **80**, 445–52.

Stuelsatz, P., Keire, P., Almuly, R. and Yablonka-Reuveni, Z. (2012). A contemporary atlas of the mouse diaphragm: myogenicity, vascularity, and the pax3 connection. *The journal of histochemistry and cytochemistry : official journal of the Histochemistry Society* **60**, 638–57.

Suzuki, T., Do, M. K. Q., Sato, Y., Ojima, K., Hara, M., Mizunoya, W., Nakamura, M., Furuse, M., Ikeuchi, Y., Anderson, J. E. and Tatsumi, R. (2013). Comparative analysis of semaphorin 3a in soleus and edl muscle satellite cells in vitro toward understanding its role in modulating myogenin expression. *International Journal of Biochemistry and Cell Biology* **45**, 476–482.

Swartz, M. E., Eberhart, J., Pasquale, E. B. and Krull, C. E. (2001). Epha4/ephrin-a5 interactions in muscle precursor cell migration in the avian forelimb. *Development (Cambridge, England)* **128**, 4669–4680.

Takayama, H., La Rochelle, W. J., Anver, M., Bockman, D. E. and Merlino, G. (1996). Scatter factor/hepatocyte growth factor as a regulator of skeletal muscle and neural crest development. *Proceedings of the National Academy of Sciences of the United States of America* **93**, 5866–5871.

Talpalar, A. E., Bouvier, J., Borgius, L., Fortin, G., Pierani, A. and Kiehn, O. (2013). Dual-mode operation of neuronal networks involved in left–right alternation. *Nature* **500**, 85–88.

Tanabe, Y., William, C. and Jessell, T. M. (1998). Specification of motor neuron identity by the mnr2 homeodomain protein. *Cell* **95**, 67–80.

Tanaka, K., Sato, K., Yoshida, T., Fukuda, T., Hanamura, K., Kojima, N., Shirao, T., Yanagawa, T. and Watanabe, H. (2011). Evidence for cell density affecting c2c12 myogenesis: Possible regulation of myogenesis by cell-cell communication. *Muscle and Nerve* **44**, 968–977.

Tang, J., Landmesser, L. and Rutishauser, U. (1992). Polysialic acid influences specific pathfinding by avian motoneurons. *Neuron* **8**, 1031–1044.

Tang, J., Rutishauser, U. and Landmesser, L. (1994). Polysialic acid regulates growth cone behavior during sorting of motor axons in the plexus region. *Neuron* **13**, 405–414.

Terada, N., Hamazaki, T., Oka, M., Hoki, M., Mastalerz, D. M., Nakano, Y., Meyer, E. M., Morel, L., Petersen, B. E. and Scott, E. W. (2002). Bone marrow cells adopt the phenotype of other cells by spontaneous cell fusion. *Nature* **416**, 542–545.

Tezuka, T., Inoue, A., Hoshi, T., Weatherbee, S. D., Burgess, R. W., Ueta, R. and Yamanashi, Y. (2014). The musk activator agrin has a separate role essential for postnatal maintenance of neuromuscular synapses. *Proceedings of the National Academy of Sciences of the United States of America* **111**, 1–6.

Thaler, J., Harrison, K., Sharma, K., Lettieri, K., Kehrl, J. and Pfaff, S. L. (1999). Active suppression of interneuron programs within developing motor neurons revealed by analysis of homeodomain factor hb9. *Neuron* **23**, 675–687.

Thor, S., Andersson, S. G. E., Tomlinson, A. and Thomas, J. B. (1999). A lim-homeodomain combinatorial code for motor-neuron pathway selection. *Nature* **397**, 76–80.

Tian, G. F., Peever, J. H. and Duffin, J. (1999). Botzinger-complex, bulbospinal expiratory neurones monosynaptically inhibit ventral-group respiratory neurones in the decerebrate rat. *Experimental Brain Research* **124**, 173–180.

Tidball, J. G. (1994). Assembly of myotendinous junctions in the chick embryo: deposition of p68 is an early event in myotendinous junction formation. *Developmental biology* **163**, 447–56.

Trotter, J. a. (2002). Structure-function considerations of muscle-tendon junctions. *Comparative Biochemistry and Physiology - A Molecular and Integrative Physiology* **133**, 1127–1133.

Uetani, N. (2006). Mammalian motoneuron axon targeting requires receptor protein tyrosine phosphatases and. *Journal of Neuroscience* **26**, 5872–5880.

Van Vactor, D. (1998). Adhesion and signaling in axonal fasciculation. *Current Opinion in Neurobiology* **8**, 80–86.

Vassilopoulos, G., Wang, P.-R. and Russell, D. W. (2003). Transplanted bone marrow regenerates liver by cell fusion. *Nature* **422**, 901–904.

Vasyutina, E., Martarelli, B., Brakebusch, C., Wende, H. and Birchmeier, C. (2009). The small g-proteins rac1 and cdc42 are essential for myoblast fusion in the mouse. *Proceedings of the National Academy of Sciences of the United States of America* **106**, 8935–8940.

Venuti, J. M., Morris, J. H., Vivian, J. L., Olson, E. N. and Klein, W. H. (1995). Myogenin is required for late but not early aspects of myogenesis during mouse development. *Journal of Cell Biology* **128**, 563–576.

von Maltzahn, J., Chang, N. C., Bentzinger, C. F. and Rudnicki, M. a. (2012). Wnt signaling in myogenesis. *Trends in Cell Biology* **22**, 602–609.

Wang, H. U. and Anderson, D. J. (1997). Eph family transmembrane ligands can mediate repulsive guidance of trunk neural crest migration and motor axon outgrowth. *Neuron* **18**, 383–396.

Wang, X., Willenbring, H., Akkari, Y., Torimaru, Y., Foster, M., Al-Dhalimy, M., Lagasse, E., Finegold, M., Olson, S. and Grompe, M. (2003). Cell fusion is the principal source of bone-marrow-derived hepatocytes. *Nature* **422**, 897–901.

Watanabe, S., Matsushita, S., Hayasaka, M. and Hanaoka, K. (2011). Generation of a conditional null allele of lbx1. *Genesis* **49**, 803–810.

Weiner, J. a., Koo, S. J., Nicolas, S., Fraboulet, S., Pfaff, S. L., Pourquié, O. and Sanes, J. R. (2004). Axon fasciculation defects and retinal dysplasias in mice lacking the immunoglobulin superfamily adhesion molecule ben/alcam/sc1. *Molecular and Cellular Neuroscience* **27**, 59–69.

Whitford, K. L. and Ghosh, A. (2001). Plexin signaling via off-track and rho family gtpases. *Neuron* **32**, 1–3.

Wichterle, H., Lieberam, I., Porter, J. a. and Jessell, T. M. (2002). Directed differentiation of embryonic stem cells into motor neurons. *Cell* **110**, 385–97.

Wu, H., Barik, A., Lu, Y., Shen, C., Bowman, A., Li, L., Sathyamurthy, A., Lin, T. W., Xiong, W.-C. and Mei, L. (2015). Slit2 as a β-catenin/ctnnb1-dependent retrograde signal for presynaptic differentiation. *eLife* **4**, 1–20.

Wu, H., Lu, Y., Barik, A., Joseph, A., Taketo, M. M., Xiong, W.-C. and Mei, L. (2012). Beta-catenin gain of function in muscles impairs neuromuscular junction formation. *Development* **139**, 2636–2636.

Yang, W., Carmichael, S. L., Harris, J. a. and Shaw, G. M. (2006). Epidemiologic characteristics of congenital diaphragmatic hernia among 2.5 million california births, 1989-1997. *Birth Defects Research Part A - Clinical and Molecular Teratology* **76**, 170–174.

Yang, X., Arber, S., William, C., Li, L., Tanabe, Y., Jessell, T. M., Birchmeier, C. and Burden, S. J. (2001). Patterning of muscle acetylcholine receptor gene expression in the absence of motor innervation. *Neuron* **30**, 399–410.

Yee, S. P. and Rigby, P. W. (1993). The regulation of myogenin gene expression during the embryonic development of the mouse. *Genes & development* **7**, 1277–1289.

Ypsilanti, A. R., Zagar, Y. and Chédotal, A. (2010). Moving away from the midline: new developments for slit and robo. *Development (Cambridge, England)* **137**, 1939–52.

Yu, H. H. and Kolodkin, a. L. (1999). Semaphorin signaling: a little less per-plexin. *Neuron* **22**, 11–4.

Yuan, W., Rao, Y., Babiuk, R. P., Greer, J. J., Wu, J. Y. and Ornitz, D. M. (2003). A genetic model for a central (septum transversum) congenital diaphragmatic hernia in mice lacking slit3. *Proceedings of the National Academy of Sciences of the United States of America* **100**, 5217–5222.

Zhadanov, A. B., Provance, D. W., Speer, C. a., Coffin, J. D., Goss, D., Blixt, J. a., Reichert, C. M. and Mercer, J. a. (1999). Absence of the tight junctional protein af-6 disrupts epithelial cell-cell junctions and cell polarity during mouse development. *Current Biology* **9**, 880–888.

Zhang, B., Luo, S., Wang, Q., Suzuki, T., Xiong, W. C. and Mei, L. (2008). Lrp4 serves as a coreceptor of agrin. *Neuron* **60**, 285–297.

Zhang, B., Xiao, W., Qiu, H., Zhang, F., Moniz, H. a., Jaworski, A., Condac, E., Gutierrez-Sanchez, G., Heiss, C., Clugston, R. D., Azadi, P., Greer, J. J., Bergmann, C., Moremen, K. W., Li, D., Linhardt, R. J., Esko, J. D. and Wang, L. (2014). Heparan sulfate deficiency disrupts developmental angiogenesis and causes congenital diaphragmatic hernia. *Journal of Clinical Investigation* **124**, 209–221.

Chapter 10

Appendix

Abbreviations

AChR Acetylcholine receptor

AER Apical ectodermal ridge

ALP Alkaline phosphatase

ALS Amyotrophic lateral sclerosis

AP Action potential

Arhgap39 Rho GTPase activating protein 39

BCIP 5-bromo-4-chloro-3-indolyphosphate

Bmp Bone morphogenic protein

BötC Bötzinger complex

CAM Cellular adhesion molecule

cAMP Cyclic adenosine monophosphate

Cdc42 Cell division cycle 42

CDH Congenital diaphragmatic hernia

cGMP Cyclic guanosine monophosphate

c-hairy1 Chicken hairy homologue 1

c-Met Met proto-oncogene

CoM Costal diaphragm muscle

COM Center of mass

COS CV-1 in Origin with SV40 genes

CPG Central pattern generator

CrM Crural diaphragm muscle

CTR Central tendon region

CUB Complement C1r/C1s, Uegf, Bmp1

DAPI 4,6-Diamidin-2-phenylindol

DCC Deleted in colorectal carcinoma

DEPC Diethyl dicarbonate

dH_2O Distilled Water

DIG Digoxigenin

DLL Dorsolateral lip

DM Dermomyotome

DMEM Dulbecco's Modified Eagle Medium

DRG Dorsal root ganglia

DSHB Developmental Studies Hybridoma Bank

Duf Dumbfounded

E.Coli Escherichia Coli

ECM Extracellular matrix

EGF Epidermal growth factor

ErbB2 Erb-b2 receptor tyrosine kinase 2

ESC Embryonic stem cell

Fah Fumarylacetoactate hydrolase

FBS Fetal bovine serum

FC Founder cell

FCM Fusion competent myoblast

Fgf Fibroblast growth factor

FoxP1 Forkhead transcription factor P1

FMI Forward migration index

FV/FVII Coagulation factor V/VIII homology

Gata4 GATA binding protein 4

gDNA Genomic DNA

GFP Green fluorescence protein

GPI Glycosylphosphatidylinositol

GTPase Guanosine triphosphatease

H Heart

HS Horse serum

HSPG Heparan sulphate proteoglycan

IOS Inspiratory off-switch

ISH *In situ* hybridization

IVC Individually ventilated cage

Kon Kon-tiki

L Liver

Lbx1 Ladybird homeobox homolog 1

LMC Lateral motor column

LPbr Lateral parabrachial subgroup

Lrp4 Lipoprotein receptor-related protein 4

Lu Lung

Mapk1 Mitogen-activated protein kinase 1

MAS Muscle attachment side

MEF Myogenic regulatory factor

MMC Medial motor column

MN Motor neurons

MPCs Muscle progenitor cells

Msx1 Msh homeobox 1

MTJ Myotendinous junction

Musk Muscle/skeletal receptor tyrosine kinase

MyoD1 Myogenic differentiation 1

NBT Nitro-blue tetrazolium

NCAM Neuronal adhesion molecule

NCC Neuronal crest cell

Ndst1 N-deacetylase/N-sulfotransferase (heparan glucosaminyl) 1

Nfasc Neurofascin

NGS Next-Generation Sequencing

NMJ Neuromuscular junction

NTS Nucleus of the solitary tract

ON Over night

OC1 One cut domain, family member 1

P Polymerase

PBS Phosphate buffered saline

Pbx1 Pre-B-cell leukemia homeobox 1

PFA Paraformaldehyd

pFRG/RTN Parafacial respiratory group or retrotrapezoid nucleus

PKFC Parabrachial Kölliker-fuse complex

PMA Progressive muscular atrophy

PMC Phrenic motor column

pMN Phrenic motor neurons

pMPC Primary muscle progenitor cell

PN phrenic nerve

PNEP Phrenic nerve entry point

Pou3f1 POU domain, class 3, transcription factor

PRG Pontine respiratory group

PSA Polysialic acid

PSI Plexin, semaphorin, and integrin domain

PSM Pre-somitic mesoderm

Ptk2 Protein tyrosine kinase 2

RA Retinoic acid

Rac1 RAS-related C3 botulinum substrate 1

RE Restriction Enzyme

Reln Reelin

RhoA Ras homolog family member A

Rockl Rho-associated coiled-coil containing protein kinase 1

RPTP Receptor tyrosine phosphatase

RS Respiratory system

RT Room temperature

RTK Receptor tyrosine kinase

Scx Scleraxis

Sdc Syndecan

SEM Standard error of mean

Sema Semaphorin

SF/HGF Scatter facor/hepatocyte growth factor

Shh Sonic hedgehog

Six Sine oculis-related homeobox

SOI Sum of intersections

ST Septum transversum

SVZ Subventricular zone

Tgfb1 Transforming growth factor, beta 1

Tnmd Tenomodulin

TPC Tendon progenitor cell

Vasp Vasodilator-stimulated phosphoprotein

VEGF165 Vascular endothelial growth factor isoform 165

VLL Ventrolateral lip

VRC Ventrolateral respiratory column

VRG Ventrolateral respiratory group

Wnt Wingless-type MMTV integration site

Zfpm2 Zinc finger protein, FOG family member 2

Acknowledgments

Lastly, I want deeply appreciate following persons who contributed in various ways to the realization of this thesis:

Andrea Huber Brösamle, for accepting me in your group as a freshman in neuroscience and for your patience during my catch up in molecular biology and developmental genetics as an engineer. You really taught me how to understand complex biological contexts and to create my own hypothesis of underlying mechanisms.

Attila Aszodi, for giving me unrestricted trust to work independently and to intervene at the right time when new ideas were stuck. I certainly appreciate your perception onto neuroscience as a musculoskeletal scientist and hopefully our future exciting projects will combine both scientific topics.

Rosa-Eva Hüttl, for your encouraging input on the study and your always incredible fast, inspiring and improving corrections of our manuscript and this thesis. I especially dignify your professional help with the mouse lines and chickens during the last four years! Finally, I hope that we can expand and deepen our future scientific cooperation.

Paolo Alberton, for being so helpful during planing, practicing and performing chemotaxis experiments with primary cells. You always pushed me further when I lost my last energy during the final phase of this thesis. Thank you so much!

Georg Luxenhofer, for your sustained frankness in answering even the most stupid questions. You're truly a born teacher.

Michaela Helmbrecht & Maria Angelica Castiblanco Urbina, for being such professional, organized and cordially graduate colleagues during my PhD thesis.

Philipp Hanuschick, for your help work on the topic during your master's thesis and the investigation of *Npn-2* and *Npn-1^{cond};Ht-PA-Cre* mutant animals.

Anne-Lena Amend, for your help during you Bachelor Thesis by staining whole-mount embryos and your always good mood.

Veronika Schönitzer, for your inspiring help during primary cell sorting and ideas for follow-up projects.

Alain Chédotal, for providing us Robo1/Robo2 double knockout mutant embryos and wiltype littermates and for your beneficial discussion on Slit-Robo signaling.

Alexander Jaworksi, for your kind review of old data and your input during fruitful discussions, suggestions and ideas for follow up projects.

Hans Polzer & Christian Prall, for your inspiring discussions on real clinical questions and the transfer from basic science towards clinics and vice versa.

Anna Truckenbrodt & Stefan Weiß, for your nice cooperation to combine and improve the *in situ* hybridization protocols and constant discussion about new candidate genes for axon pathfinding and Parkinson's Disease.

Zsuzsanna Farkas, Janice Mätsch, Anja Mantik, Martina Burggraf and Heidrun Grondinger, for providing me a perfect background environment to complete my thesis focused and without any technical restrictions.

Furthermore, I express my deepest thanks to my students ***Anita Beer***, ***Anna Scheumaier***, ***Timo Tucholski***, ***Julius Mayer*** and ***Judith Schäfers***, who I supervised during my time or still supervising as a PhD student.

Finally, I also want to thank all other colleagues at the Institute of Developmental Genetics and ExperiMed who I met during the last years.

Last but not least, I want to express my sincere gratitude to my girlfriend ***Carolin***, my ***parents*** and my whole ***family***. Their persistent support during my academic studies and my PhD thesis has made everything so much easier.

Declaration

Ich erkläre hiermit an Eides statt,

dass ich die vorliegende Dissertation mit dem Thema:

Molecular mechanisms of phrenic nerve outgrowth and innervation of the diaphragm.

selbständig verfasst, mich außer der angegebenen keiner weiteren Hilfsmittel bedient und alle Erkenntnisse, die aus dem Schrifttum ganz oder annähernd übernommen sind, als solche kenntlich gemacht und nach ihrer Herkunft unter Bezeichnung der Fundstelle einzeln nachgewiesen habe.

Ich erkläre des Weiteren, dass die hier vorgelegte Dissertation nicht in gleicher oder in ähnlicher Form bei einer anderen Stelle zur Erlangung eines akademischen Grades eingereicht wurde.

München, den 30.03.2016 Maximilian Saller